UNIVERSITÀ
DEGLI STUDI
DI PADOVA

UNIVERSITÀ DEGLI STUDI DI PADOVA

DIPARTIMENTO DI FISICA E ASTRONOMIA
'GALILEO GALILEI'

SCUOLA DI DOTTORATO DI RICERCA IN ASTRONOMIA– CICLO XXVI

TESI DI DOTTORATO

DEVELOPMENT OF A NEW TOOL FOR THE DYNAMICAL ANALYSIS OF EXOPLANETARY SYSTEMS

Direttore della Scuola di Dottorato:	Ch.mo Prof. Giampaolo Piotto
Supervisore:	Ch.mo Prof. Giampaolo Piotto
Co-supervisore:	Dr. Francesco Marzari

Studente di Dottorato: Luca Borsato

2011-2014

UNIVERSITÀ
DEGLI STUDI
DI PADOVA

UNIVERSITY OF STUDIES OF PADOVA

DEPARTMENT OF PHYSICS AND ASTRONOMY
'GALILEO GALILEI'

DOCTORAL SCHOOL OF RESEARCH IN ASTRONOMY– CYCLE XXVI
PHD THESIS

DEVELOPMENT OF A NEW TOOL FOR THE DYNAMICAL ANALYSIS OF EXOPLANETARY SYSTEMS

Director of the PhD school:	Ch.mo Prof. Giampaolo Piotto
Supervisor:	Ch.mo Prof. Giampaolo Piotto
Co-supervisor:	Dr. Francesco Marzari

PhD Student: Luca Borsato

2011-2014

Contents

Introduction **xi**

1 Extra-solar planets **1**
1.1 Techniques to detect and characterize exoplanets 2
1.1.1 Radial Velocity or Doppler effect technique 4
1.1.2 Method of the transits and Transit Time Variation 5
1.2 Inverse problem: determine parameters from observations 11
1.3 Current and future missions 13
1.3.1 Radial Velocity facilities 13
1.3.2 Ground and space-based missions for transit detection . . . 15

2 TRADES: TRAnsits and Dynamics of Exoplanetary Systems **19**
2.1 Celestial Mechanics: reference frame and dynamics 20
2.2 Calculation of the simulated observables 22
2.2.1 Transit determination 22
2.2.2 RV calculation and other constraints 23
2.3 Algorithms of the different TRADES modes 24
2.3.1 Grid search 25
2.3.2 Levenberg-Marquardt 26
2.3.3 Genetic Algorithm: PIKAIA 27
2.3.4 Particle Swarm Optimization 28
2.3.5 Bootstrap analysis 28

3 Applications **31**
3.1 Validation with a simulated systems 31
3.2 Test case: Kepler-11 system 36
3.2.1 Transit time analysis of the twelve quarters 38
3.3 Test case: Kepler-9 system 49

3.3.1 Transit time analysis of the twelve quarters 52
3.3.2 Dynamical analysis without RV points 55

4 Applications to CHEOPS and TASTE **59**
4.1 Analysis of TTV capability of the CHEOPS mission 59
4.1.1 Simulation based on Kepler-9 system 60
4.2 TASTE sample analysis 64
4.2.1 HAT-P-13 system 65
4.2.2 WASP-3 system 72

5 Conclusions and future prospectives **79**
5.1 Conclusions 79
5.2 Side projects and future prospectives 82

Bibliography **85**

List of Figures

1.1 Exoplanet discoveries techniques. 2
1.2 Mass–Period relation. 3
1.3 Transit scheme 7
1.4 LCs of HD 209458b 9
1.5 Orbital Keplerian elements 12

3.1 Synthetic system: parameters as function of noise scale 33
3.2 Synthetic system: fitted parameters for different initial a 34
3.3 Kepler-11: circular orbits 37
3.4 Kepler-11: $O-C$ diagrams for Lis2011. 42
3.5 Kepler-11: $O-C$ diagrams for solution K11-II. 43
3.6 Kepler-11: plots of M and e for initial grid($M_{\rm p}$) and $e = 0.001$ 44
3.7 Kepler-11: plots of M and e for initial grid($M_{\rm p}$) and $e = 0.1$ 45
3.8 Kepler-11: plots of M and e for initial grid($M_{\rm p}$) and different e . . . 46
3.9 Kepler-11: $O-C$ diagrams for best solution K11-III 47
3.10 Kepler-9: $O-C$ with parameters from discovery paper 51
3.11 Kepler-9: $O-C$ with parameters from solution K9-I 53
3.12 Kepler-9: $O-C$ for K9-I extended to 12 quarters 54
3.13 Kepler-9: $O-C$ after fitting 12 quarters and K9-I as initial parameters 55
3.14 Kepler-9: $O-C$ for the best solution K9-II 57

4.1 Kepler-9 for CHEOPS 63
4.2 HAT-P-13: $O-C$ diagram from Southworth et al. (2012) 65
4.3 HAT-P-13: RV diagram from Winn et al. (2010) 66
4.4 HAT-P-13: $O-C$ and RV diagrams from `TRADES` fit. 69
4.5 HAT-P-13: $O-C$ and RV diagrams from grid+`LM` search. 70
4.6 HAT-P-13: best-fit solution from the grid+`LM` search. 71

4.7 WASP-3 data 73
4.8 WASP-3 $O-C$ with only one planet 74
4.9 WASP-3 $O-C$ and RV plots for the 3-body solutions. 76
4.10 WASP-3, 3-body unstable solution. 77
4.11 WASP-3 parameters evolution for 3-body unstable solution. 78

List of Tables

3.1 Parameters of the simulated system. 32
3.2 Parameters of the Kepler-11 system. 41
3.3 Ephemeris of the Kepler-11 system. 48
3.4 Main differences in the Kepler-11 analysis for each solution. 48
3.5 Ephemeris of the Kepler-9 system. 50
3.6 Parameters of the Kepler-9 system. 52

4.1 Kepler-9 system for CHEOPS TTV analysis 62

Abstract

I have developed a software that can simultaneously fit observed radial velocities (RVs) and transit times (T_0s) data with the purpose of determining the orbital parameters of exoplanetary systems. I have called this program TRADES: TRAnsits and Dynamics of Exoplanetary Systems. I implemented a dynamical simulator for N-body systems which also fits the available data during the orbital integration and determines the best combination of the orbital parameters by using a grid search, a χ^2 minimization, a genetic algorithms, a particle swarm optimization, and a bootstrap analysis.

To validate TRADES, I tested the code on a synthetic three-body system and on two real systems discovered by the *Kepler* mission: Kepler-9 and Kepler-11. These systems are good benchmarks to test multiple exoplanet systems showing transit time variations (TTVs) due to the gravitational interaction among planets. I have found orbital parameters of Kepler-11 planets in good agreement with the values proposed in the discovery paper and with a a recent work from the same authors. I analyzed the first three quarters of Kepler-9 system and found parameters in partial agreement with the discovery paper. Analyzing transit times (T_0s) covering 12 quarters of *Kepler* data I have found a new best-fit solution for Kepler-9. This solution outputs masses that are about the 55% of the values proposed in the discovery paper; this leads to a reduced semi-amplitude of the radial velocities of about 12.80 ms^{-1}.

Furthermore, I created a synthetic data set of RVs and T_0s, based on the Kepler-9 system, that samples the future observations with ESA satellite CHEOPS. This has been done to study the CHEOPS performances in case of the detection of transit time variation (TTV) signal due to an undetected planet in an exoplanetary system. This analysis is still ongoing, and it will undergo substantial changes with further development of the next phases of the CHEOPS mission.

In addition, I have applied TRADES on few exoplanetary systems of the sam-

ple of the TASTE project (The Asiago Search of Transit timing variations of Exoplanets). In the past, a TTV has been claimed For these systems, but recently this has been excluded because of underestimated uncertainties on the transit time measurements. In the next future I will extend the dynamical analysis of these systems in view of new data that have been recently collected by the TASTE project.

Riassunto

Ho sviluppato un programma per riprodurre simultaneamente le velocità radiali (RV) e i tempi di transito (T_0s) osservati con lo scopo di determinare i parametri orbitali di sistemi esoplanetari. Ho chiamato questo programma TRADES: TRAnsits and Dynamics of Exoplanetary Systems. Il simulatore dinamico N-corpi, che ho implementato, riproduce i dati disponibili durante l'integrazione delle orbite e determina la miglior combinazione dei parametri orbitali tramite una ricerca su una griglia di parametri, una tecnica di minimizzazione del χ^2, un algoritmo genetico, una tecnia di ottimizzazione a sciami di particelle e un'analisi di tipo bootstrap.

Per validare TRADES, ho testato il codice su un sistema a 3-corpi sintetico e su due sistemi reali scoperti dalla missione *Kepler*: Kepler-9 e Kepler-11. Questi sistemi sono perfetti campioni di sistemi di esopianeti multipli, che mostrano variazioni dei tempi di transito (TTVs) per l'interazione gravitazionale tra pianeti. Ho ricavato per i pianeti di Kepler-11 dei parametri orbitali in buon accordo con i valori proposti nell'articolo della scoperta e con un recente lavoro fatto dagli stessi autori. Ho analizzato i primi tre quarti di dati del sistema Kepler-9 e ho trovato dei parametri in parziale accordo con l'articolo della scoperta. Analizzando i tempi di transito (T_0s) che coprono dodici quarti di dati del satellite *Kepler* ho ricavato una nuova soluzione che meglio riproduce i dati. Le masse di questa soluzione orbitale sono circa il 55% dei valori inizialmente proposti; questo ha come conseguenza la riduzione della semi-ampiezza delle velocità radiali di circa 12.80 ms^{-1}.

Inoltre, ho creato un campione sintetico di dati di RVs e T_0, basandomi sul sistema Kepler-9, che riproducano le osservazioni future del satellite dell'ESA CHEOPS. Ciò è stato fatto per studiare le prestazioni di CHEOPS in caso di rilevazione di segnali di TTV dovuti ad un pianeta sconosciuto in un sistema planetario. Questa analisi è ancora in corso e subirà dei sostanziali cambiamenti

durante le prossime fasi di sviluppo della missione CHEOPS.

Ulteriormente, ho applicato TRADES a qualche sistema esoplanetario del campione del progetto TASTE (The Asiago Search of Transit timing variations of Exoplanets). Per questi sistemi era stato precedentemente riscontrato la variazione del tempo dei transiti, ma di recente ciò è stato escluso perché le stime dell'incertezza sui tempi di transito erano sottostimate. Nel prossimo futuro estenderò l'analisi dinamica di questi sistemi in vista dei nuovi dati che sono stati recentemente ottenuti dal progetto TASTE.

Introduction

Nowadays, more than 1811 planets[1] have been discovered and confirmed in about 1126 planetary systems. Around 466 planetary systems are known to be multiple planet systems. Hundreds of *Kepler* planetary candidates with multiple transit-like signals are still waiting confirmation (see Latham et al. 2011; Lissauer et al. 2011b). In order to characterize this kind of systems it is fundamental to combine information coming from both transit times (T_0) and radial velocities (RVs). Another effect due to the presence of multiple planets is the transit time variation (TTV): the gravitational interaction between planets causes a deviation from the Keplerian orbit and, as a consequence, the transit times of a planet may be not strictly periodic (see Agol et al. 2005; Holman & Murray 2005; Miralda-Escudé 2002). This effect can be also used to infer the presence of an unknown planet, even if it does not transit the host star (Agol et al. 2005; Holman & Murray 2005). For examples concerning the use of this technique see *Kepler* Transit Timing Observations series (TTO, Ford et al. 2011, and references therein) and TASTE project (Nascimbeni et al. 2011a, and references therein).

The problem of the determination of the masses and of the orbital parameters of the planets in a multiple system is a difficult inverse problem. In some work, the authors have decided to use an analytic approach to the problem, e.g. Nesvorný & Morbidelli (2008); Nesvorný (2009), developing a method from the perturbation theory (Hori 1966; Deprit 1969) where the transit times are computed as a Fourier series. An example of the application of this technique can be found in Nesvorný et al. (2013) where the authors have foreseen the presence of the planet KOI-142c in the system, that has been recently confirmed in the paper by Barros et al. (2013).

The conceptually simplest, but computationally intensive, method described in this paper is based on a direct numerical N-body approach (Steffen & Agol 2005;

[1] http://exoplanet.eu/catalog, 2014 July 27^{th}.

Agol & Steffen 2007). Very recently, Deck et al. (2014) have developed TTVFast, a symplectic integrator that computes transit times and radial velocities of an exoplanetary system.

I will introduce briefly, in Chapter 1, the state of art on the exoplanet search, describing the main techniques used to detect and to characterize exoplanets. In Chapter 2, I will introduce the TRADES program, the basic formulas and how it calculates radial velocities and transit times. In Chapter 3, I will illustrate applications of TRADES on a synthetic 3-body system and on two real cases: Kepler-11 and Kepler-9. In Chapter 4, I will show some preliminary results based on simulated case for the TTV analysis for the CHEOPS mission and on systems from the sample of the TASTE (The Asiago Search for Transit timing variations of Exoplanets) project.

Capitolo 1

Extra-solar planets

The search for extra-solar planets (or exoplanets) is a relatively young, but very fascinating, astronomical and astrophyical topic fo the latest two decades. The interest in this research have grown so much that the number of the discovered exoplanets has undergone a huge increase (more than 1800 confirmed planets so far) since the discovery by Mayor & Queloz of the very first exoplanet in the 1995.

The basic idea was to search for solar-system analogs, and it was expected to find the extra-solar counterparts of our planets, especially an Earth-twin in the habitable zone (HZ). Even if it has been found that the exoplanets are quite common in the Universe, the discovered exoplanets have shown characteristics quite different from expectations. In fact, one of the most incredible discovery has been the existence of Jupiter-like exoplanets that orbit very close to their hosting star (i.e., within the orbit of Mercury). They are the so-called 'hot-Jupiter'. Furthermore, these hot-Jupiter planets have shown to be inflated due to the stellar flux, and so they have larger radii and lower density than Jupiter. Nowadays, many exoplanetary systems have been discovered and they show a wide range of characteristics, i.e., some has only one hot-Jupiter planet, others are multiple planet systems (wide or very compact), some planets orbit a star of a binary system (S-type orbit) or around the binary (P-type orbit, 'circumbinary planet'). The current and future ground- and space-based missions are moving towards the detection and the study of exoplanets with small mass and radius, in particular Neptune- and Earth-size exoplanets.

1.1 Techniques to detect and characterize extra-solar planets

There are different techniques that allow to discover and to study exoplanets and their environments. I can summarize the principal planet-finding techniques in: radial velocity (RV, or Doppler effect technique), transits and transit time tariation (TTV), astrometry, timing, gravitational microlensing, and direct imaging.

Before the launch in the 2010 of the NASA space mission *Kepler*, the most prolific technique in the exoplanet search was the Radial Velocity (RV) technique. Then the number of planets discovered by transit-based missions and surveys increased a lot. In Fig. 1.1 it is shown the trend of the exoplanet discoveries since 1989 up to July 24, 2014 for each different technique used so far. The RV and transit method together have discovered a huge number of exoplanets compared to all other techniques.

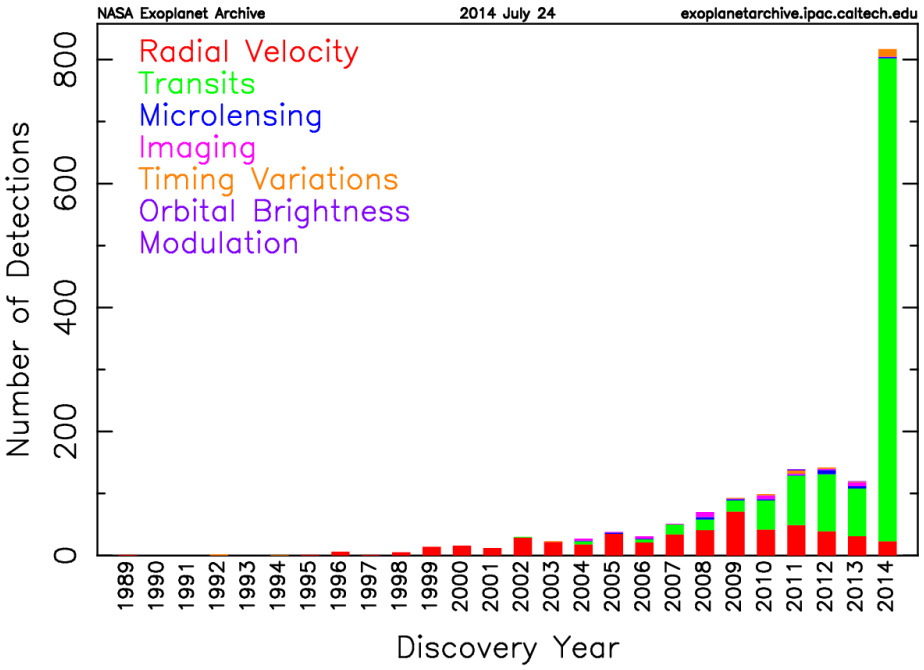

Figura 1.1: Histogram of the number of discovered exoplanets per year. The RV has been the most prolific technique for almost 20 years. The number of transiting exoplanet increased with the first data from *Kepler* mission, that reached its peak in the 2014. All other techniques contribute in a small amount compared with RV and transits method. Credits by exoplanetarchive.ipac.caltech.edu/exoplanetplots.

This is mainly due to the characteristics of the star and of the type of planet

they can detect: large planets close to their hosting star. In fact, each technique has its own sensitivities and limitations. The main biases are given by selection effects in mass (M), radius (R), and semi-major axis (a) (or period, P). A clear example of this effect is shown in Fig. 1.2, where the mass of the planets is plotted as function of the period. In particular, the transit method allows to discover high-mass planets on short periods. Future space missions, such as CHEOPS and PLATO, and new ground-based telescopes, such as the future EELT@ESO, will be able to observe lighter exoplanets with the transit technique. Also the RV technique is suitable for massive exoplanets with short periods, but at the moment it covers a slightly different part of the M-P plot (see Fig. 1.2). The future facilities shall be able to fill the gap between these techniques. At the time of writing neither of these technique have detected an Earth-analog. This is clearly visible in Fig. 1.2, where there are no points that coincide with an Earth-analog planet, that should lies at $\sim 0.003\ M_{\rm Jup}$.

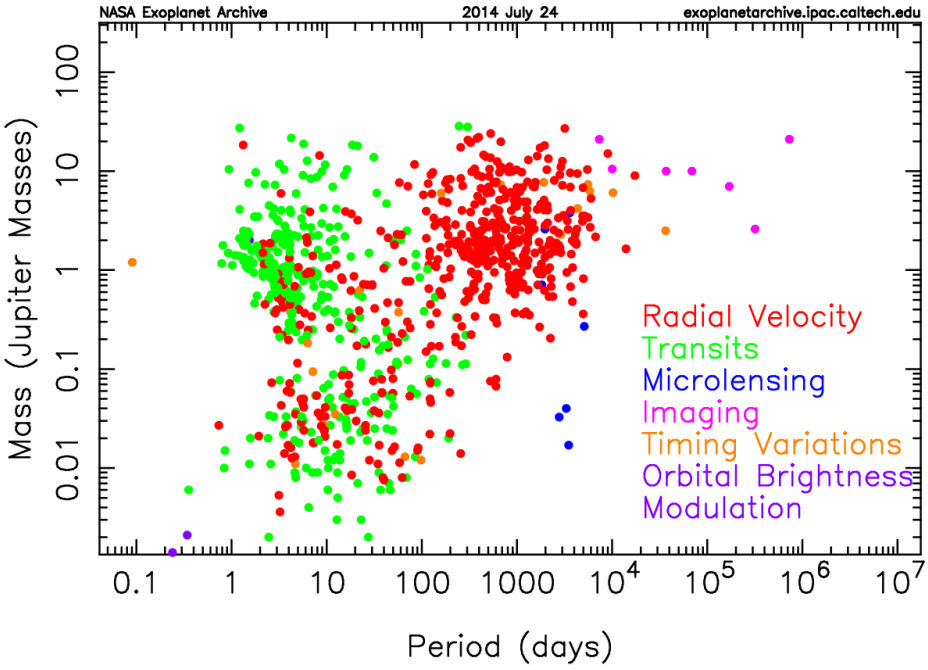

Figura 1.2: Scatter plot of the masses of the exoplanets as function of the period. Different color for each different detecting exoplanet technique. It is clear the selection effects due to the different methods. Credits by exoplanetarchive.ipac.caltech.edu/exoplanetplots.

In the next two subsections I will report a brief description of the main two techniques that allow to detect and to characterize the extra-solar planets: Radial Velocities and Transits.

1.1.1 Radial Velocity or Doppler effect technique

A Doppler shift, or a wavelength shift (or a color change), in a stellar spectrum can be used to calculate the motion of the star along our line of sight. This is the basic idea behind the Radial Velocity (RV) technique. The Doppler method has been used in the past century to study stellar kinematics, stellar binary systems, and to identify stellar pulsations. In the 1952, Struve proposed that high-precision RV could be used to detect an hypothetical planet 10 times more massive than Jupiter at a distance of 1/50 of astronomical unit (au) from its hosting star. This planet would have produced an easily detectable (at that time) RV of about 2 kms^{-1} if its orbit would have been perfectly edge-on. Only after the development of techniques able to remove the telluric lines from the spectrum, the astronomers could reach the RV precision needed to detect a signal from an extra-solar planet. This RV threshold has been achieved in the 1995, when Mayor & Queloz were able to detect the first 'true' exoplanet: 51 Pegasi b (confirmed by Marcy & Butler 1995), about 4.23 days of period, and a projected mass $M_\mathrm{p} \sin i \sim 0.5 M_\mathrm{Jup}$, with a RV precision of about 13 ms^{-1}.

Taking into account a 2-body system, the RV is the barycentric velocity of the star projected on the line of sight. Following Murray & Correia (2011) and Lovis & Fischer (2011), the projected velocity is given by the equation:

$$V_\mathrm{r} = \dot{\vec{r}}_1 \cdot \hat{k} = \gamma + K(\cos(\omega + f) + e\cos\omega) \tag{1.1.1}$$

where $\dot{\vec{r}}_1$ is the barycentric velocity of the star, $\hat{k}$ is the versor that defines the line of sight, γ is the motion of the barycenter of the system, K is the semi-amplitude of the RV that can be computed as $(V_\mathrm{r,max} - V_\mathrm{r,min})/2$. The other three parameters, ω, f, and e, are the argument of the pericenter, the true anomaly and the eccentricity of the body, respectively. The second term defines the so-called Keplerian term, that is function of the orbital parameters of the system, that determines the phase of the planet, $\phi = \omega + f$. The true anomaly f is a function of time and it is an angle measured from ω that defines the position of the planet. It is common to add to equation 1.1.1 a further linear term that takes into account instrumental drifts, massive unidentified bodies, or companions with long periods. The semi-amplitude K depends on the orbital parameters of the body and on the mass of the star and it can be written in practical units as:

$$K = \frac{28.4329\ \mathrm{ms}^{-1}}{\sqrt{1-e^2}} \frac{M_2 \sin i}{M_\mathrm{Jup}} \left(\frac{M_1 + M_2}{M_\odot}\right)^{-1/2} \left(\frac{a}{1\ \mathrm{au}}\right)^{-1/2} \tag{1.1.2}$$

where M_1 and M_2 are the masses of the star and of the planet, respectively; a is the semi-major axis of the planet in astrocentric coordinates, and i is the inclination of the orbit of the body. It is possible to express Eq. 1.1.2 in term of the period, P, through the third Kepler's Law:

$$K = \frac{28.4329\ \mathrm{ms}^{-1}}{\sqrt{1-e^2}} \frac{M_2 \sin i}{M_{\mathrm{Jup}}} \left(\frac{M_1 + M_2}{M_\odot}\right)^{-2/3} \left(\frac{P}{1\ \mathrm{yr}}\right)^{-1/3} \tag{1.1.3}$$

In order to determine the different observables, K, P or a, e, ω, and f it is necessary to obtain different values of V_r, or RV, covering the whole phase ϕ of the planet. Usually, the mass of the planet M_2 is negligible compared to the star mass M_1 that is measurable via spectroscopic analysis, photometry, parallax, and from evolutionary models. When all these information are collected it is possible to calculate the 'minimum', or projected, mass: $M_2 \sin i$. In fact, with the RV method it is not possible to disentangle the planet orbit inclination from the mass, and only the projected mass is achievable.

The common way to analyze RV data is to build a periodogram, i.e., with the Lomb-Scargle or the General Lomb-Scargle (Zechmeister & Kürster 2009) algorithms, in order to evaluate a starting period and its false alarm probability (fap, that measures the significance of the signal at that period). The periodogram can detect a periodic signal through a least-square fitting of sinusoidal taking into account measurement errors, unevenly spaced observations, and drift. Then a Keplerian fit for a single planet is used to determine the exoplanet parameters.

A model of the RV is built from the fitted parameters and it is compared to the data. If the residuals between the data and the model show a pattern, or if a periodogram of the residuals shows a significant signal at a certain period, then the fitting process will be iterate searching for further planets. This is the so-called Keplerian fit that needs $5n_\mathrm{p} + 1$ fitting parameters (or +2, taking into account a further linear term) with n_p the number of planets. The robustness of the fit could be increased using the fitted parameters in the Keplerian fit as the initial parameters for a multi-planet fit. The Levenberg-Marquardt (`LM`) and the Monte-Carlo-Markov-Chain (`MCMC`) methods are efficients, robusts, and common algorithms used for this purpose.

1.1.2 Method of the transits and Transit Time Variation

An eclipse is defined as the astronomical phenomenon during which a body obscures another body. When a planet, the smaller body, passes in front of the

host star it is called a *transit* (or *primary eclipse*). Vice versa, when the planet is behind the star it is called *occultation* (or *secondary eclipse*).

It is worthy to mention that the eclipse events are very useful to study different type of astrophysical problems. In particular, it has been possible to measure precisely the speed of light through the timing of the eclipses of Jupiter's moons, to estimate the astronomical unit (au) during the solar eclipse of Venus; and the stellar structure and evolution can be studied from the analysis of the eclipses of binary stars.

From an exoplanet point of view, observing a transit allows the direct determination of the radius ($R_{\rm p}$), the inclination (i) of the orbit, and the semi-major axis (a) of the planet. An example of a transit, and of an occultation, is reported in Fig. 1.3 (see Fig. 6.9 of Perryman 2011). Following Fig. 1.3, when the planet disk touches the star disk the observed flux (F) will be dimmed. We have the mid transit time, or central transit time or simply transit time (TT or T_0), when the flux depletion is maximum, i.e., when the planet is perfectly aligned with the center of the star. That is, when the projected distance on sky plane between the center of the planet and the star ($r_{\rm sky}$) is minimum. The flux variation, or as it is commonly called the depth of the transit, ΔF, is proportional to the ratio between the projected area covered by the planet and the stellar disk, so it can be expressed as a function of $R_{\rm p}$. For circular orbits it could be approximated by the equation:

$$\frac{\Delta F}{F} \propto \left(\frac{R\rm p}{R_\star}\right)^2 . \tag{1.1.4}$$

An extended formulation of the stellar flux variation that can be measured analyzing a light curve (LC) during a transit can be found in Mandel & Agol (2002).
In example, for the Earth $\Delta F/F$ is of the order of $\sim 8.4\times10^{-5}$, and it increases to $\sim 1.1\times10^{-2}$ for Jupiter.

In addition to the TT, other four important times can be calculated during the transit, the contact times ($t_{\rm con,i}$ with i=1,2,3,4). The planet is just before the transit and its disk touches the stellar disk at the first contact time ($t_{\rm con,1}$); the second contact time ($t_{\rm con,2}$) is defined when the planet is completely inside the stellar disk and their disks touch each other (see circles named 1 and 2 in Fig. 1.3). The $t_{\rm con,1}$ and $t_{\rm con,2}$ define the transit *ingress*. The transit *egress*, from $t_{\rm con,3}$ to $t_{\rm con,4}$, has the same definition of the ingress, but it identifies the end of the transit (see circles 3 and 4 in Fig. 1.3). In some cases, it is possible to calculate only $t_{\rm con,1}$ and $t_{\rm con,4}$ and it is called a *grazing eclipse* (or *grazing transit*); in this case the planet

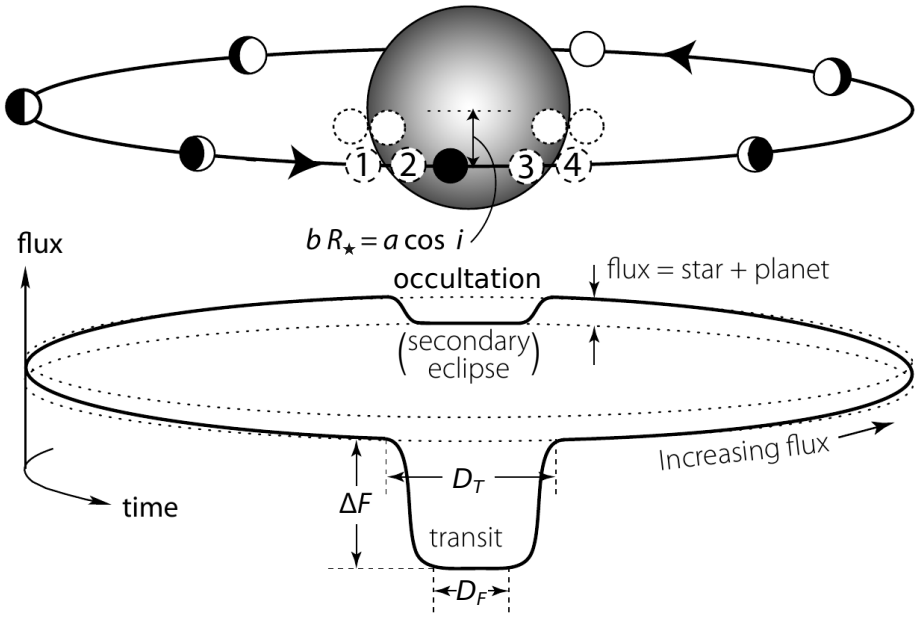

Figura 1.3: Schematic view of a transit. *Top*: orbit of a planet that passes in front of the star; the four contact times are shown as numbered circles; the halfway contact times are not shown. *Bottom*: the stellar flux variation as function of time. The labels have the same meaning of the main text.

disk is not completely within the stellar disk.

When the $t_{\mathrm{con,i}}$ are determined it is possible to calculate the total duration (D_T) and the full duration (D_F) of the transit. The D_T is the difference between $t_{\mathrm{con,4}}$ and $t_{\mathrm{con,1}}$, while D_F is given by $t_{\mathrm{con,3}} - t_{\mathrm{con,2}}$. Winn (2011) gives the equations for D_T and D_F (he called them T_{tot} and T_{full}, respectively) in case of circular and eccentric orbits in term of the Keplerian elements. The ratio between full and total duration gives information about the transit shape (Perryman 2011, Chapter 6). However, it would be better to calculate the transit duration (D) as the difference between the so-called $t_{\mathrm{con,3.5}}$ and $t_{\mathrm{con,1.5}}$, the halfway points of egress and ingress, respectively. Recalling the two previous cases of the Earth (with $P = 1$ yr) and Jupiter ($P = 11.86$ yr), the duration D of the transit would be of about 13 hours and 30 hours, respectively.

It is necessary to stress that the determination of the contact times is very delicate, because they depend on the coefficients of limb darkening (LD). The star has the edges (the limbs) fainter than the center. This cause a smaller ΔF near the edge and a deeper ΔF at the center. In a light curve this is translated in less distinct $t_{\mathrm{con,2}}$ and $t_{\mathrm{con,3}}$ and a rounded bottom at the center of the transit.

The existence of the LD effect implies that would not be appropriate to define $t_{\mathrm{con},1.5}$ and $t_{\mathrm{con},3.5}$ as the mean time of ingress ($(t_{\mathrm{con},1} - t_{\mathrm{con},2})/2$) and egress times ($(t_{\mathrm{con},3} - t_{\mathrm{con},4})/2$), respectively; it would be better to determine the times at which the projected distance of the center of the planet (r_{sky}) is equal to $R_\star$.

Furthermore, D depends on the *impact parameter* (b), that is the projected-distance between the center of the planet and of the star at the time of the conjunction. For circular orbits, and in units of stellar radius, b is approximated as:

$$b = \frac{a}{R_\star} \cos i \,. \tag{1.1.5}$$

If b is equal to zero the planet passes exactly through the center of the star, D is maximum, and the inclination is $i = 90°$. If b is greater than 0 and lower than 1, D will be shorter. When $b = 1$ the transit is grazing and $D = D_T$. A value of b higher than 1 means that the planet does not transit at all. The formulation of D and b for eccentric orbits can be found, i.e., in Ford et al. (2008), Winn (2011), and Perryman (2011).

The shape of the transit changes with D, and so with b, and the transit light curve tends towards a V–shape for b that tends to unity. Furthermore, the LC shape depends on the observation wavelength (λ). The LC during the transit appears more V–shaped and rounded at the bottom at shorter λ, while it appears more boxy at longer λ. Likewise, this effect is still due to the LD effect.

The first transiting extrasolar planet, HD 209458b, has been discovered by Henry et al. (1999, 2000) and Charbonneau et al. (2000) independently. This is a Jupiter-mass planet (inferred by previous RV) with a transit duration of about 2.5 hours and $\Delta F/F \sim 1.5\%$ that led the authors to estimate $R_{\mathrm{p}} = 1.27 \pm 0.002\ R_{\mathrm{Jup}}$. In Fig. 1.4 different LCs of planet HD 209458b are shown for different λ, in which the LD effect as function of λ is clearly visible.

The transit method allows to extract the R_{p}, a_{p}, i_{p} of a planet from a stellar LC of one transit, if $R_\star$ is already known (and well constrained). The common method is to fit a LC model, i.e., the Mandel & Agol (2002) model, with parameters $R_{\mathrm{p}}/R_\star$, $a/R_\star$, i, and T_0. As for RV, `LM` and `MCMC` are good methods to determine the best set of parameters, and an example is the program `JKTEBOP` by Southworth et al. (2004).

Observing two consecutive transits and measuring the TTs it is possible to determine precisely the period (P_{p}). If it would be possible to observe many transits for the same planet, it could obtain P_{p} with a better precision. This is

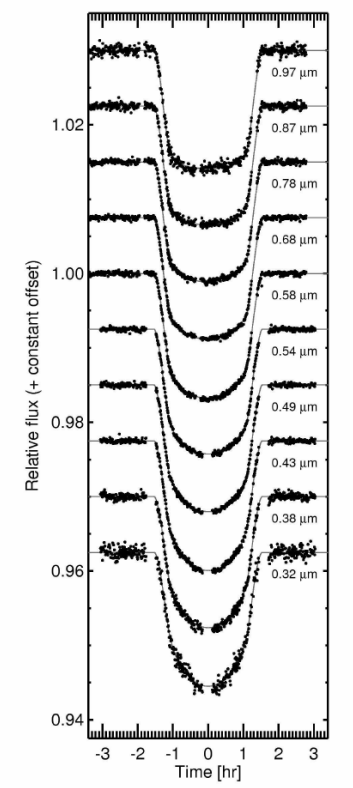

Figura 1.4: Transit LCs of HD 209458b at different λ: from 0.32 μm (bottom) to 0.97 μm (top). It is clearly visible the effect of the LD, more pronounced for shorter λ. The data were collected with the *Hubble Space Telescope* (HST) by Knutson et al. (2007).

achievable fitting a linear ephemeris of kind

$$T_{0,N} = T_{0,\mathrm{ref}} + P_{\mathrm{p}} \times N \tag{1.1.6}$$

where N is the transit number, or epoch, an integer number that identifies a transit in respect to a reference $T_{0,\mathrm{ref}}$, at which $N = 0$. This could be done only after that the TTs have been corrected for the light-time travel effect (LTE, see Irwin 1952; Perryman 2011).

Considering a 2-body system, a star and a planet, the exoplanet transit signal will be strictly periodic. So, a linear ephemeris allows to perfectly predict future transits. The difference between the observed T_0 ($T_{0,O}$) and the calculated T_0 ($T_{0,C}$) from the linear ephemeris is called $O-C$, and it is equal to zero for an unperturbed 2-body system. But, it could happen that the $O-C$ could be not zero, and it would show a so-called Transit Time Variation (TTV). The TTV amplitude (σ_{TTV}) can be evaluated as the root mean square (rms) of the $O-C$ (Agol et al. 2005).

The LC could be influenced by different phenomena that alter the TT, for

example the stellar activity and spots, or the precession of some angular parameters (Miralda-Escudé 2002) or more intriguing is the case of undetected body (or bodies) that perturbs the transiting planet (Holman & Murray 2005; Agol et al. 2005). The observed planet dynamically interacts with the perturbing planet and it undergoes a pull or a push that produces delayed or early transit times.

As shown by Agol et al. (2005), a TTV signal mainly depends on the perturber mass, period, and eccentricity and it is enhanced when planets are locked in a mean motion resonance (MMR) or just outside (or near) it. Two planets are in MMR when their gravitational interaction is periodic and regular (Perryman 2011), the ratio of their periods is given by the ratio of two small integer, and the orbits of both planets precess by 360° (Ford 2008). More precisely, in the majority of the exoplanetary systems discovered so far, we should say that two planets show a commensurability relation between their periods, rather than a MMR. This commensurability can be defined as:

$$n_2(p+q) - n_1 p \approx 0 \tag{1.1.7}$$

where n_1, n_2 are the mean motions ($n = 2\pi/P$) of inner (1) and outer (2) planet; p, q are positive integers that define the resonance $(p+q) : p$ and q is its order (Beaugé et al. 2012). An example of a strong MMR is the 2:1 resonance, for which every two orbits of the inner planet the outer does just one orbit. In this case the amplitude of the TTV is quite high even for relatively small planets, i.e., the multiple exoplanet system Kepler-9 in Sect.3.3. Another characteristic of the TTV is that the periods (or the semi-major axis) of the interacting planets could show anti-correlated variations (Beaugé et al. 2012), visible in the $O-C$ diagrams.

Another cause of the TTV would be the presence of an exomoon (Kipping 2009a). However, the TTV alone cannot disentangle the mass and the orbital separation of the exomoon. In Kipping (2009a) and Kipping (2009b), an analytical approach has been developed to infer the characteristic of the exomoon combining the TTV and the transit duration variation (TDV), breaking the degeneracy between mass and semi-major axis of the exomoon. Payne et al. (2010) proposed that TDV could be used to remove some degeneracies of the parameters of the whole system, in addition to the exomoon detection. Recently, Nesvorný et al. (2013) analyzed both TTV and TDV of planet KOI-142b inferring the presence of a non-transiting planet, KOI-142c, which mass is lighter than that of Jupiter

($M_c \sim 0.63 M_{Jup}$).

1.2 Inverse problem: determine parameters from observations

An exoplanetary system can be fully characterized if the mass and the radius of the star ($M_\star$, $R_\star$) have been measured with high precision. For every j-th planet, it has to be defined the mass (M_j), the radius (R_j), and the 6 Keplerian orbital elements: the period (P_j, or the semi-major axis a_j), the eccentricity (e_j), the argument of the pericenter (ω_j), the mean anomaly (M_j, the inclination of the orbit (i_j), and the longitude of the node (Ω_j).
The angle ω_j defines the position of the pericenter (the closest orbital position to the hosting star) of a planet from the line of the node. The angular position of the body from ω_j at a specific time is determined by the true anomaly f_j. The true anomaly does not change linearly in time with $e \neq 0$, and it is appropriated to use the mean anomaly M that is linear in time (Murray & Dermott 1999). Alternatively to M, the time of the pericenter passage (τ) can be used, and they are related by the equation:

$$\mathrm{M}_j = n_j (t - \tau_j) \tag{1.2.1}$$

where n_j is the mean motion of the j-th planet defined as $n_j = 2\pi/P_j$, and t is the time. The j-th planet is at the pericenter when $t = \tau_j$. The line of the node is defined by Ω_j and it defines the reference axis of the $\{x, y, z\}$ frame. It is impossible to determine Ω_j from the observation and it is usually common to set $\Omega = 0^\circ$ for a reference planet; for the other bodies Ω_j should be expressed as relative values. A schematic view of the Keplerian elements of a planetary orbit respect to a reference plane are shown in Fig. 1.5. As in Murray & Dermott (1999), Danby (1988), and Murray & Correia (2011), two other angles can be defined as the combination of the previous ones: the longitude of pericenter, $\varpi_j = \omega_j + \Omega_j$, and the mean longitude $\lambda = \omega_j + \Omega_j + \mathrm{M}_j = \varpi_j + \mathrm{M}_j$.

So, the parameters needed to characterize an exoplanetary systems are $N \times 8$ for N planets plus 2 parameters for the star. This is really a huge parameter space and many high-precision observations are needed to determine the whole set of parameters. Unfortunately, this is not always possible. For example, if a planet has been detected via RV, but it does not show any transit, it will be impossible to obtain the true mass of the planet and the radius. So, it will be very

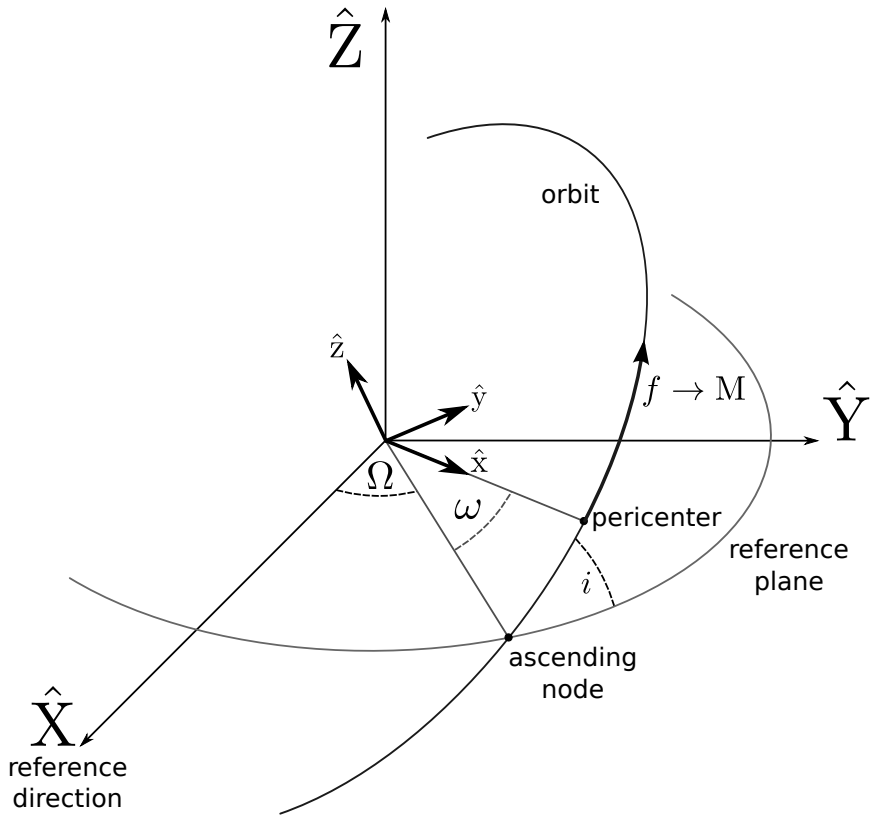

Figura 1.5: An explanatory scheme of a planet orbit in a three-dimensional space respect to a reference plane (base on Fig. 2.13 by Murray & Dermott 1999). The Keplerian element labels have the same meaning as in the main text.

difficult to fully characterize the exoplanetary system. Vice versa, if the transits of a planet have been observed, but there are no RV observations (i.e., because the star is to faint or the planet would be too small to be detected), it will not be possible to obtain the planetary mass. Determining all the parameters from the observations is a difficult inverse problem. Different observation techniques allow to determine different parameters and only combining their information would be possible to solve this problem. Sometimes, a further method, such as the TTV, is needed to infer the missing parameters.

From an analytical point view, it is possible to use the perturbation theory (Hori 1966; Deprit 1969) to computes the observables, e.g., RV and T_0, as described in Nesvorný & Morbidelli (2008) and in Nesvorný (2009). This approach

has some limitation, being developed analytically, it can only approximate the observations and cannot take into account some feature of the system, i.e., the MMR. However, this method is very fast and it allows to put some constraints on the parameter space. An example of the application of this method can be found in Nesvorný et al. (2013). They have predicted the existence of an undetected planet in the KOI-142 system, KOI-142c. Recently, this planet have been confirmed by Barros et al. (2013).

Another method is the direct numerical simulation of an N-body system (Steffen & Agol 2005; Agol & Steffen 2007). In this way it possible to take into account all the effect due to the dynamical interactions among the planets. As drawback, this method is very time consuming: it needs billions of simulations to converge to the best orbital configuration. Furthermore, the lack of constraints on the parameters could lead to some degeneracy, e.g., mass-period, mass-eccentricity, or period-eccentricity. A clear evidence of these effects can be found in Payne et al. (2010) and Veras et al. (2011), where the authors underlined the major correlations between TTV and orbital parameters of an exoplanetary system. However, with the development of new search and optimization algorithms would be possible to speed-up the computation in the determination of a best fitting set of parameters.

In my PhD work I have developed a program based on the direct approach trying to characterize exoplanetary systems solving the 'inverse problem' by fitting observed radial velocities (RVs) and transit times (T_0s). Recently, Deck et al. (2014) have published the symplectic integrator TTVFast that computes the observed transit times and radial velocities of an exoplanetary system.

1.3 Current and future missions

In this section I will give a short description of a selection of current and future facilities and missions aimed to detect and characterize extra-solar planets. I will divide the section depending on the technique used.

1.3.1 Radial Velocity facilities

HARPS After the experience gained with ELODIE and CORALIE, the High Accuracy Radial Velocity Planet Searcher, HARPS, has been built at the ESO 3.6-m telescope (La Silla) with the aim to reach a RV accuracy of about 1 ms^{-1} (Mayor et al. 2003). It is operative since 2003 (Rupprecht et al. 2004).

HARPS is an échelle spectrograph sensible from 378 nm to 691 nm with a resolution $R = 115\,000$. Two fibers, with a 1 arcsec aperture on the sky, collect light from the target and simultaneously from a thorium-argon reference spectrum or from the background sky. In order to reduce effects, such as spectral drifts, due to temperature and air pressure, the spectrograph is located into a vacuum vessel cooled to a few mK. The photon noise error for a star G2V of magnitude $V = 6$ is of about 0.9 ms^{-1}, with a signal-to-noise ration (SNR) of 110 per pixel (at 550 nm) for 60 seconds of integration. Pepe & Lovis (2008) achieved a short-term precision of 0.2 ms^{-1} and of about $0.3-0.6$ ms^{-1} on long-term radial velocity measurements.

HARPS-N At the Telescopio Nazionale Galileo (TNG, located at Roque de los Muchachos Observatory, Spain) has been mounted HARPS-north (HARPS-N), the equivalent of the HARPS spectrograph. It has been chosen to locate HARPS-N at the Northern hemisphere to allow cooperation and synergy with the NASA space satellite *Kepler*. It covers the same wavelength range of HARPS, but with $R = 120\,000$ and other updates and improvements. It should achieve a long-term RV precision lower than 1 ms^{-1} for $V = 12$ mag star, allowing the detection and the characterization of terrestrial exoplanets. The HARPS-N Project is a collaboration between the Astronomical Observatory of the Geneva University (lead), the CfA in Cambridge, the Universities of St. Andrews and Edinburgh, the Queens University of Belfast, and the TNG-INAF Observatory.

HIRES The Keck I 10-m telescope on Mauna Kea (Hawaii) hosts the instrument HIRES, High Resolution Echelle Spectrometer (Vogt et al. 1994a), another instrument with the capabilities to detect exoplanets with RV technique. HIRES has a resolving power of about $\sim 25\,000 - 85\,000$ in the spectral range from 0.3 to 1.0 microns and the calibration in wavelength are made through an iodine absorption cell.

ESPRESSO It is foreseen to mount at the VLT the ESPRESSO instrument (Echelle SPectrograph for Rocky Exoplanet and Stable Spectroscopic Observations), a super-stable spectrograph that will work on optical wavelength. Moreover it will be capable of collecting the light simultaneously from the 4 VLT-UTs, achieving high-precision measurements. The first light is scheduled for 2016.

1.3.2 Ground and space-based missions for transit detection

Ground based surveys

Many ground-based surveys use a network of two or more small telescopes in order to maximize the area of the sky monitoring a large number of stars.

HATNet An example is the Hungarian Automated Telescope net, HATNet[1], with six telescopes in the Northern hemisphere (four at the Whipple Observatory in Arizona and two at the Mauna Kea; Bakos et al. 2002, 2004) and further six telescopes in the south (three sites: Las Campanas, Chile; Siding Spring, Australia; HESS γ-ray site, Namibia). These small telescopes can achieve a photometric precision of about $3-10$ mmag at $I \sim 8-11$.

SuperWASP The UK's leading program in the detection of exoplanets is SuperWASP[2] (Super Wide-Angle Search for Planets; Pollacco et al. 2006; Collier Cameron et al. 2009). Two robotic observatories operate in both hemispheres. Each observatory is composed by eight wide-angle cameras that operate simultaneously looking for transits of exoplanets. SuperWASP-North is located on the island of La Palma amongst the Isaac Newton Group of telescopes (ING) and SuperWASP-South is located at the site of the South African Astronomical Observatory (SAAO). After pipeline processing, the typical long-term photometric rms for a non-variable star at $V = 9.5$ mag is of about 4 mmag and 10 mmag at $V = 12$ mag.

MEarth Another survey that uses small-robotic telescopes is the project MEarth[3]. The purpose is to detect transits of small planets around the smallest and coolest star in the Galaxy: M dwarf stars. M dwarf stars have smaller mass and radius than G or K stars and the transit depth of Earth-like planet is greater. So, it would be much easier to detect small-rocky planets around M dwarf stars.

XO and TrES Other two transit surveys are the XO-project and the TrES (Transatlantic Exoplanet Search). XO-project uses two 0.11 m telescopes located at Haleakala (Maui). TrES consist of three telescope with diameter of 10 cm located

[1] hatnet.org
[2] www.superwasp.org
[3] www.cfa.harvard.edu/MEarth

at Lowell Observatory, Palomar Observatory, and the Canary Islands. Both these two projected are conceived to detect exoplanets around bright stars.

NGTS Last but not the least, is the Next-Generation Transit Survey (NGTS[4]). It will be an array of fully-robotic small telescopes that will monitor K and M stars searching for Neptune-size and smaller exoplanet around bright stars ($V <$ 13). NGTS will be sited at ESO-Paranal, while a prototype operated at La Palma during 2009 and 2010.

Space missions

CoRoT On December 27, 2006, the CoRoT[5] satellite (Convection Rotation and planetary Transits) was launched and put on an polar-orbit at 900 Km of altitude. This was a space mission led by the French Space Agency (CNES) with the participation of the ESA (European Space Agency) and other international partners. The satellite was equipped with a 27-cm diameter afocal telescope with four 2k×2k CCDs, and it was dedicated to the study of the stellar seismology, measuring solar-like oscillations, and to discover exoplanets with size larger than the Earth. Over the mission lifetime (~ 7 years), CoRoT has monitored different fields, and due to the polar-orbit it has observed continuously up to 150 days in the same direction. The observations cadence was of either 512 s or 32 s, and the photometric light curves were extracted on board. It has discovered about 25 exoplanets, but on 24 June 2013, it was announced that CoRoT has been retired and would be decommissioned.

Kepler The NASA space satellite *Kepler*[6] was launched on 2009 March 6 beginning a mission of about 3.5 years. It mounts a 0.95 m aperture Schmidt telescope, 42 2k×1k CCDs for a wide field of view (FOV) of about 115 square degrees (Borucki et al. 2010; Koch et al. 2010; Jenkins et al. 2010; Caldwell et al. 2010). The theoretical shot noise for a $V = 12$ mag solar-like star is of about 14 ppm in 6.5 hours. With this configuration the *Kepler* satellite monitors more than 150 000 stars with magnitude between 8 and 15 in the constellation of the Cygnus (and Lyra). The main goal of the *Kepler* mission is to observe a great number solar-like stars determining the frequency of Earth-size exoplanets in the habitable zone

[4] www.ngtransits.org
[5] smsc.cnes.fr/COROT
[6] www.nasa.gov/mission_pages/kepler

(HZ). *Kepler* observed stars in the so-called long-cadence mode (about 30 min per image) and short-cadence mode (about 1 min per image).
The mission has discovered about 977 exoplanets, that have been already confirmed, and there are about 4 234 planet candidates. Many of this confirmed planets have been found to be in multiple-planet systems and some of these have been confirmed by the TTV analysis. Unfortunately, many stars observed by *Kepler* are too faint for ground-based follow-up in order to confirm the smaller planets by the RV method.
During the mission, two out of four reaction wheels have broken, loosing the ability to point firmly the FOV for the mission extension. Nowadays, the mission is in the so-called K2 phase, an extending phase of approximately 75 days characterized by the shift of the FOV along the ecliptic plane.

CHEOPS For the end of the 2017, it has been foreseen the launch of the CHEOPS (CHaracterizing ExOPlanet Satellite) satellite, a space ESA S-class mission. The diameter of the CHEOPS telescope is of about ~ 30 cm of diameter. The main goal is the characterization of the structure of exoplanets with Neptune to Earth radii ($1-6\ R_{\oplus}$). I will report a more detailed discussion about CHEOPS further in the text, in Section 4.1.

PLATO Recently, it has been selected a third medium-class mission in ESA's Cosmic Vision Programme aimed to the discovery and characterization of exoplanets: PLATO, PLAnetary Transits and Oscillations of stars[7]. This satellite will be launched in the 2020 and it will be injected into a Lissajous orbit around L2 Lagrangian point. The purpose of this mission is very similar to that of *Kepler*, but PLATO will mount 34 small telescopes (12 cm each) and cameras, and each camera will cover a FOV of about 1100 square degrees). Thirty-two 'normal' cameras will observe faint stars ($m_V > 8$) with a cadence of about 25 seconds, and other two cameras will work in 'fast' mode (time cadence of 2.5 s) for very bright stars ($m_V \sim 4-8$). The 'normal' telescopes-cameras will be mounted in group of eight, each group will cover the same FOV, but with an offset of about 9°.2 that allows to cover a total FOV of about 2250 square degrees. PLATO will obtain high-precision photometric light curves of more than 1 million of bright stars, that will be very suitable for a future follow-up from ground-based facilities. The total duration of PLATO mission should be of about 6 years, divided in two pha-

[7] sci.esa.int/plato

se. In the first phase PLATO will point a fixed part of the sky. The second phase will be a 'step-and-stare' phase, in which the satellite will observe different fields (up to 5 months for each field) covering almost the 50% of the sky. From the results obtained with *Kepler* it is clear that PLATO will discover a huge number of exoplanetary systems.

TESS NASA has planned for the 2017 to launch an all-sky transit survey satellite: the Transiting Exoplanet Survey Satellite (TESS[8]). The targets of TESS will be about 500 000 bright-nearby stars with the purpose to detect and characterize small planets. The mission should last for two years, during the first year TESS will map the Northern hemisphere and the Southern one in the second year. This is possible thanks to the High Earth Orbit (HEO) in a 2:1 MMR with the Moon. TESS will mount 4 CCD cameras, and each camera will have a FOV of $24^\circ \times 24^\circ$ and an effective pupil diameter of 10 cm. The cameras will observe bright stars in short-cadence mode ($\sim$ 1 min) and all other stars in long-cadence mode ($\sim$ 30 min).

JWST and GAIA Worth of mention are the missions James Webb Space Telescope (JWST[9]) and GAIA[10]. JWST is an infrared space telescope with a primary mirror of 6.5 m aperture, and it is a international collaboration among NASA, ESA, and CSA (Canadian Space Agency). One of the main goals of the JWST is the study of chemical and physical properties of extra-solar planets. GAIA will build a three-dimensional map of the Milky Way, providing unprecedented positions and radial velocities of about one billion of stars. During its five years lifetime, GAIA will observe about 70 times each sources and will could discover planets around other stars, brown dwarfs, and small bodies of our Solar System.

[8] tess.gsfc.nasa.gov
[9] jwst.nasa.gov
[10] sci.esa.int/gaia

Capitolo 2

TRADES: TRAnsits and Dynamics of Exoplanetary Systems

I have developed a computer program (in Fortran 90 and openMP) for determining the possible physical and dynamical configurations of extra-solar planetary systems from observational data: TRADES, which stands for TRAnsits and Dynamics of Exoplanetary Systems (Borsato et al. 2014, submitted to A&A). TRADES models the dynamics of multiple planet systems and reproduces the observed transit times (T_0, or mid-transit times) and radial velocities (RVs). These T_0s and RVs are computed during the integration of the planetary orbits. I have developed TRADES from zero in order to avoid black-box programs and because it would be easier to parallelize it with openMP and include additional algorithms.

The orbits of the planets in the system are calculated with the Runge-Kutta-Cash-Karp integrator (RKCK, Cash & Karp 1990; Press et al. 1996). This integrator has not the higher order available, but it allows to have a stable orbit with a variable step (it self adjusts the step-size to maintain the numerical precision during the computation of the orbits), it is quite fast for short timescale of integration and it is ease to be implemented in such a complex code. During the test phase of the program the conservation of the energy and of the angular momentum has been verified.

2.1 Celestial Mechanics: reference frame and dynamics

For the transit time determination, the propagation of the trajectories of all planets in the system is performed in a reference frame with the Z axis pointing to the observer while the X-Y plane is the sky plane. Given the Keplerian orbital elements of each planet (period P or semi-major axis a, inclination i, eccentricity e, argument of the pericenter ω, longitude of the ascending node Ω, and time of the passage at the pericenter τ or the mean anomaly M, at a given reference epoch) I first compute the initial radius $\vec{r}$ and velocity $\dot{\vec{r}}$ vectors in the orbital plane (e.g., see Murray & Dermott 2000):

$$\vec{r} = \begin{pmatrix} x \\ y \\ z \end{pmatrix} = \begin{pmatrix} a(\cos E - e) \\ a\sqrt{1-e^2}\sin E \\ 0 \end{pmatrix}, \tag{2.1.1}$$

$$\dot{\vec{r}} = \begin{pmatrix} \dot{x} \\ \dot{y} \\ \dot{z} \end{pmatrix} = \begin{pmatrix} \frac{n}{1-e\cos E}(-a\sin E) \\ \frac{n}{1-e\cos E}\left(a\sqrt{1-e^2}\cos E\right) \\ 0 \end{pmatrix} \tag{2.1.2}$$

where $n = 2\pi/P$ is the mean motion, E is the eccentric anomaly obtained from the solution of the Kepler's equation, $\mathrm{M} = E - e\sin E$, with the Newton-Raphson method (e.g., see Danby 1988; Murray & Dermott 2000; Murray & Correia 2011). Then, I rotate the state vector by applying three consecutive rotation matrices, $\mathrm{R}_l(\phi)$ (e.g., see Danby 1988; Murray & Dermott 2000; Murray & Correia 2011) where ϕ is the rotation angle and l is the rotation axis (where l is $\{1,2,3\}$ for $\{x', y', z'\}$). In order to rotate the initial state vector from the orbital plane to the observer reference frame, I have to use the transpose of the rotation matrix, $\mathrm{R}_l^{\mathrm{T}}(\phi)$ with angles: ω, i, and Ω. After this rotation the X-Y plane is the sky plane with the Z-axis pointing to the observer, and I determine the initial state vector of each *k-th* planet:

$$\begin{pmatrix} X \\ Y \\ Z \end{pmatrix} = \mathrm{R}_3^{\mathrm{T}}(\Omega)\,\mathrm{R}_1^{\mathrm{T}}(i)\,\mathrm{R}_3^{\mathrm{T}}(\omega) \begin{pmatrix} x \\ y \\ z \end{pmatrix}, \tag{2.1.3}$$

where the three rotation matrices are defined as

$$\begin{aligned} \mathrm{R}_3^{\mathrm{T}}(\omega) &= \begin{pmatrix} \cos\omega & -\sin\omega & 0 \\ \sin\omega & \cos\omega & 0 \\ 0 & 0 & 1 \end{pmatrix} \\ \mathrm{R}_1^{\mathrm{T}}(i) &= \begin{pmatrix} 1 & 0 & 0 \\ 0 & \cos i & -\sin i \\ 0 & \sin i & \cos i \end{pmatrix} \\ \mathrm{R}_3^{\mathrm{T}}(\Omega) &= \begin{pmatrix} \cos\Omega & -\sin\Omega & 0 \\ \sin\Omega & \cos\Omega & 0 \\ 0 & 0 & 1 \end{pmatrix} . \end{aligned} \tag{2.1.4}$$

The same rotations have to be applied to the initial velocity vector. The inclinations are measured from the sky-plane. Indeed, a planet with inclination of 0° has an orbit that lies on the sky-plane (X-Y plane), i.e., it is seen face-on. The orbit of a planet with $i = 90°$ is seen edge-on (it transits exactly through the center of the star) and it lies on the X-Z plane. From the initial state vector, TRADES integrates the astrocentric equation of motion (e.g. Murray & Dermott 2000; Fabrycky 2011) of planet k:

$$\ddot{\vec{r}}_k = -G\,(M_1 + M_k)\,\frac{\vec{r}_k}{r_k^3} + G \sum_{j=2;j\neq k}^{N} M_j \left(\frac{\vec{r}_j - \vec{r}_k}{|\vec{r}_j - \vec{r}_k|^3} - \frac{\vec{r}_j}{r_j^3} \right) \tag{2.1.5}$$

where M_1 is the mass of the star, N the number of bodies; the first term is the *direct* gravitational force and the second term is the *indirect* force due to mutual interaction of the planets. As I sad previously, the orbits are computed with the Runge-Kutta-Cash-Karp integrator (RKCK, Cash & Karp 1990; Press et al. 1996). It is not a symplectic integrator and it is not well suited for long–term time integrations. Instead, it uses small and variable steps, it is fast and it preserves the total energy and the total angular momentum during the time scales of our simulations.

2.2 Calculation of the simulated observables

2.2.1 Transit determination

I chose to use as first condition of an eclipse the change of sign of the X or Y coordinates between two consecutive steps of each planet trajectory. When this condition is met, following Fabrycky (2011, chap. 2.5), I have to seek roots of the sky-projected separation $\vec{r}_{s,k} \equiv (X_k, Y_k)$ with the Newton-Raphson method, solving:

$$g(X_k, \dot{X}_k, Y_k, \dot{Y}_k) = \vec{r}_{s,k} \cdot \dot{\vec{r}}_{s,k} = X_k \dot{X}_k + Y_k \dot{Y}_k = 0 \tag{2.2.1}$$

moving, iterating, by the quantity

$$\delta t = -g \left(\frac{\partial g}{\partial t} \right)^{-1} . \tag{2.2.2}$$

In this way I can determine with high precision the mid-transit time and the corresponding state vector ($\vec{r}_{\rm mid}$, $\dot{\vec{r}}_{\rm mid}$), with an accuracy equal to the selected δt. I decided to set this accuracy in `TRADES` at the machine precision, which can be fine-tuned in the source of the code and defines the type of the chosen variables.

Then, I determine if I have four contact times, or just two (in the case of a grazing eclipse), or no transit, comparing the module of the sky-projected separation at the transit time, $|\vec{r}_{s,\rm mid}|$, with the radius of the star, $R_\star$, and of the planets, R_k, as in Fabrycky (2011). If the transit (or the occultation) does exist, I move the state vector of about $\mp R_\star / |\dot{\vec{r}}_{s,\rm mid}|$ from the $t_{\rm mid}$ ($-$ for first and second contact, and + for third and fourth contact). Then, I have to solve

$$h(X_k, Y_k) = \dot{X}_k^2 + X_k \ddot{X}_k + \dot{Y}_k^2 + Y_k \ddot{Y}_k = 0 \tag{2.2.3}$$

and move of

$$\delta t = -h \left(\frac{\partial h}{\partial t} \right)^{-1} \tag{2.2.4}$$

until δt is less than the accuracy (the same adopted to find the transit time).

Differently from Fabrycky (2011), I used a bisection-Newton-Raphson hybrid method (it guarantees to be bound near the solution), and I assume that the orbital elements of the bodies are almost constant around the center of the transit, so I use $F(t_i, t_{i-1})$ and $G(t_i, t_{i-1})$ functions (called $f(t, t_0)$ and $g(t, t_0)$ in Danby 1988; Murray & Dermott 2000) to compute the planetary state vectors instead of

the integrator while seeking the transit times:

$$\begin{cases} \vec{r}_i(t) = F(t_i, t_{i-1})\vec{r}_{i-1} + G(t_i, t_{i-1})\dot{\vec{r}}_{i-1} \\ \dot{\vec{r}}_i(t) = \dot{F}(t_i, t_{i-1})\vec{r}_{i-1} + \dot{G}(t_i, t_{i-1})\dot{\vec{r}}_{i-1} \end{cases} \tag{2.2.5}$$

where

$$\begin{cases} \vec{r}_{i-1} = \vec{r}(t_{i-1}) \\ \dot{\vec{r}}_{i-1} = \dot{\vec{r}}(t_{i-1}) \end{cases} \tag{2.2.6}$$

with

$$\begin{cases} F(t_i, t_{i-1}) = \frac{a_i}{r_{i-1}} \left[\cos(E_i - E_{i-1}) - 1\right] + 1 \\ G(t_i, t_{i-1}) = (t_i - t_{i-1}) + \frac{1}{n_i} \left[\sin(E_i - E_{i-1}) - (E_i - E_{i-1})\right] \end{cases} \tag{2.2.7}$$

and

$$\begin{cases} \dot{F}(t_i, t_{i-1}) = -\frac{a_i^2}{r_i r_{i-1}} n_i \sin(E_i - E_{i-1}) \\ \dot{G}(t_i, t_{i-1}) = \frac{a_i}{r_i} \left[\cos(E_i - E_{i-1}) - 1\right] + 1 \end{cases} . \tag{2.2.8}$$

where $t_i = t_{i-1} + \delta t_{i-1}$ at the i-th iterations; E_i and E_{i-1} are the eccentric anomalies at the i-th and i-th−1 iterations. This allows the code to run faster than using the integrator, i.e., lower number of function calls, to seek the transit and contact times.

The light coming from the star is delayed due to the motion of the star around the barycenter of the system (Irwin 1952), and so TRADES corrects for the light-time travel effect (LTE = $-Z_\star^{\text{barycentric}}/c$, see Fabrycky 2011) for contact and center transit time.

2.2.2 RV calculation and other constraints

For each observed RV (when available), TRADES integrates the orbits of the planets to the instant of the RV point and calculates the RV as the opposite of the z-component of the barycentric velocity of the star ($\text{rv}_{\text{sim}} = -\dot{Z}_\star^{\text{barycentric}}$ in the right unit of measurement). The observed RV is defined as $\text{RV}_{\text{obs}} = \gamma + \text{rv}_{\text{obs}}$, where γ is the motion of the barycenter of the system and rv_{obs} is the reflex motion of the star induced by the planets. TRADES calculates γ_{sim} as the weighted mean of the difference $\Delta\text{rv}_j = \text{RV}_{j,\text{obs}} - \text{rv}_{j,\text{sim}}$ with j from one to the number of RVs. The final simulated RV is $\text{RV}_{j,\text{sim}} = \gamma_{\text{sim}} + \text{rv}_{j,\text{sim}}$. I am planning to im-

plement the $\gamma_{\rm sim}$ fitting rather than the described weighted mean method. Furthermore, I will add the possibility to simultaneously use set of RV data from different facilities. Because of this, TRADES will have to calculate a different γ value for each observed RV sample.

Furthermore, I added some constraints on the orbit during the integration, setting a minimum and a maximum semi-major-axis for the system, $a_{\rm min}$ and $a_{\rm max}$, respectively. The lower limit has been set to the star radius, while the maximum one to five times the larger semi-major axis of the system calculated from the periods of the planets (in the GA and in the PSO I have used the largest period boundary). I have used the definition of the Hill's sphere to obtain minimum distance allowed between two planets (Murray & Dermott 2000). In the case these constraints will not be respected, the integration will be stopped, and the χ^2 returned is set to the maximum value allowed by the compiler, so the combination of the parameters will be rejected.

It could happen that a combination of parameters would reproduce very well the data, but at the same time, they describe an unstable configuration that leads to a close-encounter or to the ejection of one the body. So, the stability analysis of the solutions found by TRADES is needed. I have decided to not include any other stability constraint or analysis in TRADES. The main reason is that TRADES has not been developed with this purpose in mind. The implementation of a stability tool inside TRADES would change drastically to whole structure of the program. So, I have prefered to determine the best orbital configuration that fits the data with TRADES and then to run the stability analysis *a posteriori*, i.e., integrating the planetary orbits on a longer temporal baseline with SyMBA (Levison & Duncan 2000) and subsequently applying the frequency map analysis (FMA, Laskar et al. 1992; Laskar 1993b,a; Marzari et al. 2002). The FMA gives a measurement of the stability of an orbit analyzing the evolution with time of the fundamental frequencies determined from the orbital elements of a test planet.

2.3 Algorithms of the different TRADES modes

To solve the inverse problem determining the best orbital configuration, TRADES can be run in four different modes: 1) 'grid' search, 2) Levenberg-Marquardt[1]

[1] lmdif converted to Fortran 90 by Alan Miller (http://jblevins.org/mirror/amiller/) from MINPACK.

(LM) algorithm, 3) genetic algorithm (GA, I used the implementation named PIKAIA[2], Charbonneau 1995), 4) and particle swarm optimization (PSO[3], Tada 2007). In each mode, TRADES compares observed transit times ($T_{0,\mathrm{obs}}$s) and radial velocities ($\mathrm{RV}_{\mathrm{obs}}$s) with the simulated ones ($T_{0,\mathrm{sim}}$s and $\mathrm{RV}_{\mathrm{sim}}$s).

The grid search is a good approach in case I want to map a limited subset of the parameters space or if I want to analyze the behavior of the system by varying some parameters, for example to test the effects of a growing mass for the perturbing planet. GA and PSO are good methods to be used in case of a wider space of parameters. The orbital solution determined with the GA or the PSO method can be refined with the LM mode.

2.3.1 Grid search

In the grid search method, TRADES samples the orbital elements of a perturbing body in a four-dimensional grid: the mass, M, the period, P (or the semi-major axis, a), the eccentricity, e, and the argument of the pericenter, ω. We have selected these four parameters for the grid search because they represent the minimal set of parameters required to model a coplanar system. In the future I intend to add the possibility of making the grid search over all the set of parameters for each body.

The grid parameters can be evenly sampled on a fixed grid by setting the number of steps or the step size, or with a number of points chosen randomly within the parameter bounds. For any given set of values the orbits are integrated, and the residuals between the observed and computed T_0s and RVs are computed. For each combination of parameters the LM algorithm can be called and the best case is the one with the lowest residuals (lowest χ^2).

Each single simulation of the grid can be executed on a different cpu. And for each grid combination it is possible to write the orbits, the constant of motion, the osculating Keplerian elements, and all the transits of the planets, into files indipendently, and without interfering with another cpu if TRADES has been executed in parallel.

[2] PIKAIA (http://www.hao.ucar.edu/modeling/pikaia/pikaia.php) converted to Fortran 90 by Alan Miller.

[3] based on the public Fortran 90 code at http://www.nda.ac.jp/cc/users/tada/

2.3.2 Levenberg-Marquardt

After an initial guess on the orbital parameters of the perturber, the `LM` algorithm exploits the Levenberg-Marquardt minimization method, to solve the nolinear least square problem (Moré et al. 1980), to find the solution with the lowest residuals, i.e., minimize the chi square χ^2:

$$\min\chi^2 = \min\left\{\sum_{i=1}^{n_{\rm data}} f_i(x)^2 : x \in \Re^{n_{\rm fit}}\right\} \tag{2.3.1}$$

where x are the $n_{\rm fit}$ parameters to fit, and $f_i(x)$ is the i-th weighted residual between observation and simulation for each data point (RV or T_0).

The minimization of the χ^2 requires the analytic derivative of the model respect to the parameters to be fitted, i.e., of the residual function $f(x)$, to compute the initial Jacobian matrix:

$$\left(\frac{\partial f_i(x)}{\partial x_j}\right),\ 1 \le i \le n_{\rm data}\ 1 \le j \le n_{\rm fit} \tag{2.3.2}$$

Since the T_0s are determined by an iterative method and the radial velocities are computed using the numerical integrator, I cannot express these as analytic functions of fitting parameters. So, I have adopted the method described in Moré et al. (1980) to compute the Jacobian matrix, which is determined by a forward-difference approximation.

The `epsfcn` parameter, that is the parameter that determines the first Jacobian matrix, is automatically selected in a logarithmic range from the machine precision, $\epsilon_{\rm p}$, up to $\sqrt{\epsilon_{\rm p}}$ in 10 steps; the best value is the one that returns the lower χ^2. Each simulation with a different `epsfcn` value is run on a difference cpu, if available.
This method has the advantage to be scale invariant, but it assumes that each parameter will be varied by the same `epsfcn` value (e.g., a variation of 10% of the period has a different effect than a variation of the same percentage of the argument of pericenter).

As pointed out by Moré et al. (1980), the `LM` has beend designed to find a local solution for a set of initial condition. For example, in case of an high number of fitting parameters the χ^2 space could be described by many peaks that could prevent `LM` to converge to the right solution (or minimum). Sometimes, using a slight diffent set of initial condition could allow to computed a more precise Jacobian matrix that allow a better estimation of the final parameters.

The precision used in the computation is another limitation of the LM (Moré et al. 1980). An higher precision leads to a better performance of the algorithm, because lower precision entails higher round-off error. In fact, an higher precision allows to compute a more accurate Jacobian matrix in the forward-difference approximation.

The initial conditions for the LM can be provided from a previous analysis, or from a grid of orbital configurations (see Section 2.3.1). And furthermore, it can be used to refine the solution that has been found by other more global-search algorithms, such as the genetic algorithm (see Section 2.3.3) and the particle swarm optimization (see Section 2.3.4).

At the end of the execution, LM returns the errors of the fitted parameters as the square root of the diagonal elements of the covariance matrix. It is known that this errors do not take into account physical boundaries, i.e., LM could return errors such that the mass of planet would be negative and so, sometimes, the errors of the LM algorithm should be used only as an upper limit. Furthermore, it is known that such parameter uncertainties could be underestimated and they have to be treated carefully.

2.3.3 Genetic Algorithm: PIKAIA

The GA mode searches for the best orbit by performing a genetic optimization method (e.g. Holland 1975; Goldberg 1989) where the fitness parameter is set to the inverse of the χ^2. This algorithm is part of a class of heuristic serach techniques inspired by the biological process of evolution, i.e., the combination of the natural selection, the heredity, and the variability.

The simulation starts with npop individuals. Each initial individual is a set of random orbital parameters that have to be fit and that are limited in $[0-1]$. They have to be proprerly rescaled to physical units in the orbital simulation. The individuals, and so the parameter sets, evolve during ngen generations. Each generation is a new population of 'offspring' orbital configurations, that are the results of the recombination (or crossover) and of the mutation of 'parents' pairs selected on their fitness parameter. It means that the parameters of each individual depends on the previous generation. This evolution of the parameters is defined by the adaptive plan or evolution strategy selected and are based on the fitness parameter. A more detailed explanation of the GA used, PIKAIA, can be found in Charbonneau (1995).

A drawback of the GA is the slowness of the algorithm, when compared to other optimizers. Furthermore, the evolution does not span all the parameter space, but it is strictly dependent on the best 'parents' pairs. However, the GA should converge to a global solution (if it exists) after the appropriate number of iterations.

2.3.4 Particle Swarm Optimization

PSO is another optimization algorithm that searches for the global solution of a problem. This approach is inspired by the social behavior of bird flock and fish school (e.g. Kennedy & Eberhart 1995; Eberhart 2007).

Imaging a set of parameters, i.e., a set of orbital Keplerian elements , as a 'particle' that has 'position' and 'velocity'. For each iteration this 'particle' will change its position and velocity: it will change the values of the parameters. Many particles build a 'swarm', and in this 'swarm' each particle evolves, or simply moves, following a simple rule determined by three main terms. The first term is the 'inertia' of the particle, and it depends mainly by the initial position and velocity, i.e., the initial set of parameters. The second term is the best 'position' of the particle (a local term) that it is updated for each iteration. The last term is a global term, it is the best set of parameters, or the best 'position', of the whole swarm. This is updated each iteration. The simulation is terminated after nit iterations. Each parameter is weighted by a random number during each iteration, allowing to span as much as possible the parameter space.

The selection of the local and global best is determined by a fitness parameter. In this work I decided to use the same fitness parameter of the GA, the inverse of the χ^2. The code by Tada (2007) that I implemented in TRADES needs the physical boundaries of each fitting parameters, but internally it uses $[0-1]$ limits for easier computation.

This is an interesting and promising optimization method because it does not require that the problem would be differentiable. This feature makes this algorithm quite suitable to solve the dynamical inverse problem (as already mentioned in Section 2.3.2 for the LM algorithm).

2.3.5 Bootstrap analysis

For each mode TRADES can perform a bootstrap analysis in order to calculate the interval of confidence of the best-fit parameter set. We generate a set of

T_0s and RVs from the fitted parameters and we add a Gaussian noise having the calculated value (of T_0s and RVs) as mean and the corresponding measurement error as variance. We fit each new set of observables with the `LM`. We iterate the whole process thousands of times in order to analyze the distribution for each fitted parameter determining the confidence intervals.

Capitolo 3

Applications

In order to validate TRADES I dealt with three different exoplanetary systems. In the first case, I simulated a synthetic 3-body system, aimed to test the basics of the code, the robustness of the integrator, the precision of the T_0 and RV calculations, the limits of the LM algorithm, and the grid search algorithm. Then, I used TRADES to simulate two real cases: a very complex system, Kepler-11, and a system that show a strong TTV signal, Kepler-9. I analyzed and compared my results with the discovery papers and then I extended the analysis to the first twelve quarters of *Kepler* data. The extended analysis is based on the T_0 by Mazeh et al. (2013), which purpose was to detect Kepler Object of Interest (KOI) with TTV signal by an automated approach. In this way they could analyze about 1960 KOIs, they determined the T_0s, and they found 130 KOIs that show a strong TTV signal. However, these T_0s have lesser precision and reliability compared with a careful and aimed analysis of the light curves, but a new analysis of the data will not be discussed in this work.

3.1 Validation with a simulated systems

In order to validate TRADES I simulated a synthetic system with two planets having known orbital parameters. I chose a star with mass and radius equals to the Sun, a first planet, named b, with Jupiter mass and radius ($M_{\rm Jup}$ and $R_{\rm Jup}$), and a second planet, c, with mass and radius of Saturn ($M_{\rm Sat}$ and $R_{\rm Sat}$). I assumed a co-planar system with inclination of 90° (perfectly edge-on). The input orbital elements of the system are summarized in Table 3.1.

I simulated the system with TRADES for 500 days. I computed all T_0s for each

Tabella 3.1: Parameters of the simulated system in section 3.1.

Parameter	Star	Planet b	Planet c
M	1. $M_\odot$	1. $M_{\rm Jup}$	1. $M_{\rm Sat}$
R	1. $R_\odot$	1. $R_{\rm Jup}$	1. $R_{\rm Sat}$
a		0.1 au	0.2 au
e		0.1	0.3
ω		90°	90°
M		0°	0°
i		90°	90°
Ω		0°	0°

body and I call these times the 'true' transit times ($T_{0,\rm true}$s) of the system. Then, I created sets of synthetic transit times ($T_{0,\rm synth}$s) as:

$$T_{0,\rm synth} = T_{0,\rm true} + N(0,1) \times \frac{P}{3} \times s\,, \tag{3.1.1}$$

where s is a scaling factor varying from 0.01 to 1.5 (on twenty logarithmic steps) needed to simulate good to very bad measurement cases; $N(0,1)$ is Gaussian noise with 0 as mean and 1 as variance. The $P/3$ factor is needed to scale the Gaussian noise in the right unit of time and at the same time avoiding confusion between transits and occultations. Furthermore, for each set of $T_{0,\rm synth}$s I selected a random numbers of transits (at least $N/3$, with N the total number of transits of each planet) to simulate observed transits.

I fixed the orbital parameters of planet b and I fitted P, e, ω, M, and Ω of planet c. I ran `TRADES` in `LM` mode for each scaling factor and I calculated the difference of the parameters (Δ) as the determined parameters minus the input parameters. I repeated the simulation 10 times (I calculated new Gaussian noise and the number of observed times every time). In Fig. 3.1 I plotted mean and median of the 10 simulations for each s scaling factor value. The parameters of the system derived by `TRADES` depart from the 'true' ones only for very large measurement errors.

To further test the robustness of the algorithm, I took the $T_{0,\rm true}$s (without added noise) and varied the initial semi-major axis of planet c from 0.19 au to 0.21 au with the `TRADES` `grid+LM` mode fitting the same parameters of the previous test. The algorithm nicely converged to the values from which the syn-

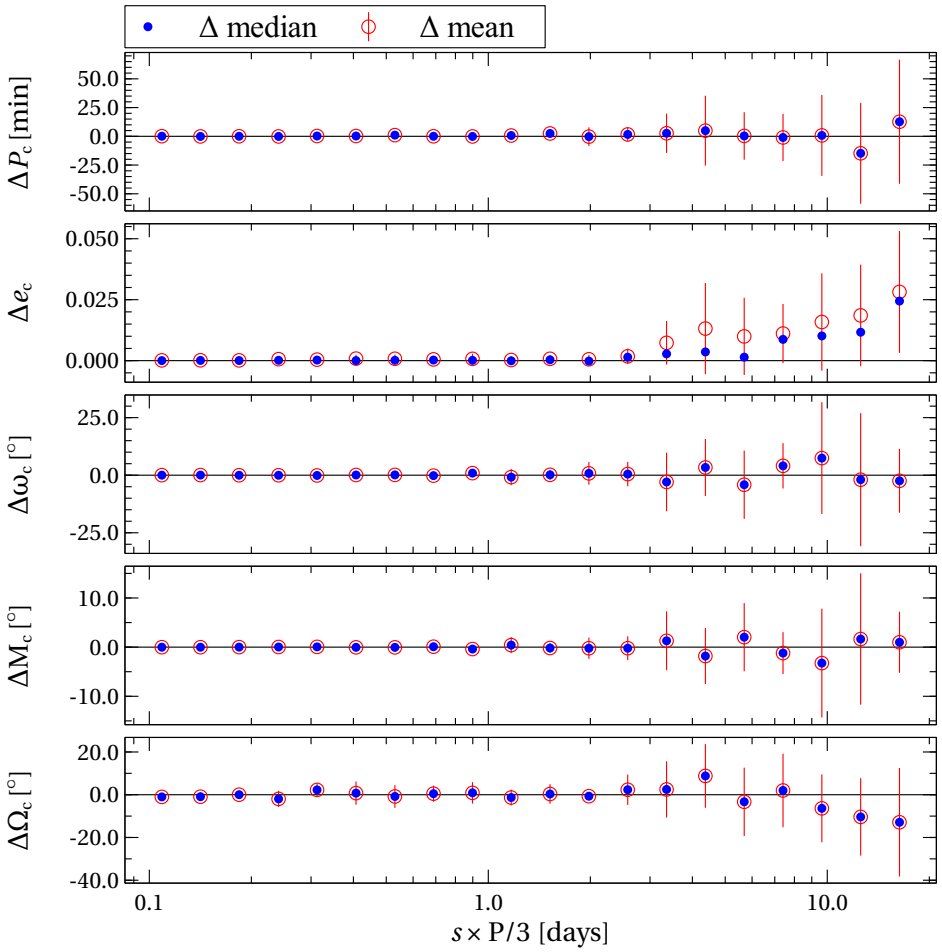

Figura 3.1: Mean (red-open circles with 1σ error bars) and median (blue-filled circles) variation (Δ) of fitted parameters of planet c for each value of the measurement errors on T_0, here parametrized as $s \times P/3$ (see text for details).

thetic data were generated, except for initial parameters too far from the right solution. This is due to the known limitation of the LM algorithm, that converges to close local minima from an initial set of parameters. Figure 3.2 shows the variation of the parameter differences (Δ) as function of the initial semi-major axis. This test shows how well TRADES recovers the parameters in case of a bad guess of the initial parameters.

I measured the computational time required by TRADES, and I found that it can integrate (initial step size of 0.0001 day) a 3-body synthetic system for 3000 days writing the orbits, the Keplerian elements and the constants of motion each 0.1 days in about 2.3 seconds. An integration of 1000 days has been performed in less than 1 second, and in less than half second for 500 days of integration

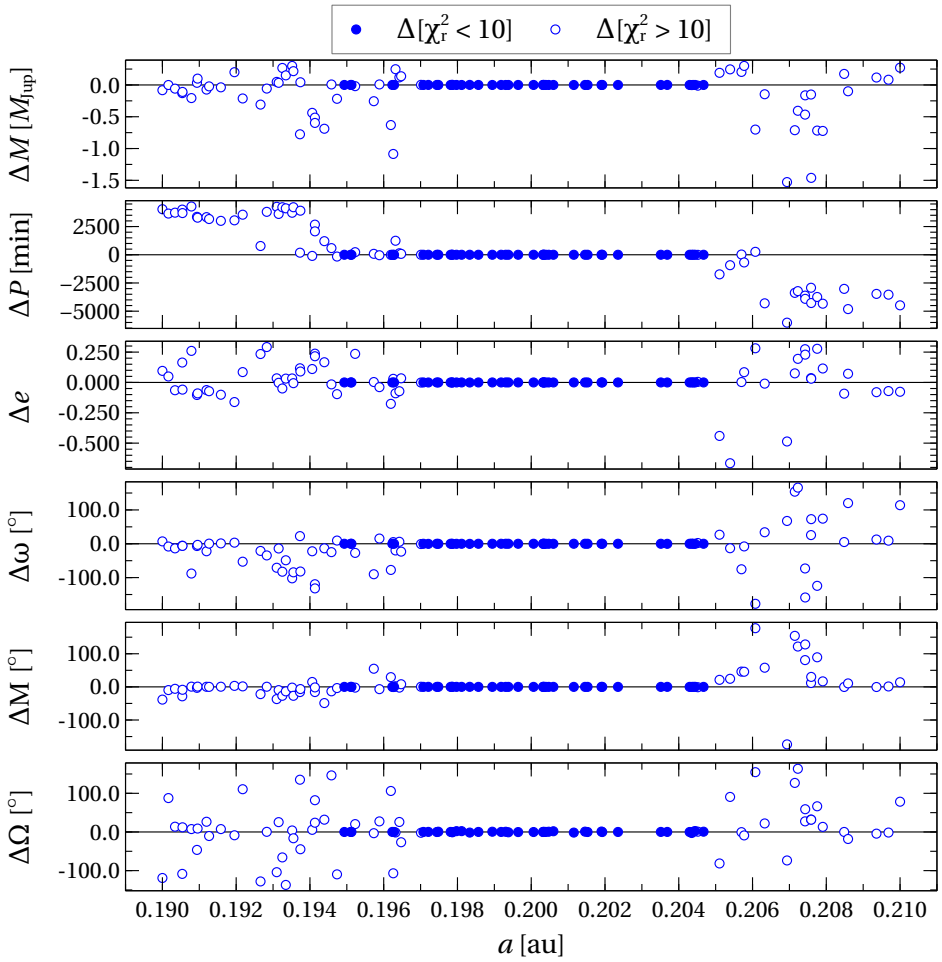

Figura 3.2: Variations of the fitted parameters for different initial values of the semi-major axis of the planet c; each point corresponds to a different simulation. In this case the input parameters (of planet c) are the parameters in Table 3.1 used to generate the exact transit times. The goodness of the fit has been color-coded so that good fits ($\chi^2_r < 10$) have been plotted as blue points and bad fits ($\chi^2_r > 10$) as open circles. The small gaps are due to the random sampling used to generate the grid in the semi-major axis a.

time, but most of the time have been spent writing files. I want to stress that TRADES write these files only at the end of the simulations, so the real computation is faster than these estimates. The time required by TRADES to complete the `grid` search was about 51 minutes with 10 processors of an Intel®Xeon®CPU E5-2680 based workstation. For each combination of the initial parameters in the grid search, TRADES runs 10 times the LM in order to select the best value for the parameter `epsfcn`, that is needed to construct the initial Jacobian.

I tested the PSO+LM algorithm fitting the same parameters of the grid search with limited boundaries except for the semi-major axis of planet c, for which I

used the same limit of the grid search (a_c = [0.19, 0.21] AU). I ran this test 4 times with 200 particles for 2000 iterations, and TRADES always returned the right parameter values in less than about 1 hour and 40 minutes with 10 processors.

3.2 Test case: Kepler-11 system

Kepler-11 (KOI-157, Lissauer et al. 2011a) system has six transiting planets packed in less than 0.5 au, making a complex and challenging case to be tested with TRADES.
From the spectroscopic analysis of HIRES high-resolution spectra, Lissauer et al. (2011a) derived the stellar parameters (effective temperature, surface gravity, metallicity, and projected stellar equatorial rotation) and determined the mass and the radius of Kepler-11 star to be $0.95 \pm 0.10\ M_\odot$ and $1.1 \pm 0.1\ R_\odot$.

I first performed an analysis of Kepler-11 system only on the data from the first three quarters of *Kepler* observations published by Lissauer et al. (2011a), and Supplementary Information (SI), for a comparison. I used as initial guess the first circular model from the Lissauer et al. (2011a, SI), which fixed the eccentricity and the longitude of the ascending node to zero for all the planets; hereafter I call this model Lis2011 (see first column in Table 3.2 for a summary of the orbital parameters). I used this model because the authors did not provide any information about the mean anomalies (or the time of the passage at the pericenter) for those planets. In this case the argument of the pericenter, ω, is undetermined so I fixed it to $\omega = 90°$ for each planet. I then calculated the initial mean anomaly, M_0 at the reference epoch $t_{\rm epoch} = 2\,455\,190.0$ ($\mathrm{BJD_{UTC}}$[1]), setting the transit time (T_0, Lissauer et al. 2011a, SI Table S4) as the time of passage at the pericenter:

$$\mathrm{M}_0 = n \cdot (t_{\rm epoch} - T_0)\ , \tag{3.2.1}$$

where n is the mean motion of the planet.

Lissauer et al. (2011a) gave an upper limit of $300\ M_\oplus$ on the mass of the planet Kepler-11g, while in the three dynamical models of the Supplementary Information they set it to zero, and I followed the same approach. Figure 3.3 shows the orbits and RVs of the Kepler-11 planets according to the Lis2011 model.

I fitted a linear ephemeris (Table 3.3) to the observed transit times of each planet for the first three quarters, and computed the Observed–Calculated ($O-C$) diagrams. Where O is $T_{0,\rm obs}$s and C the transit times calculated from the linear ephemeris.

I ran TRADES and fitted masses, periods, and mean anomalies of each planet.

[1] In the FITS header of *Kepler* data the time standard is reported as Barycentric Julian Day in Barycentric Dynamical Time ($\mathrm{BJD_{TDB}}$), but in the KSCI-19059 Subsect. 3.4 it is specified that the correct time is Barycentric Julian Day in Coordinated Universal Time ($\mathrm{BJD_{UTC}}$).

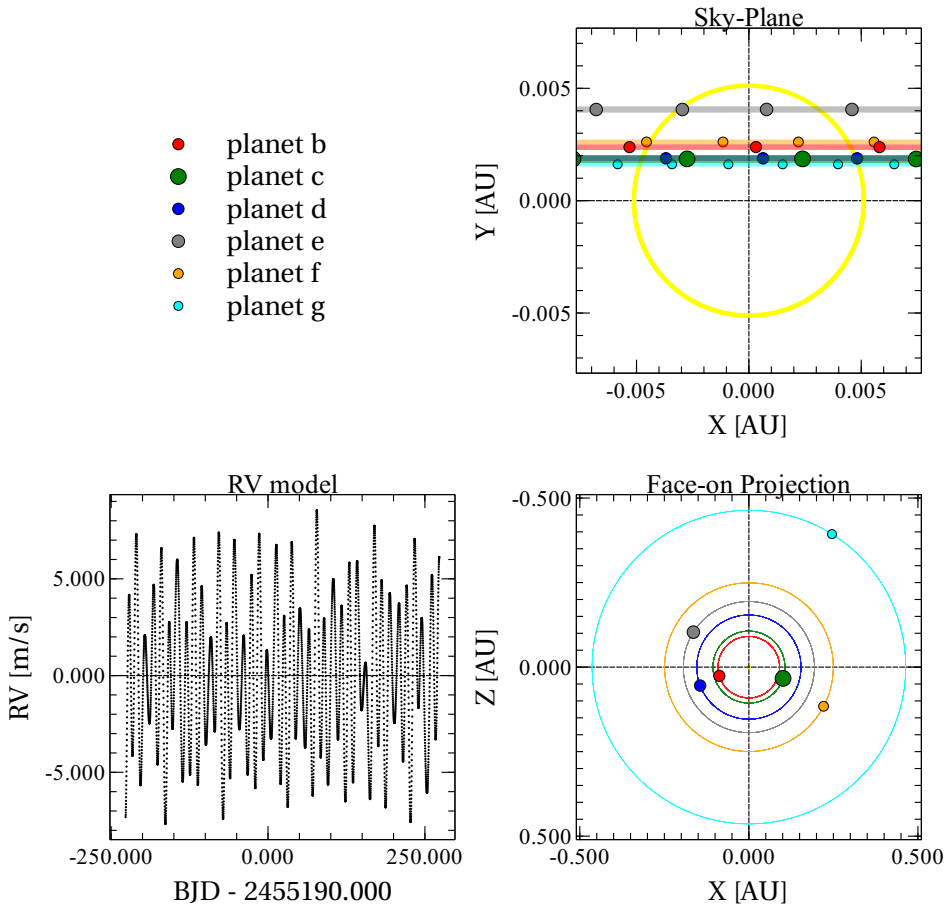

Figura 3.3: Orbits of the Kepler-11 system with initial parameters from Lis2011 model (circular model, see Table 3.2). The planet marker size is scaled with the mass of the planet. *Top-right*: 'Sky Plane', Kepler-11 system as seen from the *Kepler* satellite; I plotted only one orbit near a transit for each planet. Each circle is the position of a planet at a given integration step. *Bottom-right*: projection of the system as seen face on; the big markers are the initial points of the integration. *Bottom-left*: RV model from the simulation.

Hereafter the orbital solution I have determined with TRADES will be named with a short ID of the system (K11 for Kepler-11 and K9 for Kepler-9) and a Roman number (K11-I, K11-II, and so on). See solution K11-I in Table 3.2 for a summary of the parameters determined with TRADES (with 2σ confidence intervals from bootstrap analysis), which are in agreement with those published by Lissauer et al. (2011a). Fig. 3.4 show the $O-C$ diagrams for each body for solution K11-I. For each bootstrap analysis, I run 1000 iterations in order to obtain the confidence intervals at the 97.72 percentile (2σ) of the distribution of each parameter. I calculated the residuals as the difference between the observed and simulated

T_0s. The residuals after the TRADES-LM fit are smaller than those with simulated transit times obtained with original parameters and the final χ^2_r is around ≈ 1.25 for 88 degrees of freedom (dof, calculated as the difference between the number of data and the number of fitted parameters).

I used the same initial conditions of solution K11-I, but this time I fitted the eccentricity and the argument of pericenter of all the planets. In this case the LM did not move from the initial conditions even if it properly ended the simulation and returned reasonable errors. In the user guide of MINPACK (Moré et al. 1980) the user is warned to carefully analyze the case in which one has a null initial parameter. So, I set the initial eccentricities to a small but not zero value of 0.0001. This small change was able to let the LM algorithm to properly end the simulation and to return reasonable parameter values; see solution K11-II in Table 3.2 for a summary of the parameters. In Fig. 3.5 the O-C diagrams for the solution K11-II.

The resulting masses of the solutions K11-I and K11-II are all in agreement within 2σ with the discovery paper (Lissauer et al. 2011a) and with all the best-fit solutions determined by Migaszewski et al. (2012). In the latter work the authors presented different sets of orbital parameters determined with an approach similar to mine (direct N-body simulation with genetic algorithm, Levenberg-Marquardt, and bootstrap), but they directly fit the flux of *Kepler* light curves (so called dynamical-photometric model), without fitting the transit times.

3.2.1 Transit time analysis of the twelve quarters

Recently, Lissauer et al. (2013) analyzed the transit times covering fourteen quarters of *Kepler* data (in long and short cadence mode). Three independent extractions of T_0s from the light curves made by Lissauer et al. (2013, hereafter I call the dynamical model from this work Lis2013, see column five of Table 3.2) led the authors to change the value of some parameters of the system, e.g., they determined a mass of $2.9^{+2.9}_{-1.6}\ M_\oplus$ of the planet c that is lower than $15.82\pm2.21\ M_\oplus$ published in the discovery paper (Lissauer et al. 2011a). Unfortunately the authors have not published the T_0s. So, I used the data from Mazeh et al. (2013) that recently published the transit times for twelve quarters of the *Kepler* mission for 721 KOIs.

I used the linear ephemeris by Lissauer et al. (2013) to compute the $O-C$s for the T_0s from Mazeh et al. (2013). I found a remarkable mismatch with the $O-C$s plotted in the paper by Lissauer et al. (2013). I stress that these T_0s are

calculated with an automated algorithm. It would be advisable to analyze more carefully the light curves determining the T_0s with higher precision, but it is not the purpose of this work. I analyzed the system with all transit times from Mazeh et al. (2013) without any selection and they lead to unphysical results. I then decided to discard data with duration and depth of the transits that are 5σ away from the median values. This selection defines the sample of T_0s for the first twelve quarters of Kepler-11 exoplanets on which I based the next analysis.

I ran simulations with `TRADES` in `grid+LM` mode on twelve quarters, initial set of parameters as in K11-II; I fitted M, P, e, ω, M of each planet ($\Omega = 0°$ fixed for all the planets). In particular I varied in the grid the mass of planet g from 1 $M_\oplus$ to 100 $M_\oplus$ with a logarithmic step (ten simulations including the boundaries of 1 and 100 $M_\oplus$). I repeated this set of simulations for three different initial values of the eccentricity: in the first sample I set the initial eccentricity of all planets to 0.001; equal to 0.1 in the second sample; in the third sample I used a different value of the eccentricity for each planet, closer to the Lissauer et al. (2013) ones: $e_\mathrm{b} = 0.05$, $e_\mathrm{c} = 0.05$, $e_\mathrm{d} = 0.001$, $e_\mathrm{e} = 0.005$, $e_\mathrm{f} = 0.005$, and $e_\mathrm{g} = 0.1$. Figures 3.6, 3.7, and 3.8 show the calculated masses (upper panel) and eccentricities (lower panel) compared with the values from Lis2013 for each simulation having different initial eccentricity. With these simulations I intended to test whether, during the search for the lowest χ^2, a forest of local minima are met. According to Figs. 3.6 and 3.7, this indeed seems to be the case significantly complicating the identification of the real minimum. In fact the `LM` was not able to properly change the eccentricity of the planets that, in the majority of the cases, have been got stucked close to the initial value. Furthermore, when the initial eccentricity have been set to 0.1 the masses of planets d and f have decreased (Fig. 3.7) compared to those in the previous simulation (Fig. 3.6). Maybe, this could be an effect due to the particular sample of T_0 I used, so it would interesting to re-estimate the T_0 from the light curves and re-analyze the system. However, all the simulations have a final χ^2_r of about 2 or lower; the best simulation, solution K11-III (see Table 3.2), is the number 9 of the third set (blue-yellow marker of Fig. 3.8) with a $\chi^2_\mathrm{r} = 1.8$. The resulting $O-C$ diagrams of the best simulation are shown in Fig. 3.9. All the masses and the eccentricities of the solution K11-III are in good agreement with the values found by Lissauer et al. (2013). Some of my simulations converged to parameter values which are different from those proposed by Lissauer et al. (2013). Furthermore, some simulations show very narrow confidence intervals. This could be due both to the high complexity of

the problem and to a strong selection effect: the distribution of the parameters in the bootstrap analysis are strongly bounded to the parameter values found by the `LM` algorithm.

In Table 3.4 I report a brief summary of the main differences of the characteristics of the analysis that led us to each solution for the Kepler-11 system.

Tabella 3.2: Parameters of the Kepler-11 system. Epoch of reference: 2455190.0 (BJD_{UTC}).

Parameter	Lis2011[a]	K11-I[b]	K11-II[c]	Lis2013[d]	K11-III[e]
$M_b[M_\oplus]$	5.06 ± 0.95	$5.51^{+1.91}_{-2.04} \pm 1.15$	$5.03^{+2.29}_{-2.42} \pm 1.50$	$1.9^{+1.4}_{-1.0}$	$2.18^{+1.60}_{-0.87} \pm 0.52$
$R_b[R_\oplus]$	1.97 ± 0.19			$1.80^{+0.03}_{-0.05}$	
P_b[days]	10.3045 ± 0.0003	$10.30459^{+0.00064}_{-0.00060} \pm 0.00035$	$10.30446^{+0.00074}_{-0.00066} \pm 0.00070$	$10.3039^{+0.006}_{-0.0011}$	$10.30448^{+0.00033}_{-0.00032} \pm 0.00019$
e_b	0		$0.00018^{+0.00094}_{-0.00017} \pm 0.00494$	$0.045^{+0.068}_{-0.042}$	$0.026^{+0.026}_{-0.016} \pm 0.006$
$\omega_b[^\circ]$	90		$89.98^{+110.02}_{-112.11} \pm 220.29$	$45.00^{+101.31}_{-43.34}$	$71.46^{+2.68}_{-2.63} \pm 17.06$
$M_b[^\circ]$	73.467 ± 0.003	$73.46^{+0.17}_{-0.15} \pm 0.09$	$73.48^{111.01}_{-110.73} \pm 219.60$	–	$91.44^{+2.28}_{-2.41} \pm 16.19$
$i_b[^\circ]$	$88.5^{+1.0}_{-0.6}$			$89.64^{+0.36}_{-0.18}$	
$M_c[M_\oplus]$	15.82 ± 2.21	$16.11^{+3.66}_{-4.63} \pm 2.30$	$15.83^{+4.71}_{-4.94} \pm 3.99$	$2.9^{+2.9}_{-1.6}$	$2.09^{+2.11}_{-1.43} \pm 0.61$
$R_c[R_\oplus]$	3.15 ± 0.30			$2.87^{+0.05}_{-0.06}$	
P_c[days]	13.0247 ± 0.0003	$13.02406^{+0.00041}_{-0.00046} \pm 0.00026$	$13.02419^{+0.00045}_{-0.00054} \pm 0.00038$	$13.0241^{+0.0013}_{-0.0008}$	$13.02426^{+0.00053}_{-0.00058} \pm 0.00028$
e_c	0		$0.00005^{+0.0006}_{-0.00005} \pm 0.00375$	$0.026^{+0.063}_{-0.013}$	$0.015^{+0.011}_{-0.010} \pm 0.005$
$\omega_c[^\circ]$	90		$90.00^{+29.61}_{-34.03} \pm 100.29$	$51.34^{+128.63}_{-231.00}$	$96.43^{+0.36}_{-0.24} \pm 29.56$
$M_c[^\circ]$	288.267 ± 0.005	$288.27^{+0.06}_{-0.06} \pm 0.04$	$288.26^{+32.04}_{-31.18} \pm 99.66$	–	$281.99^{+0.26}_{-0.37} \pm 28.71$
$i_c[^\circ]$	$89.0^{+1.0}_{-0.6}$			$89.59^{+0.41}_{-0.16}$	
$M_d[M_\oplus]$	5.69 ± 1.27	$5.97^{+2.32}_{-2.57} \pm 1.36$	$5.67^{+2.70}_{-2.66} \pm 1.55$	$7.3^{+0.8}_{-1.5}$	$7.24^{+1.37}_{-1.36} \pm 0.89$
$R_d[R_\oplus]$	3.43 ± 0.32			$3.12^{+0.06}_{-0.07}$	
P_d[days]	22.6849 ± 0.0007	$22.68509^{+0.00169}_{-0.00167} \pm 0.00096$	$22.68494^{+0.00173}_{-0.00202} \pm 0.00135$	$22.6845^{+0.0010}_{-0.0009}$	$22.68440^{+0.00095}_{-0.00095} \pm 0.00055$
e_d	0		$0.0001^{+0.0001}_{-0.0001} \pm 0.0074$	$0.004^{+0.007}_{-0.002}$	$0.003^{+0.007}_{-0.003} \pm 0.001$
$\omega_d[^\circ]$	90		$90.00^{+7.72}_{-7.70} \pm 77.47$	$146.31^{+33.69}_{-146.31}$	$102.52^{+0.22}_{-0.51} \pm 24.37$
$M_d[^\circ]$	69.245 ± 0.002	$69.25^{+0.03}_{-0.04} \pm 0.02$	$69.25^{+7.48}_{-8.43} \pm 76.58$	–	$56.77^{+0.23}_{-0.50} \pm 24.25$
$i_d[^\circ]$	$89.3^{+0.6}_{-0.4}$			$89.67^{+0.13}_{-0.16}$	
$M_e[M_\oplus]$	8.22 ± 1.58	$8.44^{+3.38}_{-3.49} \pm 1.74$	$8.26^{+3.25}_{-3.43} \pm 2.03$	$8.0^{+1.5}_{-2.1}$	$7.37^{+1.78}_{-1.73} \pm 0.89$
$R_e[R_\oplus]$	4.52 ± 0.43			$4.19^{+0.07}_{-0.09}$	
P_e[days]	32.0001 ± 0.0008	$32.00102^{+0.00300}_{-0.00366} \pm 0.00189$	$32.00044^{+0.00342}_{-0.00377} \pm 0.00305$	$31.9996^{+0.0008}_{-0.0013}$	$32.00413^{+0.00173}_{-0.00207} \pm 0.00122$
e_e	0		$0.0002^{+0.0004}_{-0.0002} \pm 0.0089$	$0.012^{+0.006}_{-0.006}$	$0.013^{+0.003}_{-0.005} \pm 0.003$
$\omega_e[^\circ]$	90		$90.00^{+5.82}_{-5.20} \pm 1.11$	$-131.63^{+29.54}_{-25.75}$	$204.69^{+0.26}_{-0.36} \pm 3.22$
$M_e[^\circ]$	122.211 ± 0.003	$122.21^{+0.02}_{-0.02} \pm 0.01$	$122.21^{+5.01}_{-6.06} \pm 0.04$	–	$8.86^{+0.23}_{-0.40} \pm 3.19$
$i_e[^\circ]$	$88.8^{+0.2}_{-0.2}$			$88.89^{+0.02}_{-0.02}$	
$M_f[M_\oplus]$	1.90 ± 0.95	$2.15^{+1.85}_{-1.76} \pm 0.98$	$2.19^{+1.98}_{-1.94} \pm 1.23$	$2.0^{+0.8}_{-0.9}$	$1.98^{+1.16}_{-1.00} \pm 0.46$
$R_f[R_\oplus]$	2.61 ± 0.25			$2.49^{+0.04}_{-0.07}$	
P_f[days]	46.6908 ± 0.0010	$46.70131^{+0.00455}_{-0.00851} \pm 0.00304$	$46.70114^{+0.00641}_{-0.00627} \pm 0.00688$	$46.6887^{+0.0029}_{-0.0038}$	$46.68707^{+0.00384}_{-0.00575} \pm 0.00143$
e_f	0		$0.000003^{+0.000001}_{-0.000002} \pm 0.000242$	$0.013^{+0.011}_{-0.009}$	$0.005^{+0.010}_{-0.004} \pm 0.002$
$\omega_f[^\circ]$	90		$90.00^{+4.12}_{-4.09} \pm 0.03$	$-24.44^{+38.48}_{-47.12}$	$8.58^{+0.32}_{-0.65} \pm 3.41$
$M_f[^\circ]$	297.667 ± 0.006	$297.68^{+0.02}_{-0.06} \pm 0.02$	$297.67^{+4.05}_{-4.14} \pm 0.06$	–	$18.53^{+0.27}_{-0.66} \pm 3.38$
$i_f[^\circ]$	$89.4^{+0.3}_{-0.2}$			$89.47^{+0.04}_{-0.04}$	
$M_g[M_\oplus]$	< 300	$0.00^{+62.19}_{-0.00} \pm 0.21$	$0.70^{+0.66}_{-0.54} \pm 41.50$	< 25	$25.13^{+48.33}_{-16.83} \pm 10.07$
$R_g[R_\oplus]$	3.66 ± 0.35			$3.33^{+0.06}_{-0.08}$	
P_g[days]	118.3808 ± 0.0025	$118.39734^{+0.00907}_{-0.00959} \pm 0.00517$	$118.39766^{+0.01080}_{-0.01053} \pm 0.01505$	$118.3809^{+0.0012}_{-0.0010}$	$118.38030^{+0.00361}_{-0.00309} \pm 0.00248$
e_g	0		$0.0029^{+0.0015}_{-0.0014} \pm 0.2974$	< 0.15	$0.052^{+0.051}_{-0.030} \pm 0.012$
$\omega_g[^\circ]$	90		$90.01^{+0.63}_{-0.72} \pm 0.05$	$34.51^{+145.41}_{-214.50}$	$97.00^{+0.29}_{-0.17} \pm 30.41$
$M_g[^\circ]$	211.997 ± 0.005	$212.01^{+0.02}_{-0.02} \pm 0.01$	$212.00^{+0.71}_{-0.64} \pm 0.05$	–	$205.71^{+0.29}_{-0.18} \pm 27.38$
$i_g[^\circ]$	$89.8^{+0.2}_{-0.2}$			$89.87^{+0.05}_{-0.06}$	
χ^2/dof	110.34/89	110.15/88	110.74/76		341.75/190
χ^2_r	1.24	1.25	1.46		1.80

Masses (M), periods (P), eccentricities (e), argument of pericenters (ω), and mean anomaly (M), of the best fit simulation with 2σ confidence intervals from bootstrap analysis and $\pm 1\sigma$ from LM. Inclinations (i) fixed to the Lis2011 model.

[a] Dynamical model as reported in Lissauer et al. (2011a, SI) with circular orbit for each planet, e fixed to 0 and ω fixed to 90° ($e\cos\omega$ and $e\sin\omega$ set to zero in the discovery paper).

[b] Orbital solution from the analysis of T_0s from Lissauer et al. (2011a) for the first 3 quarters of *Kepler* data. Parameters fitted: M, P, and M. e fixed to 0 and ω fixed to 90°

[c] Orbital solution from the analysis of T_0s from Lissauer et al. (2011a) for the first 3 quarters of *Kepler* data. Parameters fitted: M, P, e, ω, and M.

[d] Dynamical model from (Lissauer et al. 2013). Parameters determined from the analysis of 14 quarters of *Kepler* data. The values of the mean anomaly were not reported in the paper (neither the time of passage at the pericenter).

[e] Best orbital solution (simulation number 9) of Fig. 3.8 from the analysis of T_0s from Mazeh et al. (2013) for the first 12 quarters of *Kepler* data. Parameters fitted: M, P, e, ω, and M.

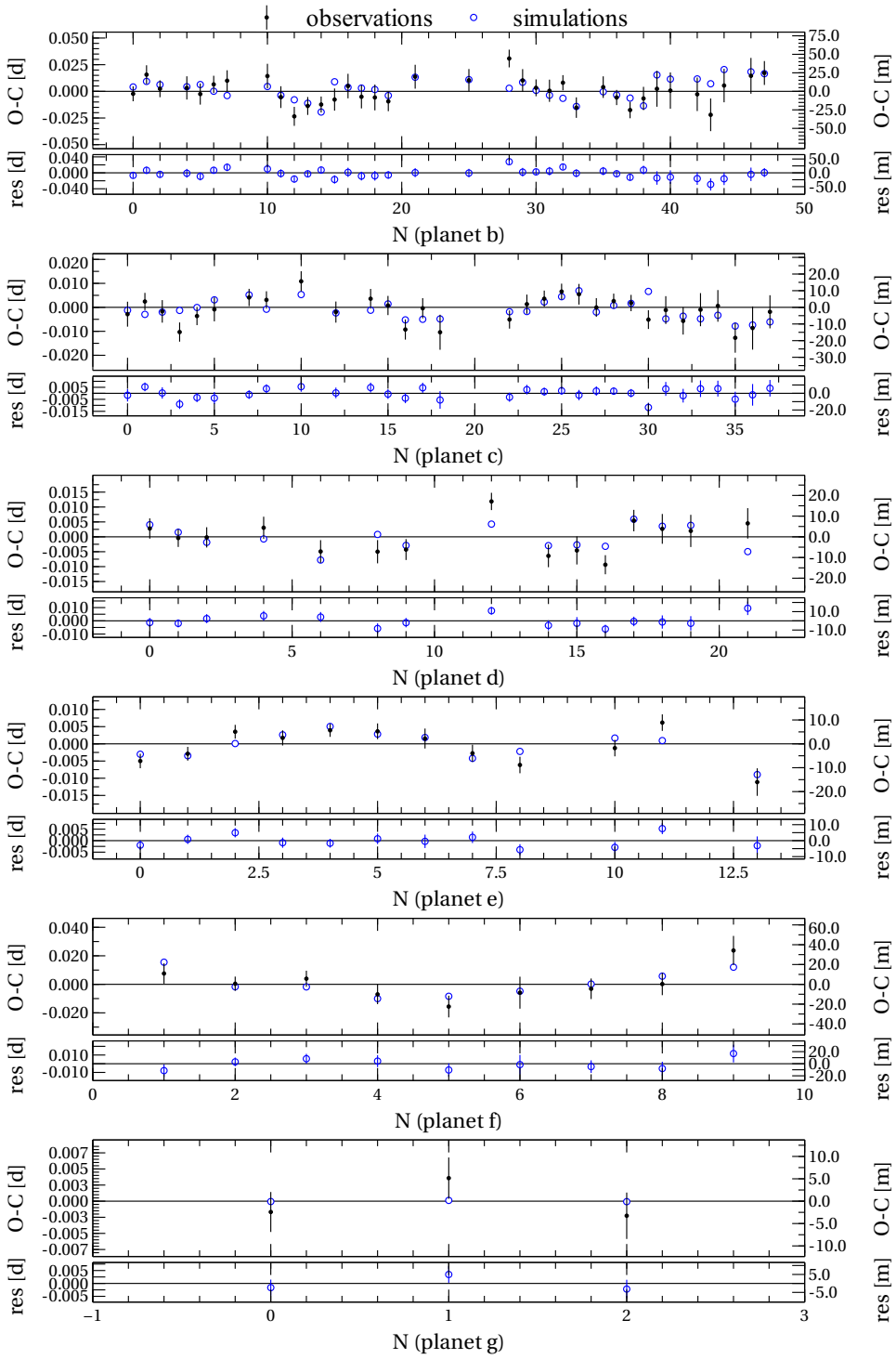

Figura 3.4: $O-C$ diagrams of Kepler-11 system. Planets b, c, d, e, f, and g from to to bottom. The black filled circles are the observed points fitted by a linear ephemeris, the blue open circles are the simulated points fitted by the same linear ephemeris of the observations. The simulated points are calculated from the TRADES program with the initial parameters from the best model in Lissauer et al. (2011a). Residual plots, as the difference between observed and simulated central time ($T_{0,\mathrm{obs}} - T_{0,\mathrm{sim}}$), in the lower panel of each $O-C$ plot. The unit of measurement of the left $O-C$ y-axis is days (d) and minutes (m) for the right one. The N in the abscissa identifies the transit number respect to the reference transit time of the ephemeris of each body (second column of Table 3.3).

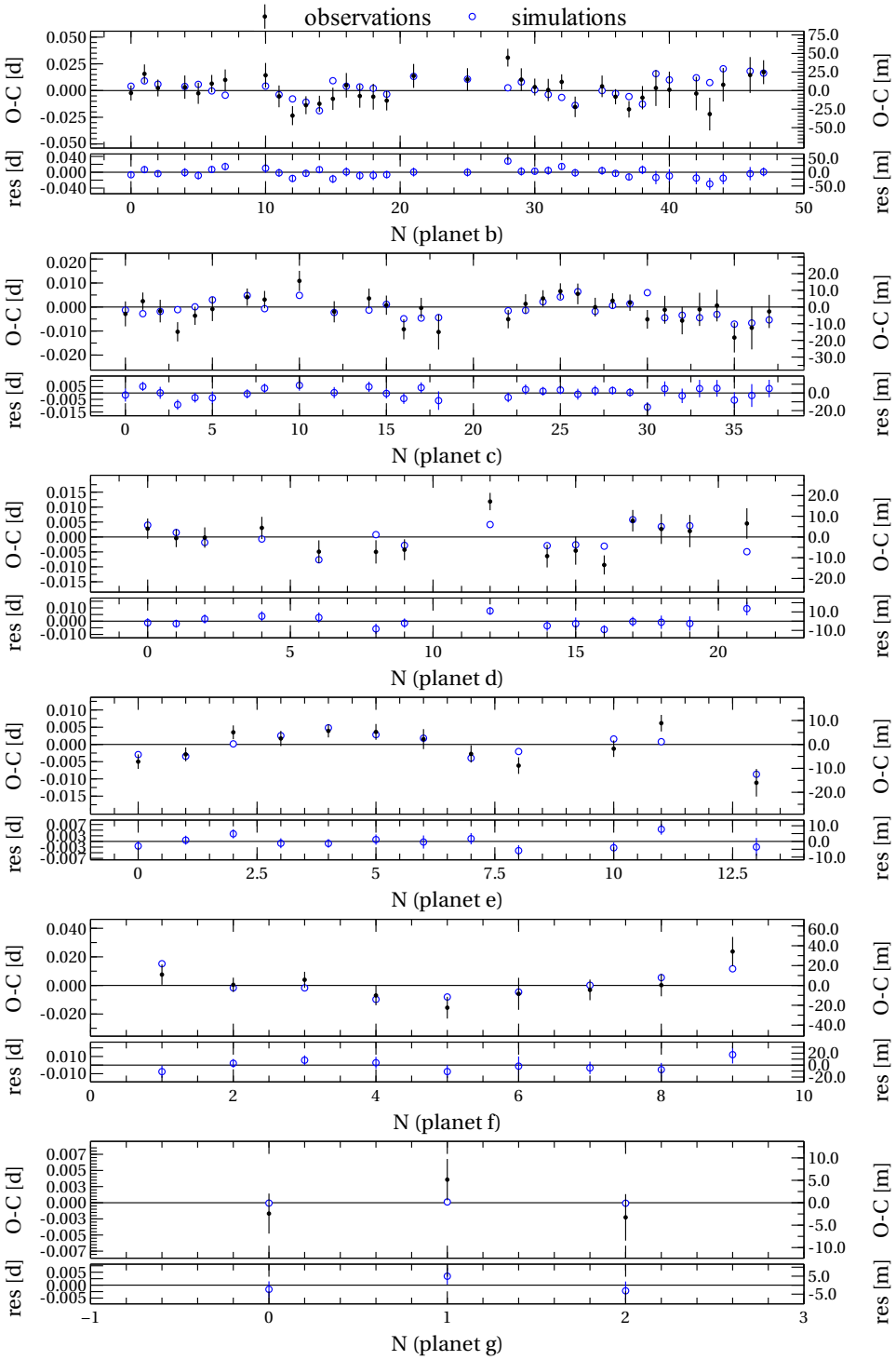

Figura 3.5: Same plots as in Fig. 3.4, but with the parameters determined with the TRADES-LM (solution K11-II in Table 3.2).

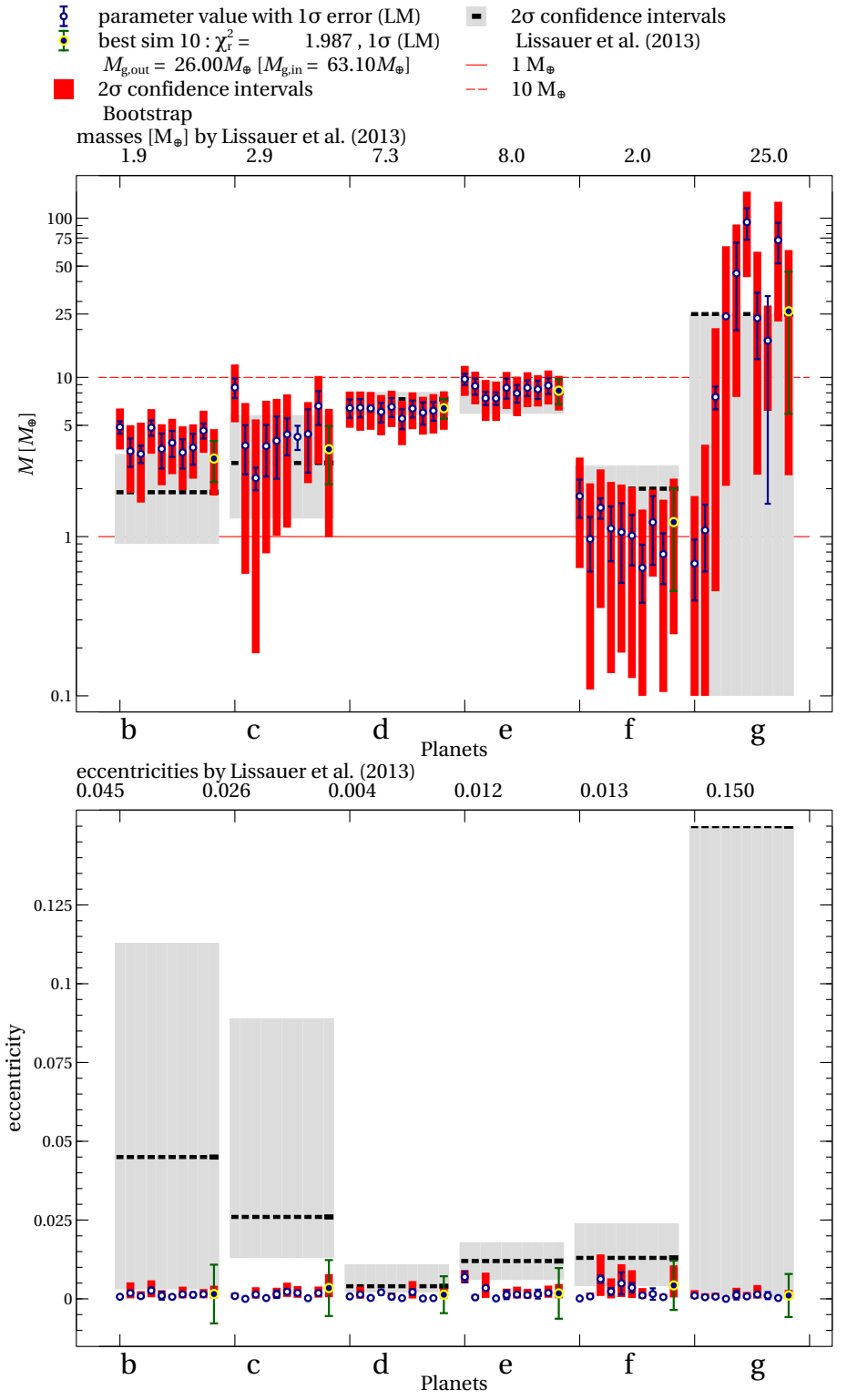

Figura 3.6: Masses (*upper-panel*) and eccentricities (*lower-panel*) for the Kepler-11 planets, calculated with `TRADES` in `grid+LM` mode (white-blue circle with blue error bars, see the legend on top of the upper plot) and 2σ confidence intervals from bootstrap analysis (red filled bars), with initial eccentricity of 0.001 for each planet. The blue-yellow circle (dark-green error bars) is the best simulation (number 10, χ^2_r, calculated mass, $M_{g,out}$, and input mass, $M_{g,out}$, are reported in the legend at the top of the plots). The different simulations (different initial mass of planet g, $m_{g,in}$) have been plotted from left (first simulation) to right (eleventh simulation) for each planet. Masses and eccentricities by Lissauer et al. (2013) plotted as black lines (values on top of the plots) with the 2σ confidence intervals (light-gray filled bars). Red lines at 1 $M_\oplus$ (solid) and at 10 $M_\oplus$ (dashed).

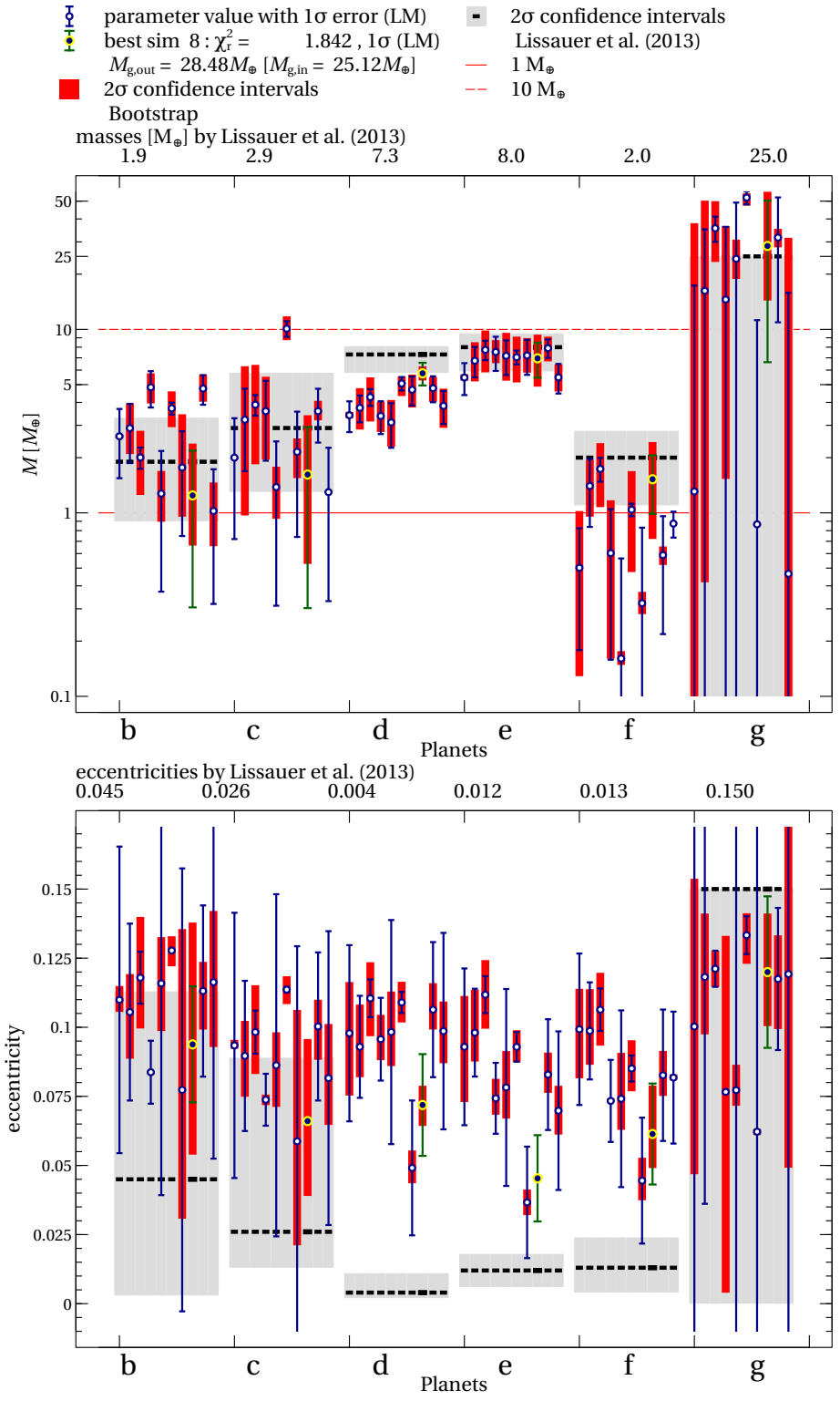

Figura 3.7: Same plot as in Fig. 3.6, but for simulations with initial eccentricities of 0.1.

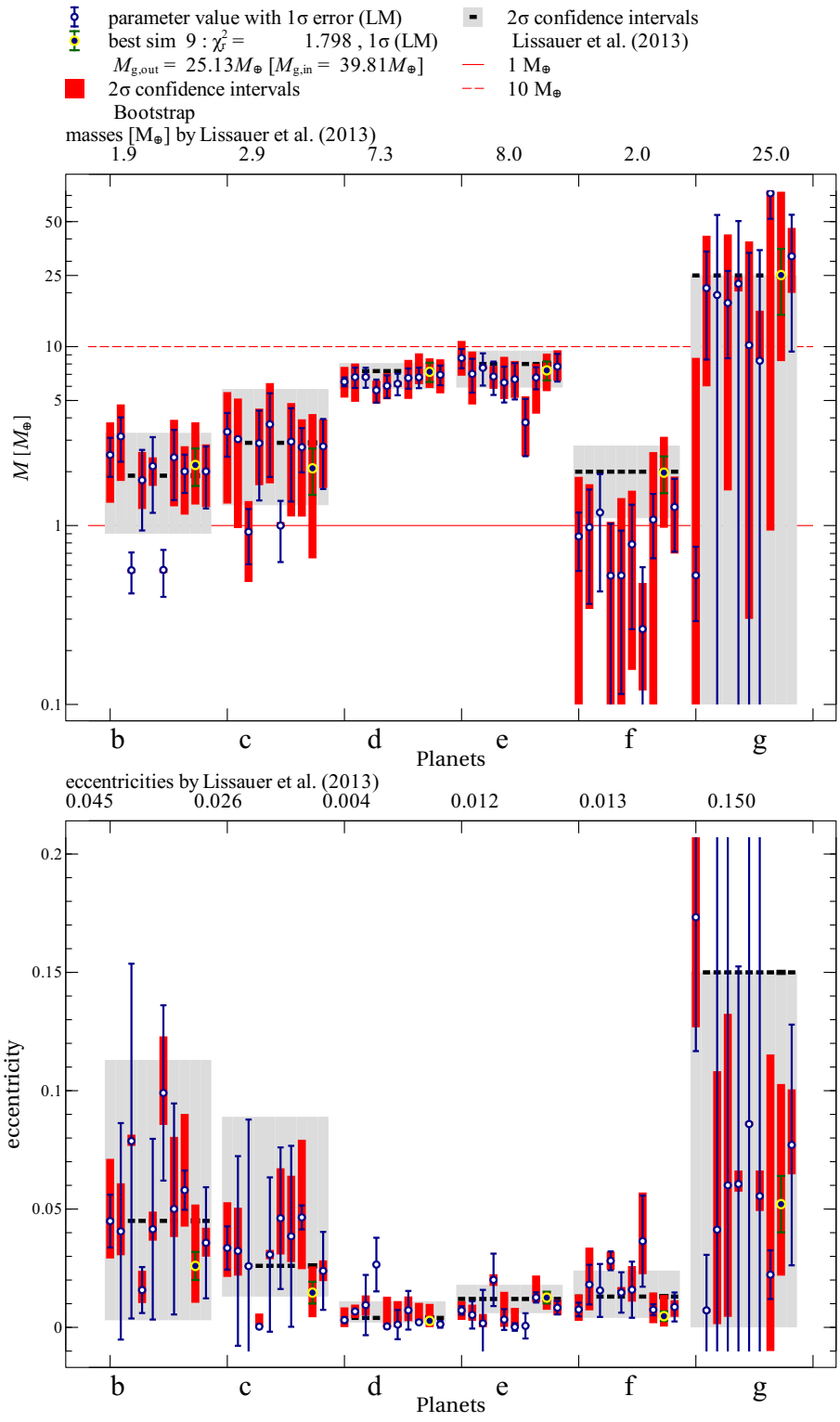

Figura 3.8: Same plot as in Fig. 3.6, but for simulations with different initial eccentricities: e_b = 0.05, e_c = 0.05, e_d = 0.001, e_e = 0.005, e_f = 0.005, e_g = 0.1. The best solution of this plot is the so-called K11-III solution; see Table 3.2 for the summary of the final parameters.

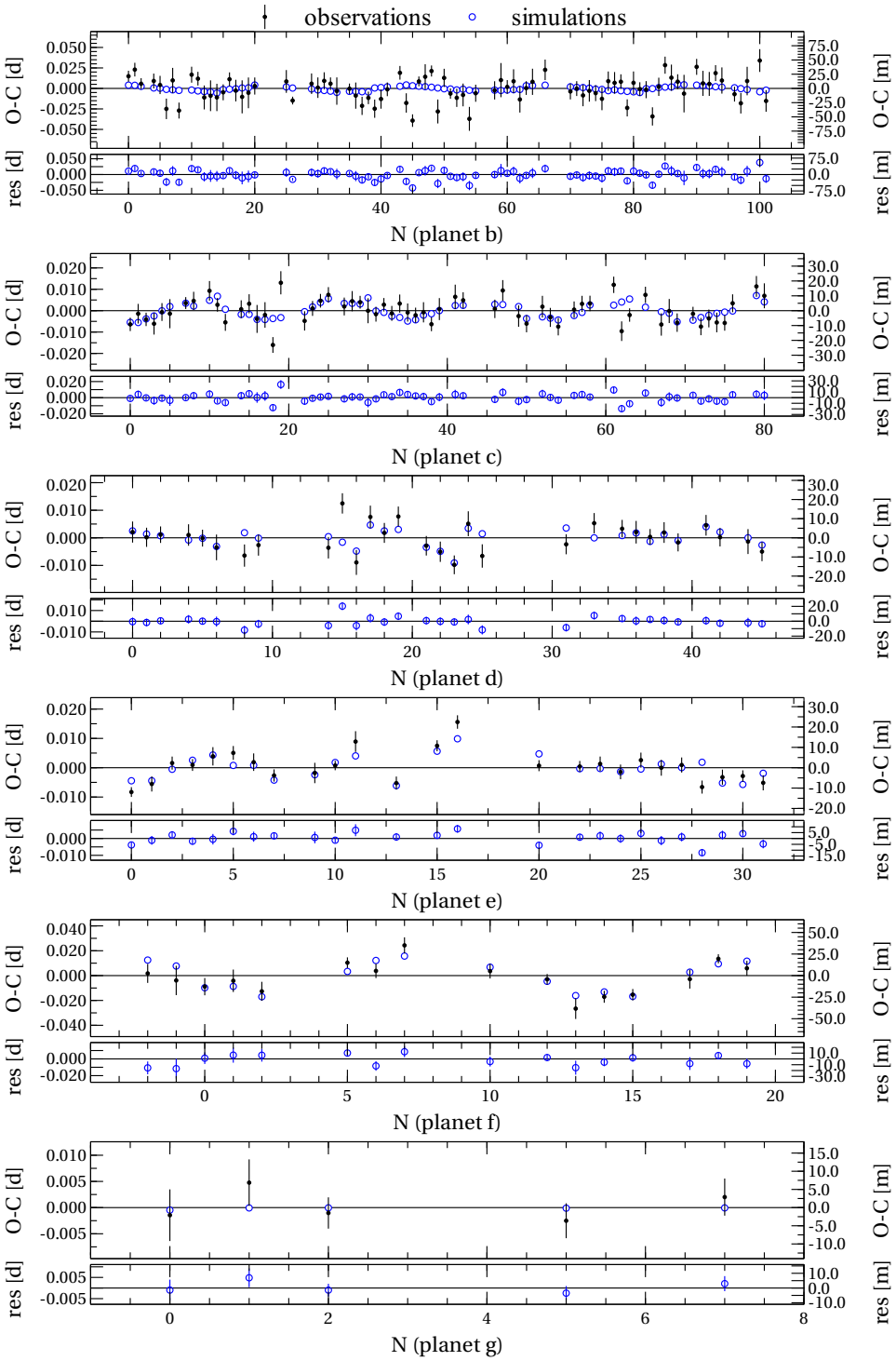

Figura 3.9: O-C plots (observed with black solid circle, simulated with blue open circle) for the solution K11-III (best simulation in Fig. 3.8) for the planets of the Kepler-11 system. For each plot the lower panel shows the residuals. The N (x-axis) has the same meaning as in Fig. 3.4.

Tabella 3.3: Ephemeris fitted to the first three quarters of data of the Kepler-11 system.

Planet	T_0 [BJD$_{\rm UTC}$]	P [days]
b	$2\,455\,187.88389 \pm 0.00028$	10.30375 ± 0.00002
c	$2\,455\,205.62519 \pm 0.00014$	13.02502 ± 0.00001
d	$2\,455\,185.63958 \pm 0.00027$	22.68718 ± 0.00004
e	$2\,455\,147.13846 \pm 0.00021$	31.99589 ± 0.00006
f	$2\,455\,151.40372 \pm 0.00089$	46.68877 ± 0.00036
g	$2\,455\,120.29008 \pm 0.00286$	118.37774 ± 0.00237

Tabella 3.4: Main differences in the Kepler-11 analysis for each solution.

	K11-I	K11-II	K11-III
Quarters	1 to 3	1 to 3	1 to 12
Initial parameters	Lis2011[a]	K11-I	K11-II and e from Lis2013[b]
Number of fitted parameters	18	30	30
Degrees of freedom (dof)	88	76	190
`TRADES` mode	`LM`	`LM`	`grid` ($M_{\rm g}$) + `LM`
Bootstrap	yes	yes	yes
$\chi^2_{\rm r}$	1.25	1.46	1.80

[a] Lissauer et al. (2011a) [b] Lissauer et al. (2013)

3.3 Test case: Kepler-9 system

Another ideal benchmark for testing TRADES is the multiple planet system Kepler-9 (KOI-377). Kepler-9 is a G2 dwarf Solar-like star with a magnitude V = 13.9 (Holman et al. 2010), mass of $1.07 \pm 0.05\ M_{\odot}$ and radius $R_{\star} = 1.02 \pm 0.05\ R_{\odot}$ (Torres et al. 2011). From the first three quarters of the *Kepler*data, Holman et al. (2010) identified two transiting Saturn-sized planet candidates (Kepler-9 b and c with radii of about $\sim 0.8\ R_{\rm Jup}$) near the 2:1 mean motion resonance (MMR). They detected an additional signal related to a third, smaller planet (KOI-377.03, estimated radius $\sim 1.5\ R_{\oplus}$), validated with BLENDER in Torres et al. (2011) but still unconfirmed. The last planet will not be input in my simulations given that there is no confirmation by spectroscopic follow-up so far (the expected RV semi-amplitude, of about ~ 1.5 ms^{-1}, would not increase the scatter in the RV data). Moreover, Holman et al. (2010) stated that the dynamical influences of the fourth body on other planets is undetectable on *Kepler*data (TTV amplitude of the order of ten seconds).

From the analysis of the $\mathrm{d}P/\mathrm{d}t$ of the parabolic fit (quadratic ephemeris) of the T_0s of each planet Holman et al. (2010) inferred the masses of Kepler-9b and Kepler-9c to be $0.252 \pm 0.013\ M_{\rm Jup}$ and $0.171 \pm 0.013\ M_{\rm Jup}$, respectively; they used the RV measurements, from six spectra with the HIRES Rachelle spectrograph at Keck Observatory (Vogt et al. 1994b), only to put a constraint on the masses. Holman et al. (2010) set an upper limit to the mass of the KOI-377.03 of about $7\ M_{\oplus}$, but they could not fix the lower mass limit (the authors proposed $1\ M_{\oplus}$ for a volatile-rich planet with a hot extended atmosphere). Torres et al. (2011) could not determine a mass value for KOI-377.03, but estimated a radius of $1.64^{+0.19}_{-0.14}\ R_{\oplus}$.

I assumed the orbital parameters of the two planets at $t_{\rm epoch} = 2\,455\,088.212$ $\mathrm{BJD_{UTC}}$ from Table S6 in Holman et al. (2010, Supporting On-line Material, SOM), and set $i_{\rm c} = 89\overset{\circ}{.}12$ (Holman 2012, priv. comm.; the value of $88\overset{\circ}{.}12$ reported in the Supporting On-line Material is inconsistent with the transit geometry). I simulated the system with TRADES, without fitting any parameter, spanning the first three quarters of the *Kepler*observations. I fitted a linear ephemeris (see Table 3.5) to the observations and compared the resulting $O-C$ diagrams with those from the simulations (Fig. 3.10). With the parameters from Holman et al. (2010) I obtained a simulated $O-C$ for Kepler-9c which is systematically offset from the observed data points by ~ 300 minutes (see Fig. 3.10, middle pa-

nel). In the bottom panel of the Fig. 3.10 I plot the RV model compared to the observations and the residuals.

I reported in Table , also, the quadratic ephemeris for a compariso with the discovery paper. My linear and quadratic ephemeris in Table 3.5 adopt the transit closest to the median epoch as time of reference for each body, while Holman et al. (2010) used the last transit time as reference for Kepler-9c.

Tabella 3.5: Linear and quadratic ephemeris (in BJD_{UTC}) fitted to data of Kepler-9 system.

ephemeris	Kepler-9b	Kepler-9c
linear	$2\,455\,073.448177 \pm 0.000069$	$2\,455\,086.276884 \pm 0.000121$
	19.243719 ± 0.000020	38.972972 ± 0.000072
quadratic	$2\,455\,073.433861 \pm 0.012302$	$2\,455\,086.311873 \pm 0.014707$[a]
	19.243164 ± 0.002317	38.962410 ± 0.006893
	0.001271 ± 0.000846	-0.013413 ± 0.004030

[a] I used the central transit time as reference for the quadratic fitting, while Holman et al. (2010) used the last time.

In order to investigate whether this behavior is due to bugs in TRADES, I ran a second analysis with the MERCURY package (Chambers & Migliorini 1997). I simulated the same system with MERCURY and used the same technique described in Sect. 2.2.1 to calculate the central time of the simulated transits. The difference between the mid-transit times from TRADES and MERCURY (with RADAU15 and Hybrid integrator) has a maximum absolute value of ~ 0.16 seconds for an integration of 500 days. I did the calculation of the Keplerian orbital elements both for TRADES and MERCURY, and I verified the trend of the X coordinate (the coordinate used as *alarm* in case of eclipses for Kepler-9) of each planet as function of time (in a range of time around an observed transit): I did not find any difference or unexpected behavior between TRADES and MERCURY.

The period of Kepler-9c in the SOM at the reference epoch $2\,455\,088.212$ BJD_{UTC} is neither compatible with period of 38.93486 days calculated from the quadratic ephemeris in Holman et al. (2010), nor with periods in Table 3.5 for my linear and quadratic ephemeris. These tests support my results showing that the problem is not in the integrator or in the subroutine used to calculate the transit times.

Then, I fitted M, P, e, ω, and M (mean anomaly) of both planets and Ω of planet c using the LMalgorithm in TRADES. I found that for all the fitted parameters the new values are consistent with those by Holman et al. (2010, see co-

lumn one and two of Table 3.6 for a comparison). Only one parameter, P_c, is in agreement with the discovery paper within 2σ. The small changes in the parameter values are enough to explain the $O-C$ offset of planet c. The mean longitudes ($\lambda = \Omega + \omega + M$) of the two planets differs from the two solution only by few degrees, but this determines a small misalignement of the initial condition that could have a strong effect in MMR configuration. This simulation gives a $\chi^2 \approx 28.39$, for 10 dof, resulting in a $\chi^2_r \approx 2.839$. The results in Table 3.6 (solution K9-I) and in Fig. 3.11 the $O-C$s and the RV diagrams (notations and colors as in Fig. 3.10).

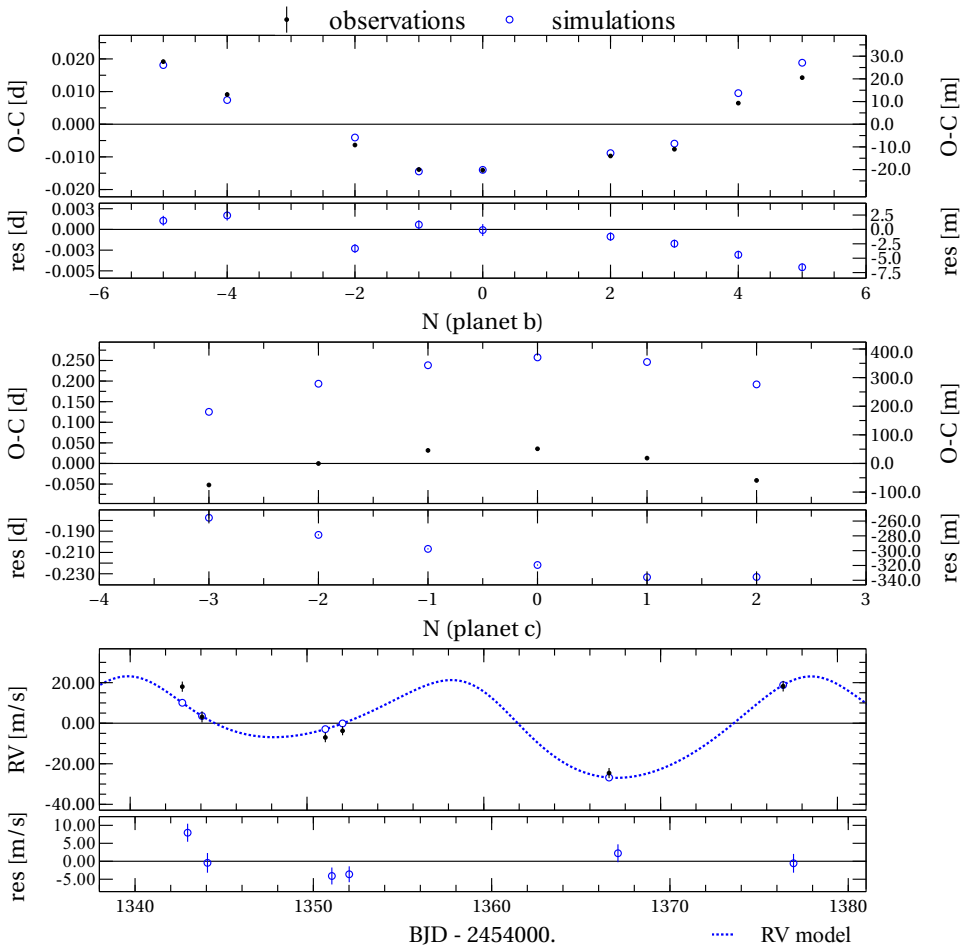

Figura 3.10: $O-C$ diagrams (with residuals) from linear ephemeris for planet Kepler-9b (top panel) and Kepler-9c (middle panel) with the discovery paper's parameters (see column two of Table 3.6); observations plotted as solid black circles, simulations plotted as open blue circles. N, in the abscissa, has the same meaning of Fig. 3.4. *Bottom panel* shows the RV observations as solid black circles, simulations at the same BJD_{UTC} as open blue circles, the dotted blue line is the RV model for the whole simulation.

Tabella 3.6: Parameters of the Kepler-9 system at epoch $t_{\rm epoch} = 2\,455\,088.212$ $\rm BJD_{UTC}$.

Parameter	Holman et al. (2010)[a]	K9-I[b]	K9-II[c]
$M_\star [M_\odot]$	1.0 ± 0.1		
$R_\star [R_\odot]$	1.1 ± 0.09		
$M_{\rm b} [M_{\rm Jup}]$	0.252 ± 0.013	$0.246^{+0.008}_{-0.008} \pm 0.014$	$0.137^{+0.001}_{-0.001} \pm 0.002$
$R_{\rm b} [R_{\rm Jup}]$	0.842 ± 0.069		
$P_{\rm b}$[days]	19.2372 ± 0.0007	$19.23686^{+0.00041}_{-0.00032} \pm 0.00051$	$19.23876^{+0.00004}_{-0.00004} \pm 0.00006$
$e_{\rm b}$	0.151 ± 0.034	$0.131^{+0.008}_{-0.006} \pm 0.016$	$0.058^{+0.001}_{-0.001} \pm 0.002$
$i_{\rm b}[^\circ]$	88.55 ± 0.25		
$\omega_{\rm b}[^\circ]$	18.56 ± 13.69	$18.91^{+0.60}_{-0.92} \pm 14.58$	$356.06^{+0.11}_{-0.21} \pm 0.44$
$\rm M_b[^\circ]$	332.15 ± 14.06	$333.79^{+0.89}_{-0.97} \pm 14.27$	$3.78^{+0.22}_{-0.20} \pm 0.60$
$\Omega_{\rm b}[^\circ]$	0 (fixed)		
$M_{\rm c} [M_{\rm Jup}]$	0.171 ± 0.013	$0.169^{+0.005}_{-0.006} \pm 0.017$	$0.094^{+0.001}_{-0.001} \pm 0.002$
$R_{\rm c} [R_{\rm Jup}]$	0.823 ± 0.067		
$P_{\rm c}$[days]	38.992 ± 0.005	$38.97897^{+0.00182}_{-0.00222} \pm 0.00336$	$38.98610^{+0.00020}_{-0.00021} \pm 0.00043$
$e_{\rm c}$	0.133 ± 0.039	$0.119^{+0.004}_{-0.003} \pm 0.012$	$0.068^{+0.001}_{-0.001} \pm 0.001$
$i_{\rm c}[^\circ]$	89.12 ± 0.17[d]		
$\omega_{\rm c}[^\circ]$	101.31 ± 47.05	$102.85^{+0.43}_{-0.51} \pm 8.04$	$167.57^{+0.01}_{-0.01} \pm 0.01$
$\rm M_c[^\circ]$	6.89 ± 47.20	$7.48^{+0.41}_{-0.35} \pm 6.10$	$307.43^{+0.06}_{-0.05} \pm 0.07$
$\Omega_{\rm c}[^\circ]$	2 ± 3	$1.63^{+0.07}_{-0.11} \pm 1.19$	$359.89^{+0.30}_{-0.98} \pm 0.02$
χ^2/dof		28.382/10	80.852/56
$\chi^2_{\rm r}$		2.84	1.44

Results for the analysis of the Kepler-9 system with `TRADES` using as fitting parameters the masses, the period, the eccentricity, the argument of pericenter and, the mean anomaly of both planets and the longitude of node of Kepler-9c.

[a] Parameters from the SOM of Holman et al. (2010).

[b] Analysis with `TRADES` with initial parameters and T_0s from Holman et al. (2010, SOM). Transits and RVs fit.

[c] Analysis with `TRADES+PSO+LM` and T_0s from Mazeh et al. (2013). Initial parameter boundaries were large enough to contains both solutions K9-I and by Holman et al. (2010). I fit only transits, ignored 6 RV points.

[d] The authors confirmed a typo in the inclination of Kepler-9c in the SOM (Holman 2012, priv. comm.), considering that the value of 88.°12 reported is inconsistent with the transit geometry.

3.3.1 Transit time analysis of the twelve quarters

As for the Kepler-11 system, I extended the analysis of Kepler-9 to the first twelve quarters of *Kepler*data using the transit times from Mazeh et al. (2013). I did not find any transit time to discard using the same criteria used for Kepler-11. First of all I extended the integration of the orbits of the planets from the solution K9-II to the twelve quarters (I did not fit any parameters in this simu-

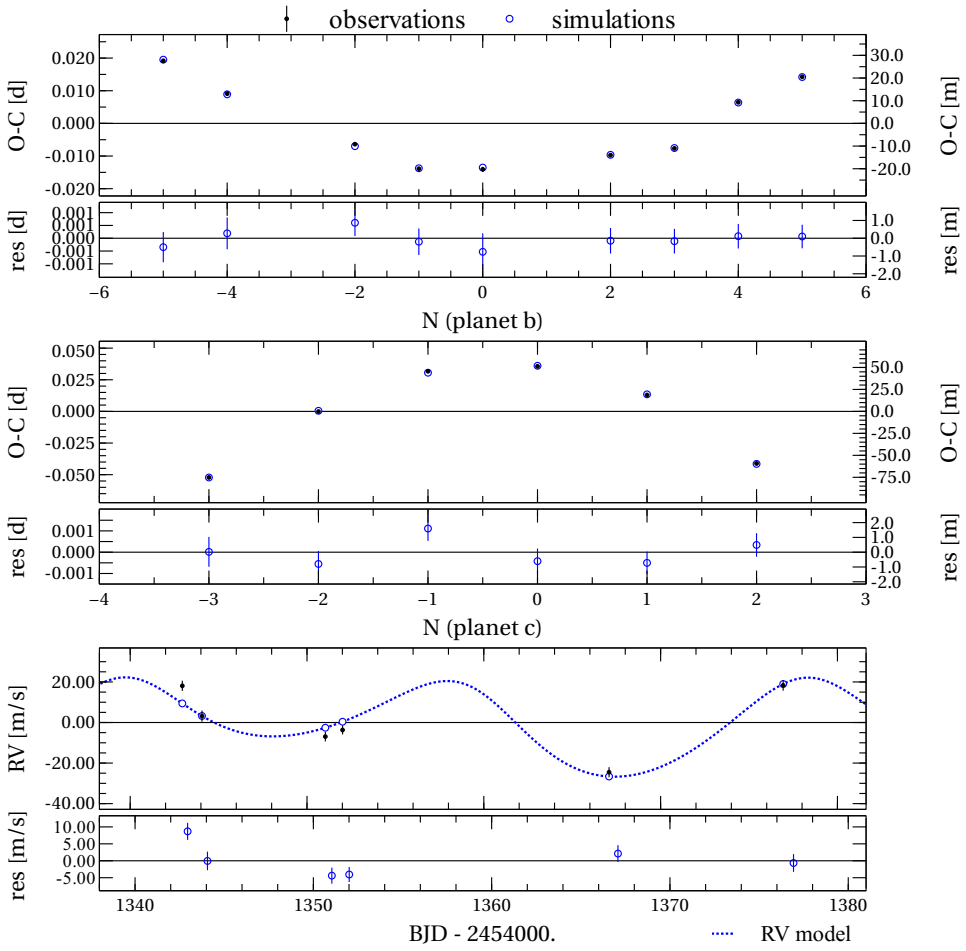

Figura 3.11: Kepler-9 system: same plots as in Fig. 3.10, but with the parameters determined with `TRADES-LM` (K9-I of Table 3.6).

lation) and I compare the observed T_0s and RVs with the simulated ones. In Fig. 3.12 it is clear that the simulation diverges quite soon from the observations. I run a simulation with the `MERCURY` package with same initial parameters of `TRADES` and comparing the resulting $O-C$ diagrams: I found the same behavior. Furthermore, I calculated the transit time differences between `TRADES` and `MERCURY` and I found that the maximum absolute difference is of about 12 seconds, which is really smaller than the error bars of the T_0s.

I considered the orbital solution K9-I in Table 3.6 and I run a simulation on the T_0s of Mazeh et al. (2013) for the same first 3 quarters of Holman et al. (2010). The six RV points are taken into account. The fitted orbital solution has all the parameters in agreement with the solution K9-I.

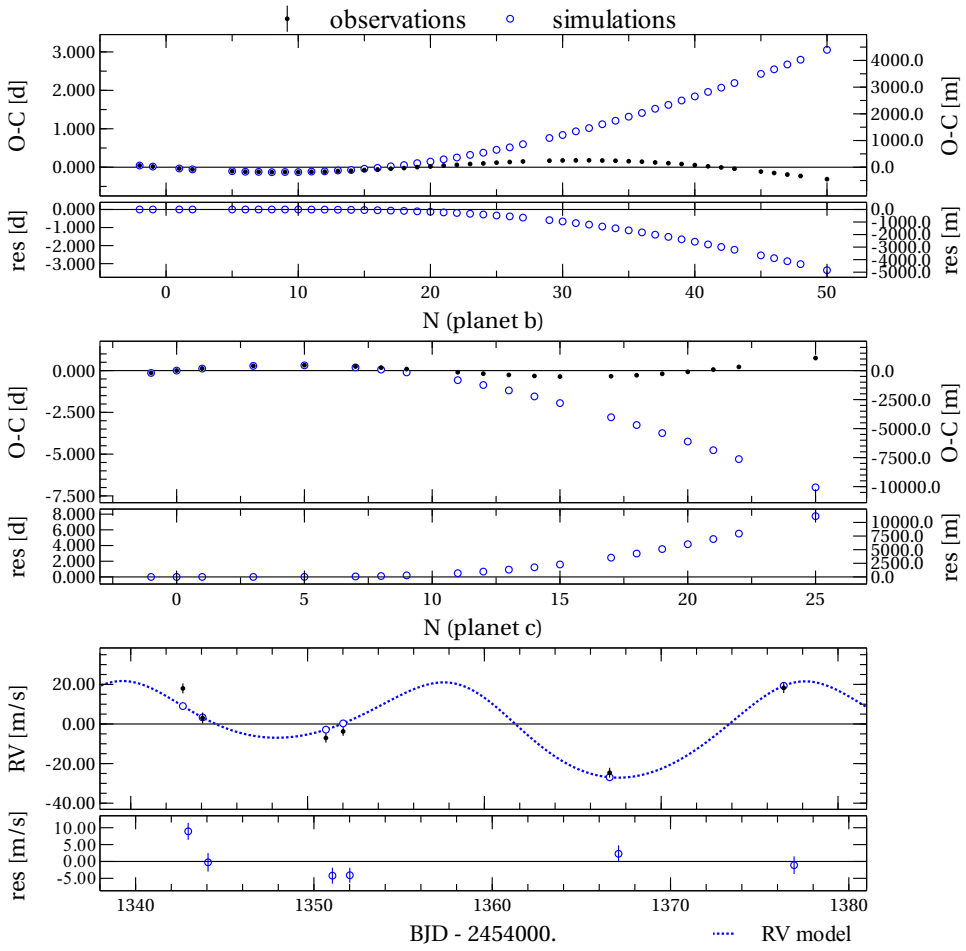

Figura 3.12: Kepler-9 system: $O-C$ diagrams from the parameters obtained (solution K9-I in Table 3.6) with TRADES on the data from Holman et al. (2010) extended to the twelve quarters of *Kepler*. The simulations are compared with the T_0s from Mazeh et al. (2013), while the RVs are from the discovery paper. The epoch of the transits (N in x-axis) are calculated from the linear ephemeris from Mazeh et al. (2013).

Then, I fit all the 12 quarters with initial condition from solution K9-I. The final χ^2_r is ~ 33 (for 62 dof). The $O-C$ diagrams (Fig 3.13) are fitted better than those in Fig. 3.12, and the RV plot shows a lower amplitude.

In order to investigate the origin of this disagreement between observations and simulations when fitting 12 quarters (Figs. 3.12 and 3.13), I analyzed the T_0s by Mazeh et al. (2013) with N simulations, each one fitting 3 adjacent quarters of data (I called it '3 moving quarters') and the 6 RV, e.g., I consider quarter 1 to 3, 2 to 4, and up to 10 to 12. I set the parameters from solution K9-I as the initial parameters of each simulations. I had good fits up to the simulation with quarters

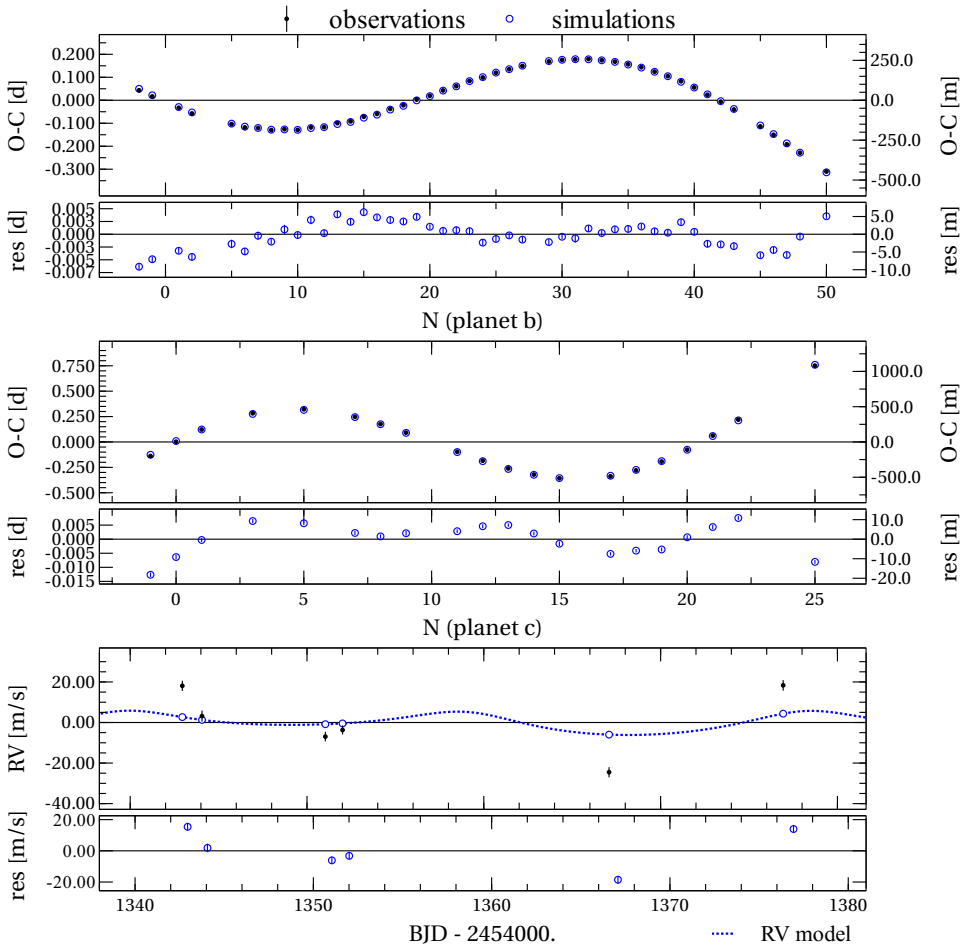

Figura 3.13: Kepler-9 system: $O-C$ diagrams from the fit with TRADES on the data from the twelve quarters of *Kepler*. T_0s from Mazeh et al. (2013), while the RV are from the discovery paper. Initial parameters from the solution K9-I. $\chi^2_r \approx 33.57$ for 62 dof. Given the high value of the χ^2_r I did not report the parameters of this solution.

6, 7, 8; the following simulations showed increased χ^2_r (> 700) that dropped to ≈ 44 only for the last 3 moving simulation (quarters 10, 11, 12). In this analysis I found that the bad fit starts when the solution K9-I diverges in Fig. 3.12. This could be an hint that the original solution determined analyzing only the first 3 quarters of data is biased by the short time scale.

3.3.2 Dynamical analysis without RV points

Due to the high χ^2 in Fig. 3.13 I re-analyzed the Kepler-9 system in a different way. I chose to run many simulations with GA+LM and PSO+LM on all 12 quarters with and without fitting the RV points. I set quite wide bounds on the

parameters, in particular I set the masses to be bound between 10^{-6} $M_{\rm Jup}$ and 1 $M_{\rm Jup}$ and the eccentricities between 0 and 0.3. The best solution (K9-II) has been obtained with the `TRADES` mode `PSO+LM`) without RV fitting. This solution has a $\chi^2_{\rm r}$ of about 1.44 for 56 dof (summary of the final parameters in Table 3.6). The masses of solution K9-II are about 55% of the masses published by Holman et al. (2010). Furthermore, the eccentricities are smaller than the published ones (calculated from the SOM of Holman et al. 2010) and of the order of 0.06. These small values of the masses and the eccentricities imply a RV semi-amplitude of about 16.11 ms^{-1}, smaller than the one from the solution K9-I ($\sim$ 28.91 ms^{-1}) extended to all 12 quarters. Furthermore, using the FMA tool (Marzari et al. 2002) I found that this solution is stable.

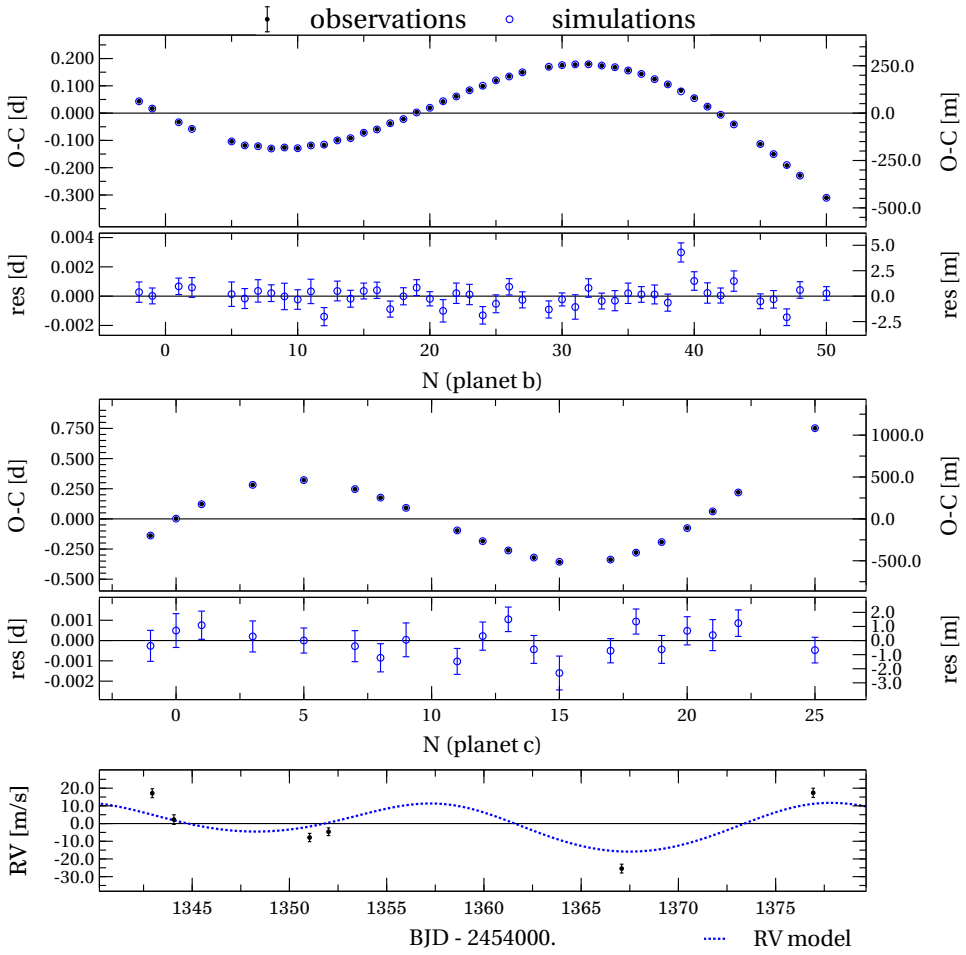

Figura 3.14: $O-C$ diagrams (top and middle plot) for the solution K9-II in Table 3.6 from the fit of the T_0s for the 12 quarters and neglecting the 6 RV points. Colors and markers as in Fig. 3.13 $\chi^2_r \approx 1.44$ for 56 dof. In the bottom panel, the RV model (blue dots) from the solution K9-II with over-plotted RV observations (black dots with error-bars). I cannot have the RV residuals from `TRADES`. The RV model has a lower RV semi-amplitude of about 12.80 ms^{-1} respect to the RVs from the discovery paper.

Capitolo 4

Applications to the CHEOPS Mission and TASTE project

In this chapter I will present some preliminary results coming from the TRADES analysis. The simulations are based on specific characteristics of two projects I am involved in: CHEOPS (CHaracterizing ExOPlanet Satellite) and TASTE (The Asiago Search of Transit timing variations of Exoplanets).

As first case I will show simulations of the Kepler-9 system as if observed by the CHEOPS satellite. In particular, the available data is a synthetic set of few transit times of the planet b (planet c not detected) and stellar RVs. In the second part of the chapter, I will show few simulated systems from the TASTE project sample.

4.1 Analysis of TTV capability of the CHEOPS mission

CHEOPS (CHaracterizing ExOPlanet Satellite[1]) is a space S-class mission that has been recently selected by ESA and the launch is foreseen for the end of the 2017. CHEOPS is as small telescope, of about ~ 30 cm of diameter, which goal is to observe exoplanets with Neptune to Earth radii ($1-6\ R_{\oplus}$) and to characterize their structure. This will be achieved from the analysis of transits in high precision photometric series of bright stars. CHEOPS will be able to detect atmosphere for planets with Neptune- to Earth-like masses hosted by a G5 dwarf star with $V \sim 9$ mag, if the signal-to-noise (S/N) ratio would be of the order of

[1] CHEOPS web page at cheops.unibe.ch

10. The precision needed to achieve this goal should be of about 20 ppm for 6 hours of integration time.

This satellite will not point stars blindfold, but it will target stars hosting known planets, previously detected via accurate RV observations (i.e., from HARPS-N) or from transit surveys (ground-based, i.e., NGTS, or space mission, i.e., TESS). In case of previous detection of exoplanets by RV, CHEOPS will search for a transit signal in order to break the M-i degeneracy, allowing to determine the planet density. If a planet is already known to transit, CHEOPS will do a 'follow-up' observation to obtain a measurement of the radius of the planet with a precision of 10% or better. The sample of bright stars should be of about 150 targets and it is foreseen that the mission will last for about 3.5 years.

CHEOPS will observe only few transits of a planet, maybe up to 10 transits covering up to 2 days of observations for each planet, with a time cadence of about 30 seconds. The right amount of time and transits needed per target will be defined during the phase of the target selection. The satellite will reach the maximum number of transits only if some peculiar behavior will be detected. In particular with 10 transits it is possible to detect a TTV signal even for Neptune-size (and smaller) planets. The presence of a TTV would add more information to the transits and to other previous observations, and sometimes it could be the only method able to detect the presence of a further exoplanet in the system.

4.1.1 Simulation based on Kepler-9 system

I have simulated a test case for CHEOPS based on the Kepler-9 system, knowing the mission goal and hypothesizing the observation strategy. I have used TRADES to integrate the orbits of Kepler-9 system with initial parameters from the solution K9-II in Sect. 3.3.2 for the duration of the CHEOPS mission, 3.5 years. I have selected 10 random transits from the transits of planet b by Mazeh et al. (2013), while I have assumed that planet c would not be detected by transits. I have selected a total of 30 RV points, from the simulated model, in 3 observational seasons (3 alternating blocks of 6 months). I have assumed an uncertainty of 5 m/s for the simulated RVs. This value is of the order of that expected from high precision observations. These 30 random RVs would allow the detection of the periods of both planets by using the GLS periodogram (Zechmeister & Kürster 2009).

I have assumed to know completely the parameters of planet b, so I have fixed them to the solution K9-II. I have used `TRADES` in `GA` and `PSO` mode and

then I have refined the solution with LM fitting M, P, e, ω, M, and i of planet c. First, I have limited the boundaries of P_c covering some strong MMR (i.e., 2:1, 3:1, and so on) and I have set the maximum mass of c to be 13 M_{Jup}. But from these kind of simulation, without any other limit on the inclination, TRADES has returned unstable solutions in most of the cases. Then, I have set the boundaries to: $M_c = 0-13$ M_{Jup}, $P = 30-45$ d, $e = 0-0.5$, $\omega = 0^\circ - 360^\circ$, M = $0^\circ - 360^\circ$, and $i = 80^\circ - 100^\circ$. I have put a strong limit to P_c because it was detectable from the periodogram of the RVs. While, I have set $\Delta i = 20^\circ$ around 90° in order to look for a quasi-coplanar solution.

Some simulations have shown a $\chi^2_r < 2$, but using the FMA tool I have found that only one orbital configuration could be stable. In particular, a simulation has returned a $\chi^2_r \simeq 1.4$, but it was unstable. The stable orbital solution (C-K9-I, for here on) has a $\chi^2_r \approx 1.69$ for 34 degrees of freedom. The values of the parameters of the two solutions (the stable and the unstable) are quite similar and within the error bar. Furthermore, the mean longitude (λ) of both solutions is equal to $\approx 136^\circ$. The difference between the solutions is the value of the ω_c and of the M_c, that defines the position of the planet at the epoch of refence. This small difference is enough to determine the unstability of one the orbital configuration. The $O-C$ diagrams and the RV plots of the stable solution in Fig. 4.1a are just alike those of the unstable solution in Fig. 4.1b. The differences in the figures could be barely seen. This is a clear example of the degeneracy of the parameters in the inverse problem and it shows the necessity of a stability analysis of the solution.

The mass of planet c of the solution C-K9-I is of about 0.223 M_{Jup}, quite higher than the value found in solution K9-II and K9-I. This is probably due to the uncertainty of ~ 5 m/s associated to the RV points that allows quite high mass values. The summary of the solution C-K9-I is in Table 4.1.

At time of writing the analysis of the TTV capability of the CHEOPS satellite is still in an early phase and these are only preliminary results. However, TRADES was able to identify a stable solution that has put strong limits on the possible orbital configurations of the system. I will do many more analysis of simulated systems that properly reflects the possible targets of the CHEOPS mission. I will use more precise transit times, reasonable RV uncertainties, and exoplanetary systems with different characteristics and configurations, such as system with planet pairs trapped in different MMRs.

Tabella 4.1: Orbital solution C-K9-I based on the Kepler-9 system at epoch $t_{\text{epoch}} = 2\,455\,088.212$ BJD$_{\text{UTC}}$.

$M_{\text{c}}[M_{\text{Jup}}]$	0.223	±	0.018
P_{c}[days]	39.1097	±	0.0131
e_{c}	0.0056	±	0.0097
$\omega_{\text{c}}[^\circ]$	28.7	±	135.3
$\text{M}_{\text{c}}[^\circ]$	108.7	±	137.0
$i_{\text{c}}[^\circ]$	96.9	±	3.8

The parameters for the planet c are determined after a simulation with `TRADES` in mode `PSO+ LM`.
Final χ^2_{r} of about 1.69 for 34 dof.

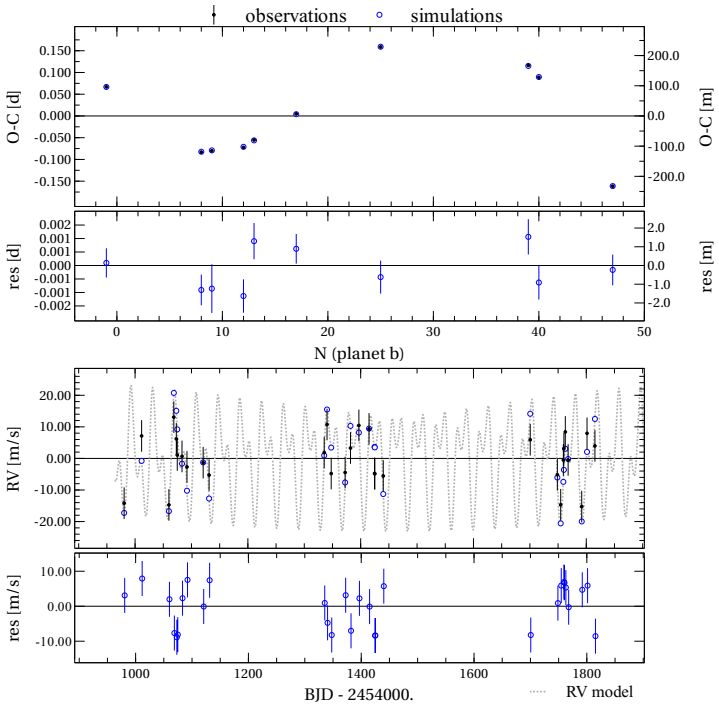

(a) Stable solution C-K9-I for the Kepler-9 system. $\chi^2_r \approx 1.69$.

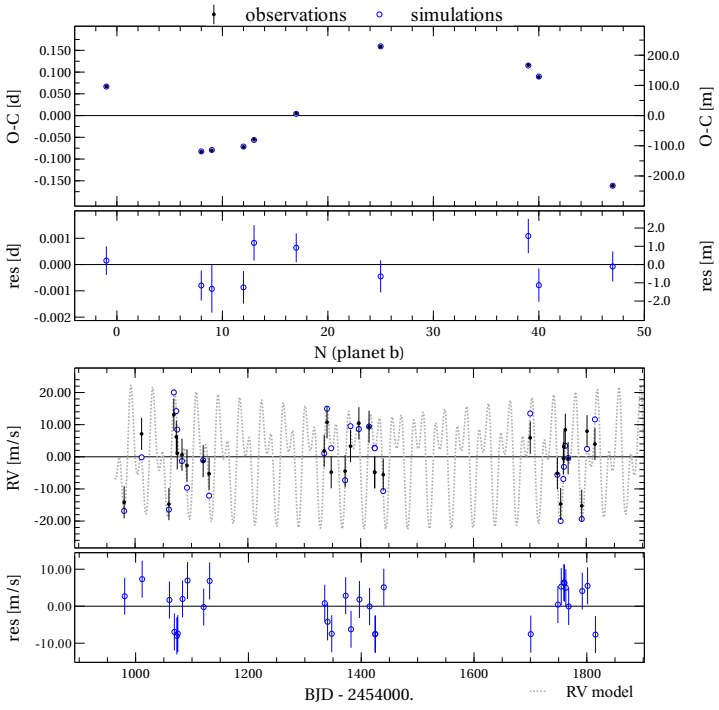

(b) Unstable solution for the Kepler-9 system. $\chi^2_r \approx 1.4$.

Figura 4.1: Simulations obtained with `TRADES` in mode `PSO+LM`. In both figures: *upper panel*, $O-C$ diagram for the T_0 of the planet c and residuals; *bottom panel*, RV diagram and residuals.

4.2 TASTE sample analysis

I am involved in TASTE, The Asiago Search of Transit timing variations of Exoplanets, a project based on small/medium ground-based telescopes. Its goal is to obtain short cadence high-precision photometric series (or light curves, LCs) of a sample of transiting exoplanets for which has been claimed a TTV signal. Initially, TASTE used the Asiago observatory[2] in cooperation with Osservatorio Astronomico della Valle d'Aosta[3] (OAVdA), but now it has been extended to other worldwide facilities, such as IAC-80 telescope[4], UDEM 0.36 m telescope (Universidad de Monterrey, Mexico), and many others.

The proposed strategy, that characterize the TASTE observations, is based on monitoring and reducing all those sources of systematic trends: the so-called *red noise* (or *correlated noise*) that afflicts many ground-based telescopes (Tamuz et al. 2005). At this purpose, it has been developed a pipeline reduction able to monitor and to correct these sources of noise with an empirical, iterative algorithm: STARSKY (Nascimbeni et al. 2011a).

The data collection is characterized by defocus technique minimizing flat-field variation and collecting many photons without reaching the saturation level of the camera. Usually it is used the windowing of the CCD reducing the read time of the images allowing an high duty cycle. The CCD window is properly chosen to contain at least few reference stars. Furthermore, the observations start about an hour before the ingress of the transit (pre-ingress) and stop about an hour after the egress (post-egress). In this way it is possible to correct for the presence of trends, i.e, due to the varying air-mass of the object, and it is possible to estimate the photometric precision of the series. The LC of the target is obtained with STARSKY, that uses an approach based on differential photometry weighted for the reference stars in the field. These reference stars are carefully chosen before the observations in order to minimize systematics due to magnitude or color effects.

The original sample of 12 TTV candidates for the TASTE project can be found in the first paper by Nascimbeni et al. (2011a); this sample has been changed with time after new analysis performed by the authors and other works. The first analysis of the TASTE sample have been done on: HAT-P-3b and HAT-P-14b (Nascimbeni et al. 2011a), HAT-P-13b (Nascimbeni et al. 2011b), WASP-3b

[2] Asiago telescopes at www.oapd.inaf.it
[3] www.oavda.it
[4] www.iac.es

(Nascimbeni et al. 2013), and recently HAT-P-20b and WASP-1b (Granata et al. 2014).

4.2.1 HAT-P-13 system

The HAT-P-13 system has been discovered by Bakos et al. (2009) and it shows the presence of two planets. HAT-P-13 is a G4 bright dwarf star (Bakos et al. 2009). The planet HAT-P-13b is an 'hot-Jupiter' on an orbit of about 2.9 days. HAT-P-13c is a massive body, with mass of the order of 14 $M_{\rm Jup}$. The planet b have been observed by the transit method, while planet c has been discovered only by RV. The transit of HAT-P-13c has been searched by Szabó et al. (2010) in a multi-site campaign without any success. In Pál et al. (2011) has been claimed an unusual TTV signal of planet b, but the true nature of this signal is still uncertain (Nascimbeni et al. 2011b; Fulton et al. 2011).

I have taken the T_0s from the work by Southworth et al. (2012); these T_0s contains, also, some data points from non-professional astronomers (see Fig. 4.2). In addition, I have used the RVs published by Winn et al. (2010). In the latter work has been used the RV points from Bakos et al. (2009) and from the analysis of the Rossiter-McLaughlin effect (RV variation during the transit of an exoplanet). Winn et al. (2010) found a trend in the residuals of the RV plot (see Fig. 4.3). The authors interpreted this trend as a variation of the proper motion of the system ($\dot{\gamma}$) that could be due to a farther fourth body.

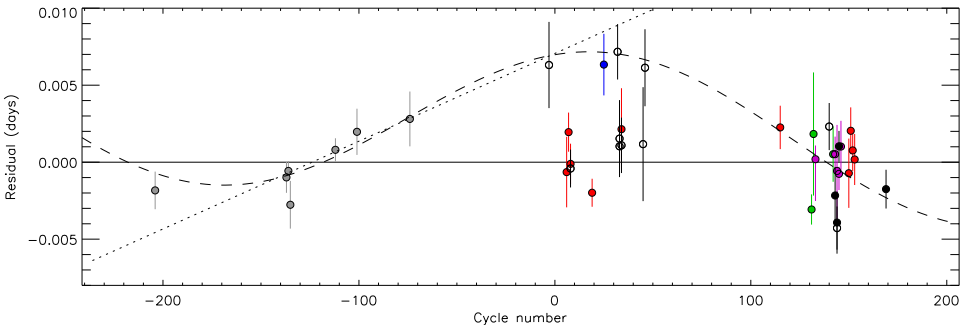

Figura 4.2: $O-C$ diagram (by Southworth et al. 2012) calculated respect to the linear ephemeris proposed by Southworth et al. (2012). Black dots from Southworth et al. (2012), gray dots from Bakos et al. (2009), blue from Szabó et al. (2010), lilac from Pál et al. (2011), green from Nascimbeni et al. (2011b), red from Fulton et al. (2011), and open circles from non-professional timings. Dotted line is the linear ephemeris by Bakos et al. (2009), while the dashed line is the sinusoidal signal proposed by Nascimbeni et al. (2011b).

Some parameters, such as the mean anomaly (M) of both bodies, are missing in both works by Southworth et al. (2012) and Winn et al. (2010). I have used a

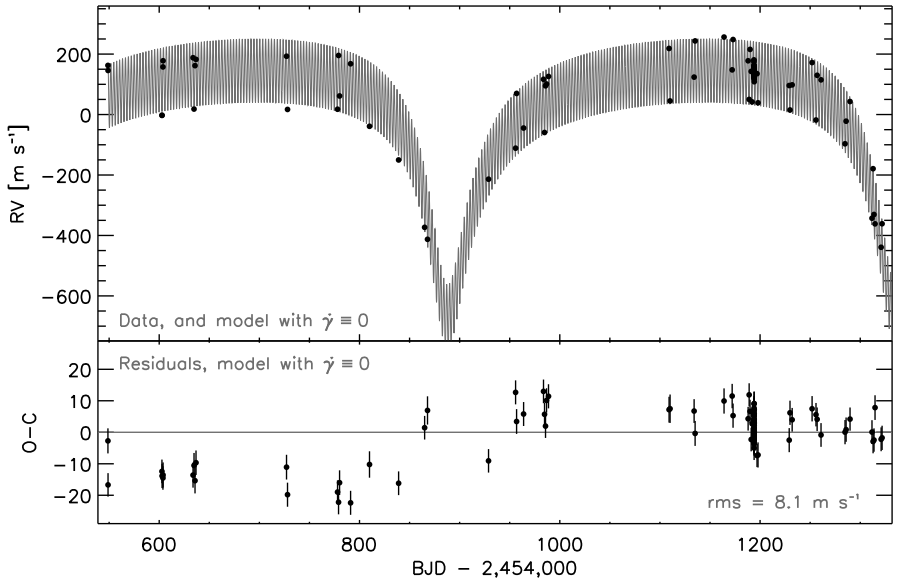

Figura 4.3: RV plot as in Winn et al. (2010). Black dots observational data, RV model (gray line in the upper panel) calculated from a Keplerian fit with planet b and c. The trend parameter $\dot{\gamma}$ has been set equal to 0.

rough value of the parameters from the two papers, I have set the M of b and c to random values between 0° and 360°, and I have set the orbit of planet c co-planar with b ($i_c = i_b = 89.^\circ13$). I have set mass and radius of the star and the radius of the planet b to the Southworth et al. (2012) values: $M_\star = 1.32\ M_\odot$, $R_\star = 1.756\ R_\odot$, $R_b = 1.487\ R_{Jup}$; I have assumed the radius of planet c equal to $1.2\ R_{Jup}$.

I have fitted 12 parameters with `TRADES` in `LM` mode: M, P, e, ω, and M for both HAT-P-13b and HAT-P-13c, i and Ω only for planet c. In Fig. 4.4a I show how `TRADES` has reproduced the plots presented in Southworth et al. (2012) and Winn et al. (2010), with the same trend in the residuals of the RV panel taking into account only planets b and c. The χ^2 of the simulation is of about 2876.37 with 126 dof, that is $\chi^2_r \simeq 22.65$.

Then, I have removed the RV points that have been used for the analysis of the Rossiter-McLaughlin effect and I have repeated the analysis. This orbital solution has a lower $\chi^2 \simeq 2188.74$ than the previous, but for less degrees of freedom (84), that outputs an higher χ^2_r of about 26.06 (see Fig. 4.4b for the $O-C$ and RV plots).

I have used the parameters found by `TRADES`, without RVs from RM analysis, for the next step of the analysis: search for an additional fourth body. Winn et al.

(2010) proposed that the $\dot{\gamma}$ term in the RV residuals would imply a fourth body with different combinations of mass and distance, in particular a 2.5 $M_{\rm Jup}$ body at 5 au, or a 10 $M_{\rm Jup}$ planet at 10 au, or a star of 90 $M_{\rm Jup}$ at 30 au. I have tried to search this hypothetical body (named 'd') by the PSO algorithm with very large boundaries on the fitted mass and semi-major axis of planet d that could cover the values proposed by Winn et al. (2010). I have set the upper limit of the eccentricity of this planet to 0.5, I have let ω and M freely varying between 0 and 360 degress. I have fixed $\Omega = 0^\circ$ and $i_{\rm d} = i_{\rm b}$ (coplanar). The fitted parameters were: $M_{\rm d}$, $a_{\rm d}$ ($P_{\rm d}$), $e_{\rm d}$, $\omega_{\rm d}$, and $\rm M_d$. I have fixed all the parameters of HAT-P-13b and HAT-P-13c. Until now, all the simulations did not returned a $\chi^2_{\rm r}$ lower than 2000.

Then, I have run a grid+LM search with mass and semi-major axis covering the proposed values by Winn et al. (2010) and fitting the same parameters of the PSO search. I used logarithmic steps in the grid for 66 combinations of parameters. I set the initial $e_{\rm c} = 0.0663$, a random number between 0.1 and 0.002, $\omega_{\rm d} = 62\overset{\circ}{.}165$ and $\rm M_d = 81\overset{\circ}{.}9312$, random numbers between 0° and 360°. The grid+LM simulation ended with 47 orbital solutions with a $\chi^2_{\rm r} < 26.6$ (the value of HAT-P-13 system with planets b and c), and 19 of them had a $\chi^2_{\rm r} < 16$, for 91 degrees of freedom. These better-fit orbital configurations show an high degeneracy in the parameter space $M_{\rm d} - P_{\rm d}$. In particular, the first three best simulations (subscripts 1, 2, and 3) have returned $\chi^2_{\rm r}$ very close to 15, but different values of mass and period (semi-major axis): $\chi^2_{\rm r,1} = 15.28$, with $M_{\rm d,1} = 8.2\,M_{\rm Jup}$ and $P_{\rm d,2} = 12\,808.8$ days ($a_{\rm d,1} = 11.776$ au); $\chi^2_{\rm r,2} = 15.34$, with $M_{\rm d,2} = 5.9\,M_{\rm Jup}$ and $P_{\rm d,2} = 9\,957.4$ days ($a_{\rm d,2} = 9.950$ au); $\chi^2_{\rm r,3} = 15.38$, with $M_{\rm d,3} = 11.1\,M_{\rm Jup}$ and $P_{\rm d,3} = 14\,404.1$ days ($a_{\rm d,3} = 12.743$ au).

As it can be seen in Fig. 4.5a, 4.5b, and 4.6, the different masses and periods of the first three best-fit orbital configurations have almost the same effect: they do not reproduce the scattered T_0s (the claimed TTV) and they have removed a linear slope of the RV residuals, but a sinusoidal long-time RV term is still visible. Taking into account only the T_0s I cannot exclude the solution with only planets b and c. Furthermore, the best-fit orbital configuration with an additional fourth body cannot reproduce neither the TTV nor the features in the RV residuals. The analysis needs observations on more long time base and further it is needed to understand if the uncertainties on the T_0s have been underestimated. If the latter is true, a linear ephemeris of HAT-P-13b cannot be excluded and the T_0 would not increase the information on the system. The only clue about an addi-

tional body would be the particular trend in the RV residuals. I am still working on this system and this is only an early analysis, but quite interesting.

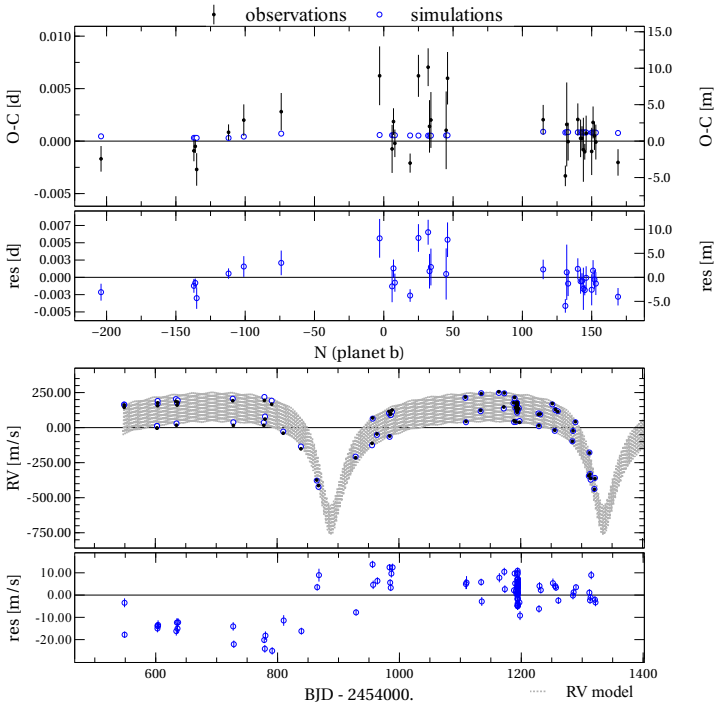

(a) Resulting plots from the simulation with TRADES starting with rough initial parameters and fitting 12 parameters. Data from Southworth et al. (2012) and Winn et al. (2010). $\chi^2_r \approx 22.65$ for 126 dof.

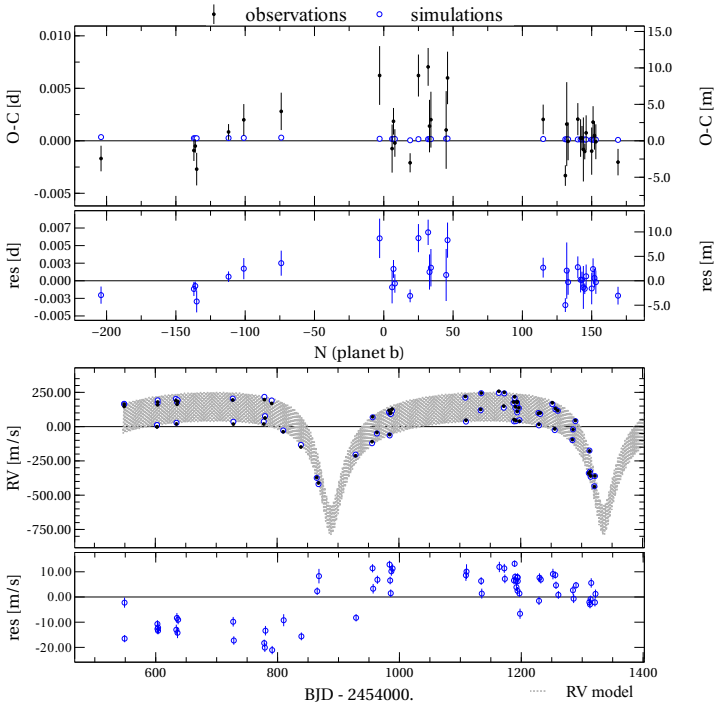

(b) Resulting plots from the simulation with TRADES starting with initial parameters as in Fig. 4.4a, fitting 12 parameters, but neglecting the RVs from the analysis of the Rossiter-McLaughlin effect. $\chi^2_r \approx 26.06$ for 84 dof.

Figura 4.4: Resulting plots from the simulation with TRADES starting with rough initial parameters and fitting 12 parameters. The RV plots (*bottom panels* in both figures) show the same trend feature in RV residuals as in Fig. 4.3.

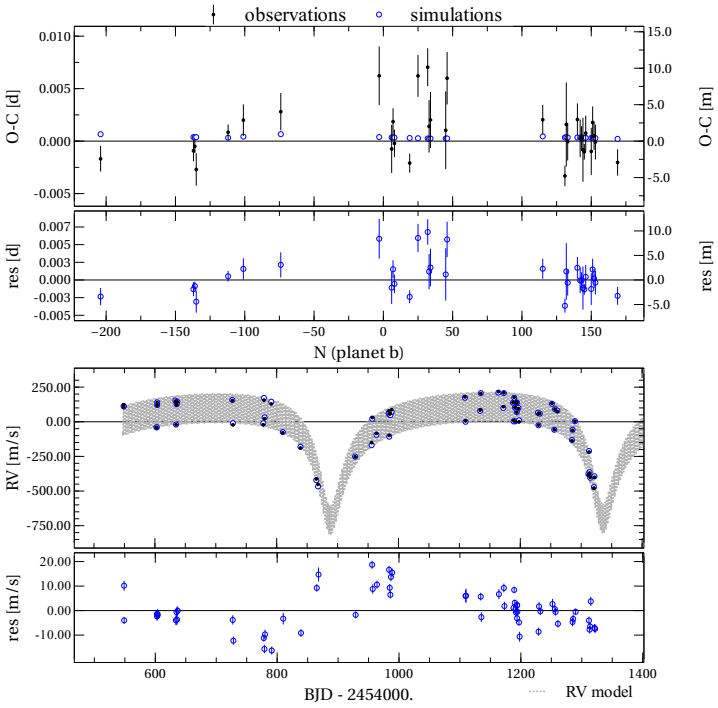

(a) Third best-fit simulation in the grid+LM search. $M_{d,3} = 11.1\,M_{Jup}$, $P_{d,3} = 14\,404.1$ days ($a_{d,3} = 12.743$ au), $\chi^2_{r,3} \approx 15.38$ for 91 dof.

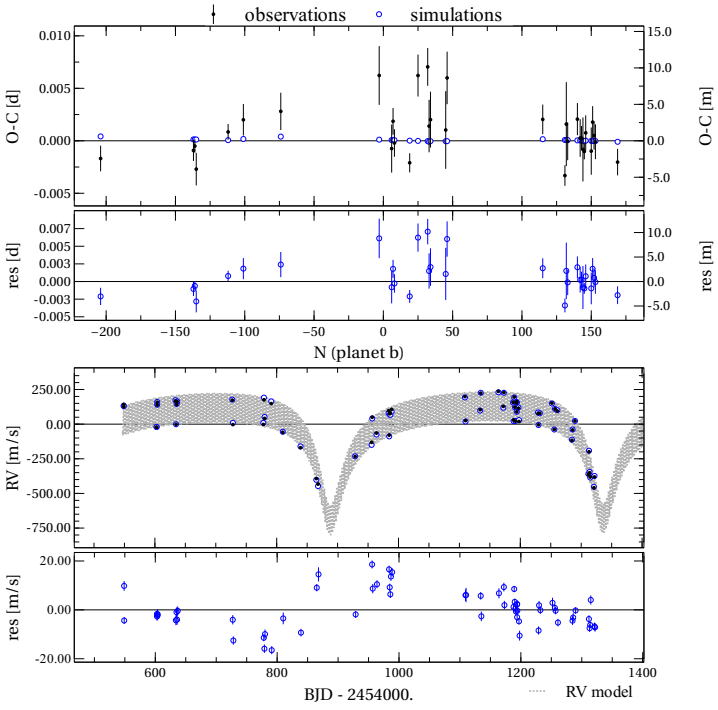

(b) Second best-fit simulation in the grid+LM search. $M_{d,2} = 5.9\,M_{Jup}$, $P_{d,2} = 9\,957.4$ days ($a_{d,2} = 9.950$ au), $\chi^2_{r,2} \approx 15.34$ for 91 dof.

Figura 4.5: $O - C$ and RV diagrams from grid+LM search on mass and semi-major axis of an hypothetical HAT-P-13d.

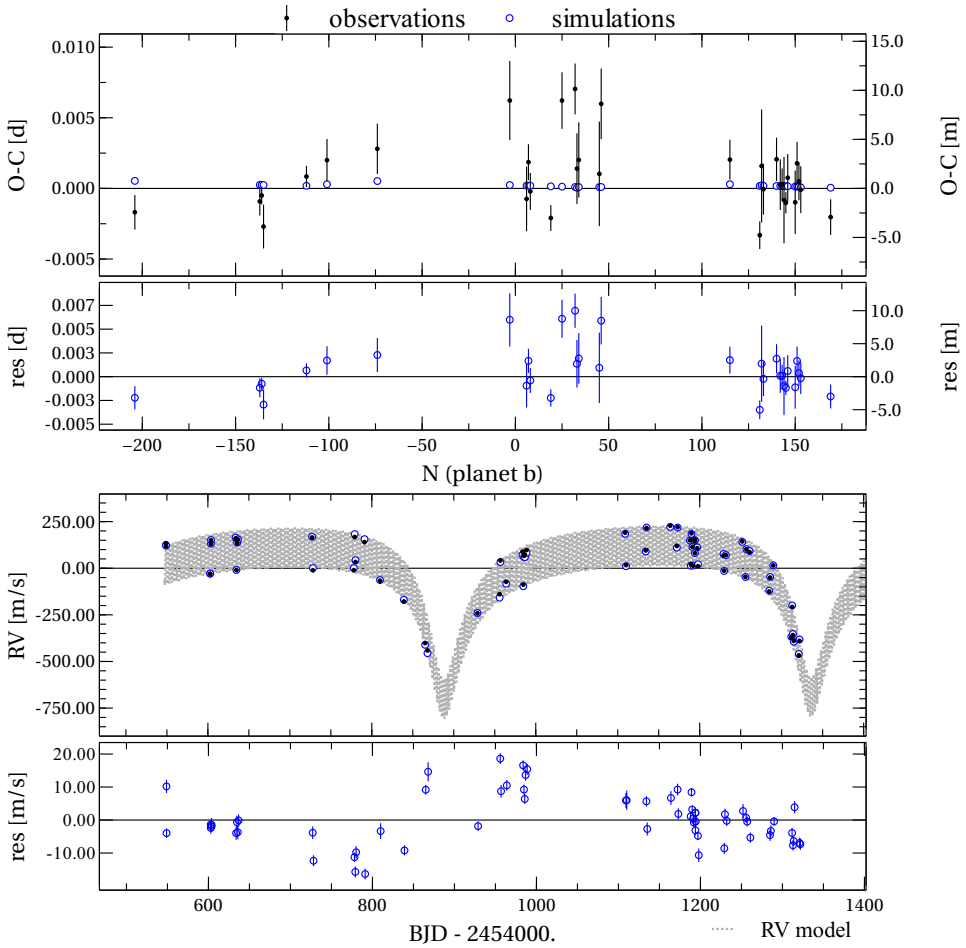

Figura 4.6: First best-fit simulation in the grid+LM simulation, searching for an hypothetical HAT-P-13d in the system. $M_{\mathrm{d},1} = 8.2\,M_{\mathrm{Jup}}$, $P_{\mathrm{d},1} = 12\,808.8$ days ($a_{\mathrm{d},1} = 11.776$ au), $\chi^2_{\mathrm{r},1} \approx 15.28$ for 91 dof.

4.2.2 WASP-3 system

WASP-3 is an F7-8 dwarf star, $V \simeq 10.6$ mag, with mass and radius of 1.110 $M_\odot$ and 1.298 $R_\odot$, respectively. This star hosts an hot-Jupiter planet, WASP-3b (Pollacco et al. 2008), with mass $M_\mathrm{b} = 1.76\ M_\mathrm{Jup}$, radius $R_\mathrm{b} = 1.31\ R_\mathrm{Jup}$, and period $P_\mathrm{b} \simeq 1.8468$ days.

After the discovery of WASP-3b, different analysis have done on this system with ground-based facilities. In particular, the first claim of a periodic TTV signal can be found in the work by Maciejewski et al. (2010). The authors estimated a perturbing planet in an outer 2:1 MMR with a mass of about 15 $M_\oplus$. The TTV periodicity found by Maciejewski et al. (2010) was confirmed by Eibe et al. (2012) including the TDV analysis, but later it was excluded by Montalto et al. (2012). In the latter work has been proposed that the stellar activity could be a source of the TTV. Then, in Nascimbeni et al. (2013), the TTV signal was described by a chaotic orbital configuration. Maciejewski et al. (2013) analyzed new high-precision transit data and different set of RV points. They excluded that the activity could affect their transit LCs and they stated that the periodic and chaotic TTV previously proposed would be due to underestimated uncertainties and systematic effects of the photometric series. Also, they analyzed the sensitivity of their data to a perturber with different mass and period, but the RV fit and the T_0s re-estimation would be consistent with a 2-body system with only the planet WASP-3b in a circularized orbit.

These TTV claims and retractions would make the WASP-3 system a quite interesting case. I would like to see what I could obtain with `TRADES` among the different results proposed in literature. I have taken the T_0s from the TASTE archive (Table 3 by Nascimbeni et al. 2013); for each available observation, I have used the median T_0s of the 'selected' sample and I have calculated as uncertainty the mean of the absolute value of the negative and positive error. For the simultaneous observations of the same transit I have used the weighted average of the T_0 and its associated error. The RV sample is the published data set in Table 2 by Maciejewski et al. (2013). I have not taken all the RV data set used in that work, because they have different RV offsets (different system velocity, γ, values) and I have not implemented the fit of multiple RV set in `TRADES`, yet. The T_0s and the RVs, I have used in the next simulations, are shown in Fig. 4.7.

I have used as initial parameters the values found in Maciejewski et al. (2013) and in Nascimbeni et al. (2013). In particular, in Maciejewski et al. (2013) has been sad that the eccentricity could be consistent with zero value, but their best

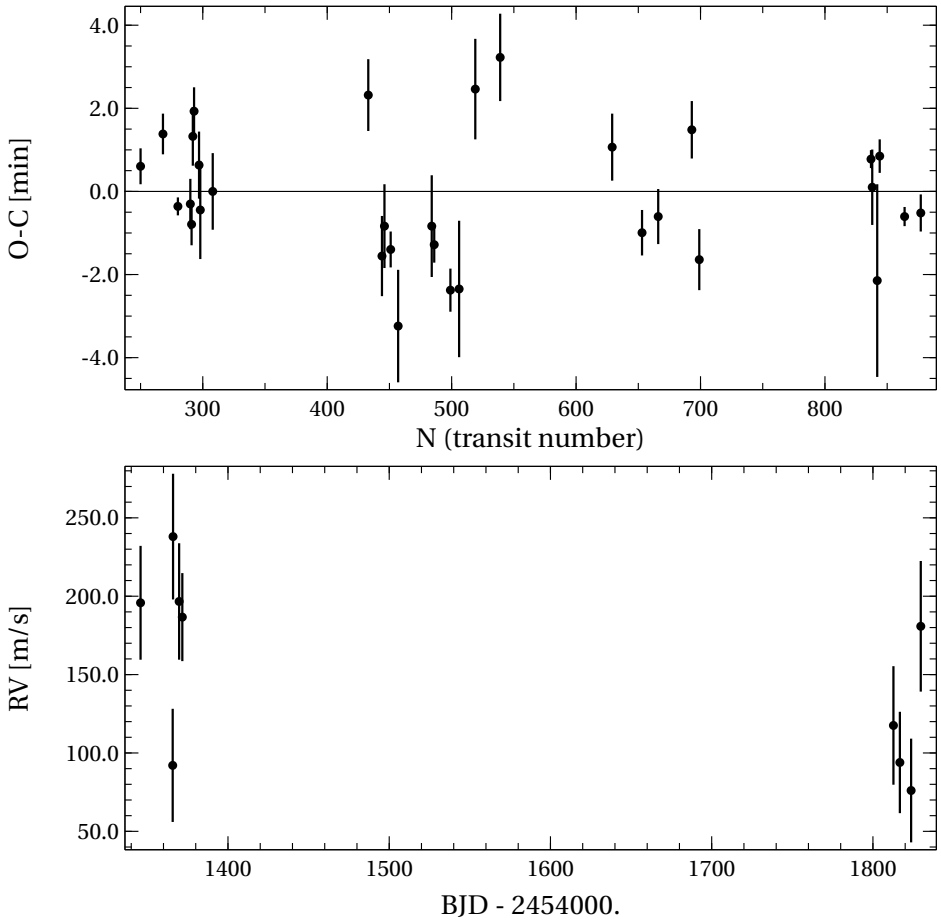

Figura 4.7: *Top-panel*: $O-C$ diagram built with the T_0s by Nascimbeni et al. (2013). *Bottom-panel*: observed RVs by Maciejewski et al. (2013).

Keplerian fit gave a small non zero value of 0.02. When $e = 0$, ω is undefined and M has not been determined. Indeed, I have set e to an initial random value between 0 and 0.02. I have done the same for the two missing angles choosing them randomly between 0 and 360 degrees. Then, I have let `TRADES` in `LM` mode to determine the proper values fitting M, P, e, ω, and M of WASP-3b. The simulation gave a χ^2_r of about 3.65 for 44 dof. In Figure 4.8 I report the $O-C$ and the RV plot of the simulation. In this case the simulated $O-C$ (open-blue circles in top panel of Fig. 4.8) are perfectly at zero, because I have simulated a 2-body system that has strictly periodic transits.

I have searched for a third body, a planet c, by using `TRADES` in `GA` and `PSO` modes. I have fixed the parameters of WASP-3b to the 2-body values, and I ha-

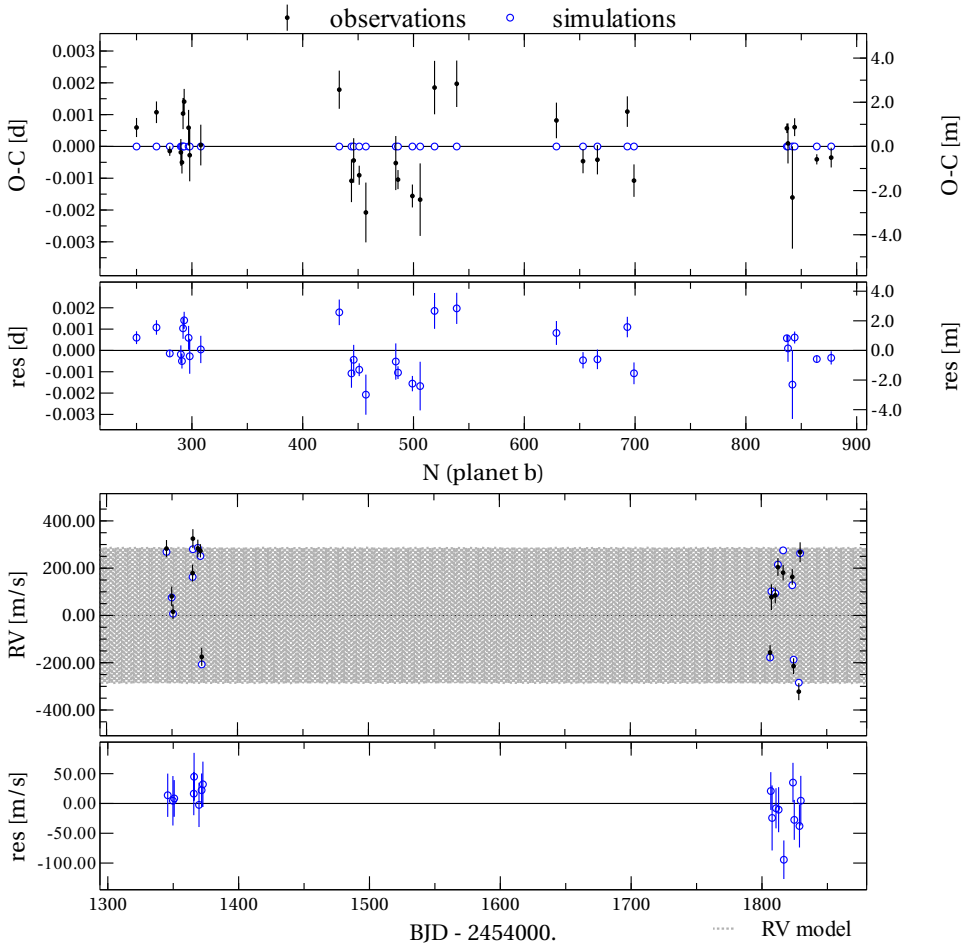

Figura 4.8: *Top*: $O-C$ diagram of WASP-3b in case of a 2-body system: star and planet. The simulated $O-C$ (open-blue circles) are correctly aligned to zero value. *Bottom*: RV plot, with the model in light-gray dots. The RV offset ($\gamma = -86.93 \pm 8.61$ ms^{-1}), found by TRADES, has been subtracted by the RVs.

ve fitted the parameters of the hypothetical planet c. I have used wide boundaries on the parameters of planet c in order to take into account the values proposed in the literature. I have set upper limits of the parameters as follow: $M_c = 13\ M_{Jup}$, $P_c = 365.25$ days, $e_c = 0.5$. The inclination has been constrained between 80 and 100 degrees (quasi co-planar case). I have let The other three angles varying freely between 0 and 360 degrees. I have found a best-fit solution with a $\chi^2 \simeq 98.70$ ($\chi^2_r \simeq 2.35$ for 42 dof, see Fig. 4.9a). The mass ($M_c \simeq 8.9\ M_\oplus$) and period ($P_c \simeq 3.369$ days) of this solution are quite in agreement with the proposed solution by Maciejewski et al. (2010). I have simultaneously done a series of global search simulations fixing the longitude of the node $\Omega_c = 0°$.

From this 'second' series of simulations I have found a best-fit simulation with $\chi^2 \simeq 143.03$ ($\chi^2_r \simeq 3.33$ for 43 dof, see Fig. 4.9b), whose mass and period values are of $M_c \simeq 4.1\ M_\oplus$ and $P_c \simeq 6.386$ days, respectively. Both these two best-fit solutions have a χ^2_r lower than the 2-body solution. Despite the good data fit of both solutions, the stability analysis with the FMA tool has found that the solution with the lower χ^2_r is unstable; an hint of this could be the peculiar orbit of planet c in Fig. 4.10a, probably due to the value of $\Omega_c \simeq 63°$. However, the FMA tool has found that the second best-fit solution is stable (see the plots of the orbits in Fig. 4.10b). This is another case where the stability analysis is needed to disentangle degenerate orbital solutions. I have reported in Fig. 4.11 the 'evolution' of the fitted parameters as function of the number of the iteration during the `PSO` simulation (500 particles for 1000 iterations) of the best-fit stable solution; the darker gray regions are the accumulation regions due to best local configurations.

I have extended the global search (refined by the `LM`) fitting parameters of planet c (same previous boundaries, fixing $\Omega_c = 0°$), and some parameters of planet b. They have been tightly constrained, i.e., I have set the upper limit of the mass to $3\ M_{Jup}$ and I have limited the period of b between 1.8 and 1.9 days. I did not have found any solution better than the previous ones or better than the 2-body case. In particular, these solutions have shown χ^2_r of the order of $4-5$ or I have found they were unstable.

This is a preliminary analysis that cannot still shed light on the doubtful TTV of WASP-3, and the 2-body solution cannot be excluded. The linear fit on the T_0s has a χ^2_r of about 4.95 for 30 dof. Following the statement by Maciejewski et al. (2013), if I double the uncertainties on the T_0s and fit a linear ephemeris I find $\chi^2_r \simeq 1.24$. This could strengthen the hypothesis of the one-planet configuration.

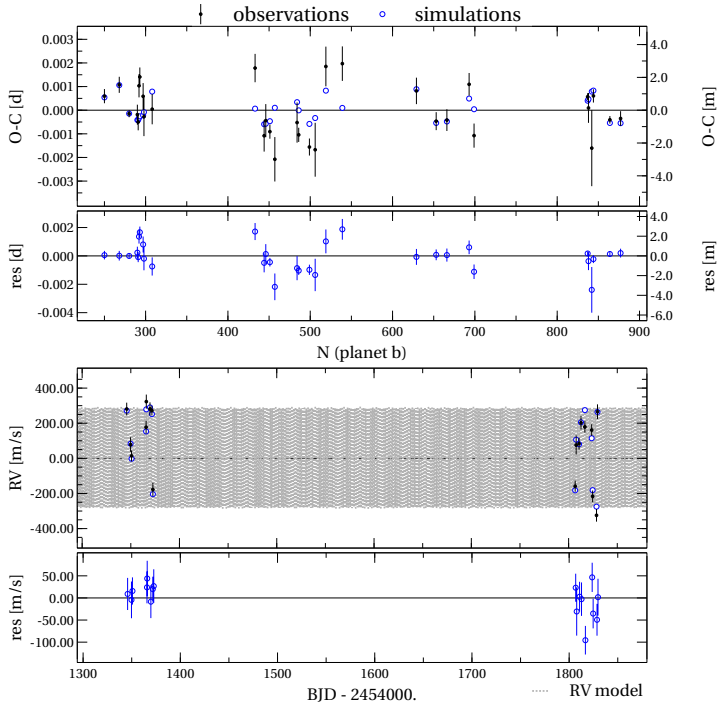

(a) [WASP-3 $O-C$ and RV plots for 3-body unstable solution. $O-C$ (*top panels*) and RV (*bottom panels*) diagrams for the unstable 3-body solution. $\chi^2_r \simeq 2.35$ for 42 dof.

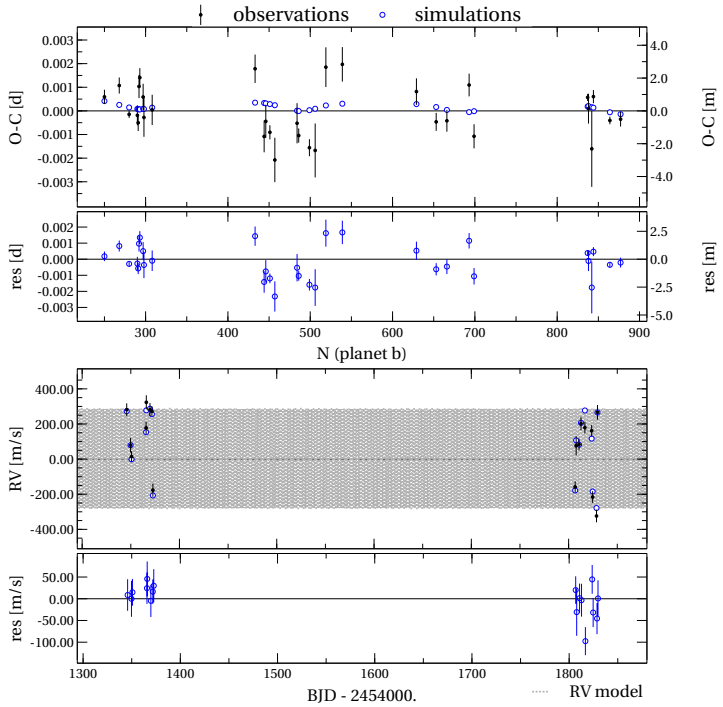

(b) WASP-3 $O-C$ and RV plots for 3-body stable solution. $O-C$ (*top panels*) and RV (*bottom panels*) diagrams for the unstable 3-body solution. $\chi^2_r \simeq 3.33$ for 43 dof.

Figura 4.9: $O-C$, RV, and orbits of the unstable and stable 3-body solutions found by `TRADES` in `PSO` mode.

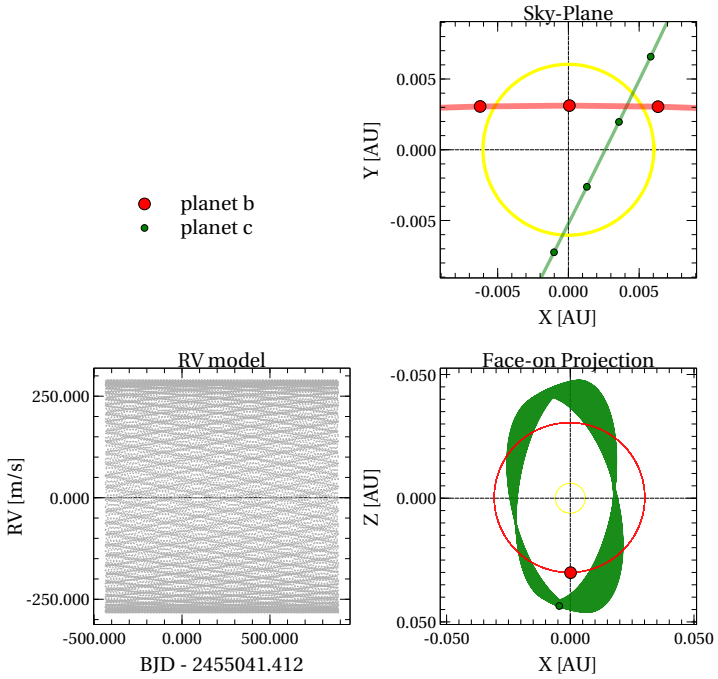

(a) WASP-3 orbits and RV model for 3-body unstable solution.

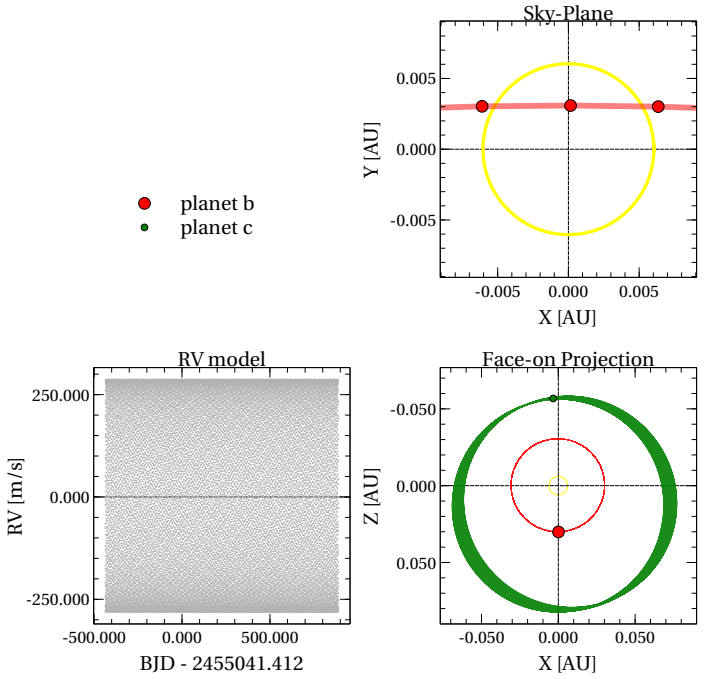

(b) WASP-3 orbits and RV model for 3-body stable solution.

Figura 4.10: $O-C$, RV, and orbits of the unstable 3-body solution found by `TRADES` in `PSO` mode. Plot of the sky-projected orbits (*top-right panel*) with the planets transiting the star (colored circles at given integration step). Orbit-projection plot (*bottom-right panel*) of the system (colored circles are the positions of the planets a the initial conditions, and the sizes have been scaled with masses). In the *bottom-left panel* the RV model for the whole integration time.

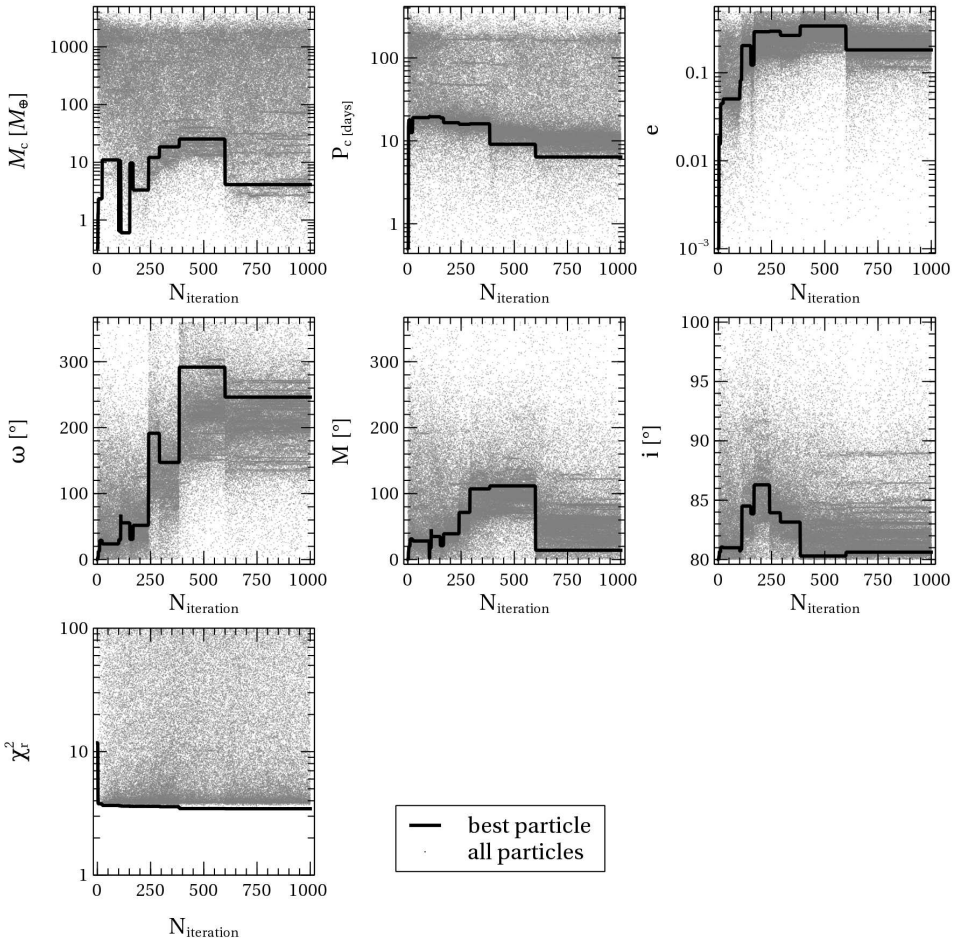

Figura 4.11: Fitted parameters evolution during the PSO simulation. Number of particles and iterations used was 500 and 1000, respectively. The total number of single configurations evaluated by the algorithm was 500 000 (gray dots). The black line is the best orbital configuration for each iteration.

Capitolo 5

Conclusions and future prospectives

5.1 Conclusions

I have developed a program, TRADES, that simulates the dynamics of exoplanetary systems and that does a simultaneous fit of radial velocities and transit times data.
Analyzing a simulated planetary system, I have shown that TRADES can determine the parameters even from low precision data or for a rough guess of the initial orbital elements.

I have validated TRADES by reproducing the packed exoplanetary system Kepler-11. The orbital parameters I have determined are in agreement with the values of the discovery paper and the recent analysis of 14 quarters by Lissauer et al. (2013). Furthermore, my analysis is in agreement with the results by Migaszewski et al. (2012), that used a similar approach. My best simulation (K11-III) has returned a value for the mass of the planet g of about 25 $M_{\oplus}$, in agreement within the error bars and the confidence interval proposed by Lissauer et al. (2013). Furthermore, all my simulations have showed a final $\chi^2_{\rm r} \lesssim 2$ and the final mass of planet g is in agreement with the previous works. However, the complexity of the system did not allow an easy determination of the parameters, because of high degeneration fo the orbital configurations. The parameter space is clearly characterized by a forest of minima of the χ^2, so the guess in the initial parameters is very awkward.

I have reproduced the Kepler-9 system (without KOI-377.03) and I have found

that the parameters from the SOM of the discovery paper (Holman et al. 2010) cannot properly reproduce the $O-C$ diagram of Kepler-9c. I have tested the orbits and the $O-C$ diagrams with an independent program, `MERCURY`, and I have found the same result. A difference of a few degrees in λ for both planets is enough to explain the offset of about 300 minutes in the $O-C$ diagram. I have found the same results after analyzing the T_0s by Mazeh et al. (2013) that cover the same quarters of Holman et al. (2010).

Extending the analysis I have found that the original solution is not compatible to the whole set of data from the 12 quarters by Mazeh et al. (2013). It shows a divergence of the simulated $O-C$ compared to the observed one (Fig. 3.12). The solution K9-I, that I have obtained with the same temporal baseline of the discovery paper cannot explain the observed transit time for the whole set of T_0s.

Only using the combination of a 'quasi' global optimized search algorithm, such as genetic (`PIKAIA`) or particle swarm (`PSO`), and the `LM` it has been possible to improve the fit on all 12 quarters, but only discarding the six RV points. With this approach I have found a new stable solution (K9-II) with a $\chi^2_{\rm r} \approx 1.4$ for 56 dof. This solution has led to mass values that are about 55% of the mass values given in the discovery paper, and smaller eccentricities. These values imply an RV model that has a smaller semi-amplitude, of about 12.80 ms^{-1}, than that calculated with the six HIRES RV observations.

I need to study better this system, e.g., obtaining more RV points, because it can shed light on the issue of the different masses of the exoplanets calculated from RV data and from the TTV (see Masuda et al. 2013, for a similar case). Follow-up transit observations with CHEOPS will extend the time coverage and are advisable.

In both *Kepler* systems I have carried out the analysis of twelve quarters using the transit times calculated by Mazeh et al. (2013) using an automated algorithm. I point out that it would be advisable to analyze in more details the light curves of the KOIs that show TTV signals and recompute the transit times of the planets.

It is known that the `LM` algorithm cannot return reliable errors (with physical meaning) in presence of correlated errors and complex parameter spaces. For some parameters the bootstrap analysis returned small intervals of confidence. A possible explanation is that the parameter distributions in the bootstrap analysis are limited to values close to those found by the `LM` algorithm. This is

probably due to a strong selection effect of the forest of minima in the χ^2 space. Furthermore, for the Kepler-9 case the measurement errors have tiny effect compared to the TTV signal that dominates the distribution of the parameters.

I have started optimizing and testing TRADES for the CHEOPS mission. The purpose is to study the capabilities of this mission in case of the detection of a TTV signal. This will help to characterize further the planets hosting systems. I have simulated an hypothetical CHEOPS case based on the Kepler-9 system. Fixing the parameters of planet b and creating a feasible data set of T_0s and RVs I have found a possible orbital solution near to the real one combining a global and a local search in the parameter space. In this case I have found some degenerate solutions that could well reproduce the data. Only analyzing their stability with the FMA tool it was possible to determine which is the stable and best-fit solution. However, a susequently analysis from a stability point of view is needed in order to disentangle degenerate-unstable solutions.

I have presented few cases from the TASTE project sample, i.e., HAT-P-13 and WASP-3. These systems have shown a doubful TTV signal. The HAT-P-13 system is made of transiting planet, HAT-P13b, and by another massive planet that has been detected by RV method. Winn et al. (2010) observed a trend in the RV residuals of this system and they proposed that it could be attributed to an additional fouth body. I have done grid+LM search on mass and semi-major axis covering the values proposed by Winn et al. (2010). I have found some degenerate solutions in mass and period that outputs better χ^2_r, remove a linear trend in the RV residuals, but left a sinusoidal term. This fourth additional body cannot describe the scattered T_0s, and the original solution with planet b and c cannot be excluded.

Most of the solutions for the WASP-3 system with more than one planet, that I determined with TRADES, have been found to be unstable. Or, they have shown a slightly higher χ^2 than the solution for the 2-body case.

The main cause of these doubful TTV could be an unprecise analysis of the photometric series that produces underestimated transit time uncertainties. These are only very preliminary results and I am still analysing the dynamics of these systems. More photometric and spectroscopic data are needed to shed light on the nature of these exoplanetary systems.

5.2 Side projects and future prospectives

In the near future, I will add a Monte-Carlo-Markov-Chain (MCMC) algorithm (or an another Bayesian algorithm , e.g., multiNEST, Feroz et al. 2009) in `TRADES` to perform parameter estimation and model selection using a Bayesian approach. The idea is to provide the initial parameters to the Bayesian algorithm via the `LM` algorithm or using a grid search. Furthermore, I plan to include the transit duration in the fitting procedure, to put further constraint on the parameter determinatio. Also, I will implement the possibility to simultaneously fit multiple RV set obtained from different facilities. From a numerical point of view, it would be advisable to test combination of parameters to be fitted in order to avoid parameter correlations, i.e., $e\cos\omega$ and $e\sin\omega$.

I am selecting a wide sample of exoplanetary systems from Mazeh et al. (2013) list showing TTV signals. The number of the multiple planetary systems in the list that show TTV signal is quite high, more than 300 at time of writing. So, I will do a screening of the more interesting cases. This could be based on the TTV amplitude, or on the shape of the TTV signal, or simply it could be based on observational parameters that could allow further follow-up with ground-based facilities.

As already mentioned in section 4.2, I am cooperating with the TASTE project, and in particular I am in the pool of the project observers. Furthermore, I work on the dynamical analysis and on the data processing, as can be found in the following articles: Nascimbeni et al. (2011b, 2013) and Granata et al. (2014).

I have a role in one of the working group (WG) of the CHEOPS mission responsible for the study of the dynamics of the exoplanetary systems that CHEOPS will discover. In particular, I am studying the TTV capability, and feasibility, of the CHEOPS satellite. I will extend the analysis presented in Section 4.1 to different set of synthetic data, reproducing different sample possibilities, i.e., a different number of observed T_0, non-consecutive transits, different set of RVs from different facilities, different mass and size of the observed planets, and so on.
In addition, I have the task to interface the Italian Science Team of the CHEOPS mission with the Science Operation Center (SOC). The SOC is a team whose task is to develop all the common software structure needed by the CHEOPS mission, from the on-board pre-processing, the on-board quicklook, the simulator of the performances of the satellite and of the camera, the definition of image formats and compressions, the pipeline data reduction, and it is responsible of

the administration of the data archive. All these programs needed to be checked from a scientific point of view in order to fullfill all the mission requirements.

I am involved in a project that is mainly based on the HARPS-N observations: Global Architecture of Planetary Systems (GAPS,[1] Covino et al. 2013). The main objectives of the GAPS project can be summarized in: i) frequencies analysis of low-mass planets as a function of stellar mass, stellar metallicity, density of the stellar environment, ii) characterization of known exoplanetary systems, iii) analysis of the stellar activity and of its influence on the determination of the planetary parameters, and iv) determine accurate planetary mass from asteroseismologic analysis of the host star.

The *Kepler* mission has shown that exists a great number of exoplanetary systems with a wide range of characteristics, and about 10% of them show TTV signal. With the PLATO mission the number of stars observed will be greater than *Kepler*, and it would be logical to expect an even higher number of exoplanetary systems. As member of one of the PLATO working packages (WPs), I will apply the knowledge and skills I have learnt from the `TRADES` development to the dynamical analysis of the exoplanetary systems that will be discovered by PLATO. At the same time, I am in charge in the WP responsible for the interface between the 'Target and Field Characterization and Selection' and the 'PLATO CCD IMAGE Simulator' WPs.

[1] GAPS at INAF-OACT

Bibliografia

Agol, E., Steffen, J., Sari, R., & Clarkson, W. 2005, MNRAS, 359, 567

Agol, E. & Steffen, J. H. 2007, MNRAS, 374, 941

Bakos, G., Noyes, R. W., Kovács, G., et al. 2004, PASP, 116, 266

Bakos, G. Á., Howard, A. W., Noyes, R. W., et al. 2009, ApJ, 707, 446

Bakos, G. Á., Lázár, J., Papp, I., Sári, P., & Green, E. M. 2002, PASP, 114, 974

Barros, S. C. C., Diaz, R. F., Santerne, A., et al. 2013, ArXiv e-prints

Beaugé, C., Ferraz-Mello, S., & Michtchenko, T. A. 2012, Research in Astronomy and Astrophysics, 12, 1044

Borucki, W. J., Koch, D., Basri, G., et al. 2010, Science, 327, 977

Caldwell, D. A., Kolodziejczak, J. J., Van Cleve, J. E., et al. 2010, ApJ, 713, L92

Cash, J. R. & Karp, A. H. 1990, ACM Trans. Math. Softw., 16, 201

Chambers, J. E. & Migliorini, F. 1997, in Bulletin of the American Astronomical Society, Vol. 29, AAS/Division for Planetary Sciences Meeting Abstracts #29, 1024

Charbonneau, D., Brown, T. M., Latham, D. W., & Mayor, M. 2000, ApJ, 529, L45

Charbonneau, P. 1995, ApJS, 101, 309

Collier Cameron, A., Pollacco, D., Hellier, C., et al. 2009, in IAU Symposium, Vol. 253, IAU Symposium, ed. F. Pont, D. Sasselov, & M. J. Holman, 29–35

Covino, E., Esposito, M., Barbieri, M., et al. 2013, A&A, 554, A28

Danby, J. M. A. 1988, Fundamentals of celestial mechanics

Deck, K. M., Agol, E., Holman, M. J., & Nesvorný, D. 2014, ApJ, 787, 132

Deprit, A. 1969, Celestial Mechanics, 1, 12

Eberhart, R. C. 2007, Computational Intelligence: Concepts to Implementations (San Francisco, CA, USA: Morgan Kaufmann Publishers Inc.)

Eibe, M. T., Cuesta, L., Ullán, A., Pérez-Verde, A., & Navas, J. 2012, MNRAS, 423, 1381

Fabrycky, D. C. 2011, Non-Keplerian Dynamics of Exoplanets, ed. S. Piper, 217–238

Feroz, F., Hobson, M. P., & Bridges, M. 2009, MNRAS, 398, 1601

Ford, E. B. 2008, in IAU Symposium, Vol. 249, IAU Symposium, ed. Y.-S. Sun, S. Ferraz-Mello, & J.-L. Zhou, 441–446

Ford, E. B., Quinn, S. N., & Veras, D. 2008, ApJ, 678, 1407

Ford, E. B., Rowe, J. F., Fabrycky, D. C., et al. 2011, ApJS, 197, 2

Fulton, B. J., Shporer, A., Winn, J. N., et al. 2011, AJ, 142, 84

Goldberg, D. E. 1989, Genetic Algorithms in Search, Optimization and Machine Learning, 1st edn. (Boston, MA, USA: Addison-Wesley Longman Publishing Co., Inc.)

Granata, V., Nascimbeni, V., Piotto, G., et al. 2014, ArXiv e-prints

Henry, G. W., Marcy, G., Butler, R. P., & Vogt, S. S. 1999, IAU Circ., 7307, 1

Henry, G. W., Marcy, G. W., Butler, R. P., & Vogt, S. S. 2000, ApJ, 529, L41

Holland, J. 1975

Holman, M. J., Fabrycky, D. C., Ragozzine, D., et al. 2010, Science, 330, 51
Holman, M. J. & Murray, N. W. 2005, Science, 307, 1288
Hori, G. 1966, PASJ, 18, 287
Irwin, J. B. 1952, ApJ, 116, 211
Jenkins, J. M., Caldwell, D. A., Chandrasekaran, H., et al. 2010, ApJ, 713, L87
Kennedy, J. & Eberhart, R. 1995, in Neural Networks, 1995. Proceedings., IEEE International Conference on, Vol. 4, 1942–1948 vol.4
Kipping, D. M. 2009a, MNRAS, 392, 181
Kipping, D. M. 2009b, MNRAS, 396, 1797
Knutson, H. A., Charbonneau, D., Noyes, R. W., Brown, T. M., & Gilliland, R. L. 2007, ApJ, 655, 564
Koch, D. G., Borucki, W. J., Basri, G., et al. 2010, ApJ, 713, L79
Laskar, J. 1993a, Physica D: Nonlinear Phenomena, 67, 257
Laskar, J. 1993b, Celestial Mechanics and Dynamical Astronomy, 56, 191
Laskar, J., Froeschlé, C., & Celletti, A. 1992, Physica D: Nonlinear Phenomena, 56, 253
Latham, D. W., Rowe, J. F., Quinn, S. N., et al. 2011, ApJ, 732, L24
Levison, H. F. & Duncan, M. J. 2000, AJ, 120, 2117
Lissauer, J. J., Fabrycky, D. C., Ford, E. B., et al. 2011a, Nature, 470, 53
Lissauer, J. J., Jontof-Hutter, D., Rowe, J. F., et al. 2013, ApJ, 770, 131
Lissauer, J. J., Ragozzine, D., Fabrycky, D. C., et al. 2011b, ApJS, 197, 8
Lovis, C. & Fischer, D. 2011, Radial Velocity Techniques for Exoplanets, ed. S. Seager, 27–53
Maciejewski, G., Dimitrov, D., Neuhäuser, R., et al. 2010, MNRAS, 407, 2625
Maciejewski, G., Niedzielski, A., Wolszczan, A., et al. 2013, AJ, 146, 147
Mandel, K. & Agol, E. 2002, ApJ, 580, L171
Marcy, G. W. & Butler, R. P. 1995, in Bulletin of the American Astronomical Society, Vol. 27, American Astronomical Society Meeting Abstracts, 1379
Marzari, F., Tricarico, P., & Scholl, H. 2002, ApJ, 579, 905
Masuda, K., Hirano, T., Taruya, A., Nagasawa, M., & Suto, Y. 2013, ApJ, 778, 185
Mayor, M., Pepe, F., Queloz, D., et al. 2003, The Messenger, 114, 20
Mayor, M. & Queloz, D. 1995, Nature, 378, 355
Mazeh, T., Nachmani, G., Holczer, T., et al. 2013, ArXiv e-prints
Migaszewski, C., Słonina, M., & Goździewski, K. 2012, MNRAS, 427, 770
Miralda-Escudé, J. 2002, ApJ, 564, 1019
Montalto, M., Gregorio, J., Boué, G., et al. 2012, MNRAS, 427, 2757
Moré, J. J., Garbow, B. S., & Hillstrom, K. E. 1980, User guide for MINPACK-1, Tech. Rep. ANL-80-74, Argonne Nat. Lab., Argonne, IL
Murray, C. D. & Correia, A. C. M. 2011, Keplerian Orbits and Dynamics of Exoplanets, ed. S. Piper, 15–23
Murray, C. D. & Dermott, S. F. 1999, Solar system dynamics
Murray, C. D. & Dermott, S. F. 2000, Solar System Dynamics
Nascimbeni, V., Cunial, A., Murabito, S., et al. 2013, A&A, 549, A30
Nascimbeni, V., Piotto, G., Bedin, L. R., & Damasso, M. 2011a, A&A, 527, A85
Nascimbeni, V., Piotto, G., Bedin, L. R., et al. 2011b, A&A, 532, A24
Nesvorný, D. 2009, ApJ, 701, 1116
Nesvorný, D., Kipping, D., Terrell, D., et al. 2013, ApJ, 777, 3
Nesvorný, D. & Morbidelli, A. 2008, ApJ, 688, 636
Pál, A., Sárneczky, K., Szabó, G. M., et al. 2011, MNRAS, 413, L43

Payne, M. J., Ford, E. B., & Veras, D. 2010, ApJ, 712, L86
Pepe, F. A. & Lovis, C. 2008, Physica Scripta Volume T, 130, 014007
Perryman, M. 2011, The Exoplanet Handbook
Pollacco, D., Skillen, I., Collier Cameron, A., et al. 2008, MNRAS, 385, 1576
Pollacco, D. L., Skillen, I., Collier Cameron, A., et al. 2006, PASP, 118, 1407
Press, W. H., Teukolsky, S. A., Vetterling, W. T., & Flannery, B. P. 1996, Numerical recipes in Fortran 90 (2nd ed.): the art of parallel scientific computing (New York, NY, USA: Cambridge University Press)
Rupprecht, G., Pepe, F., Mayor, M., et al. 2004, in Society of Photo-Optical Instrumentation Engineers (SPIE) Conference Series, Vol. 5492, Ground-based Instrumentation for Astronomy, ed. A. F. M. Moorwood & M. Iye, 148–159
Southworth, J., Bruni, I., Mancini, L., & Gregorio, J. 2012, MNRAS, 420, 2580
Southworth, J., Maxted, P. F. L., & Smalley, B. 2004, MNRAS, 351, 1277
Steffen, J. H. & Agol, E. 2005, MNRAS, 364, L96
Struve, O. 1952, The Observatory, 72, 199
Szabó, G. M., Kiss, L. L., Benkő, J. M., et al. 2010, A&A, 523, A84
Tada, T. 2007, Journal of Japan Society of Hydrology & Water Resources, 20, 450
Tamuz, O., Mazeh, T., & Zucker, S. 2005, MNRAS, 356, 1466
Torres, G., Fressin, F., Batalha, N. M., et al. 2011, ApJ, 727, 24
Veras, D., Ford, E. B., & Payne, M. J. 2011, ApJ, 727, 74
Vogt, S. S., Allen, S. L., Bigelow, B. C., et al. 1994a, in Society of Photo-Optical Instrumentation Engineers (SPIE) Conference Series, Vol. 2198, Instrumentation in Astronomy VIII, ed. D. L. Crawford & E. R. Craine, 362
Vogt, S. S., Allen, S. L., Bigelow, B. C., et al. 1994b, in Society of Photo-Optical Instrumentation Engineers (SPIE) Conference Series, Vol. 2198, Society of Photo-Optical Instrumentation Engineers (SPIE) Conference Series, ed. D. L. Crawford & E. R. Craine, 362
Winn, J. N. 2011, Exoplanet Transits and Occultations, ed. S. Piper, 55–77
Winn, J. N., Johnson, J. A., Howard, A. W., et al. 2010, ApJ, 718, 575
Zechmeister, M. & Kürster, M. 2009, A&A, 496, 577